FLORIDA DEPARTMENT OF TRANSPORTATION

Analysis and Modeling of Fiber-Wrapped Columns and Concrete-Filled Tubes

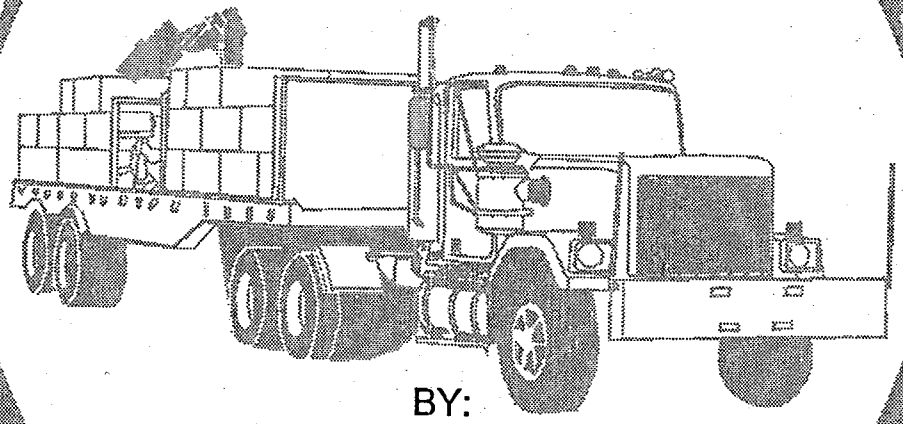

BY:

Mohsen Shahawy
Thomas E. Beitelman
and
Amir Mirmiran

STRUCTURAL RESEARCH CENTER

FLORIDA DEPARTMENT OF TRANSPORTATION
STRUCTURAL RESEARCH CENTER
2007 E. DIRAC DRIVE
TALLAHASSEE, FL 32310

FINAL REPORT
for

ANALYSIS AND MODELING OF FIBER-WRAPPED COLUMNS AND CONCRETE-FILLED TUBES

Structural Research Center
The Florida Department of Transportation
Tallahassee, Florida

Mohsen Shahawy
Tom Beitelman
and Amir Mirmiran

June 10, 1998

TABLE OF CONTENTS

Description	Page
List of Tables	iii
List of Figures	iv
Executive Summary	vi
Problem Statement	vi
Objective	vi
Findings	vi
Conclusions	vii
1 Introduction	1
1.1 Problem Statement	1
1.2 Research Objectives	1
1.3 Report Outline	2
2 Literature Review and General Information	3
2.1 Fiber-Wrapping Applications	3
2.2 Modeling Procedures	4
3 Experimental Work	6
3.1 Uniaxial Compression Tests	6
3.2 Analysis of Results	13
4 Confinement Modeling	49
4.1 Proposed Model	49
4.2 Verification of the Model	52
4.3 Results and Discussion	52
5 Finite Element Modeling	65
5.1 Introduction	65
5.2 Plasticity Approach	65
5.3 Modeling	67
5.4 Results and Discussion	68
6 Conclusions	81
References	83

List of Tables

Table	Page
3.1 Concrete mix design	6
3.2 Material properties of carbon wraps	7
3.3 Test results for the 3 ksi specimens	9
3.4 Test results for the 6 ksi specimens	11
4.1 Input values for the confinement model	55

List of Figures

Figure	Page
3.1 Instrumentation	7
3.2 Typical failure of carbon-wrapped concrete	8
3.3 Stress-strain curves for the 3 ksi specimens with l layer	14
3.4 Stress-strain curves. for the 3 ksi specimens with 2 layers	15
3.5 Stress-strain curves for the 3 ksi specimens with 3 layers	16
3.6 Stress-strain curves for the 3 ksi specimens with 4 layers	17
3.7 Stress-strain curves for the 3 ksi specimens with 5 layers	18
3.8 Stress-strain curves for the 6 ksi specimens with player	19
3.9 Stress-strain curves for the 6 ksi specimens with 2 layers	20
3.10 Stress-strain curves for the 6 ksi specimens with 3 layers	21
3.11 Stress-strain curves for the 6 ksi specimens with 4 layers	22
3.12 Average stress-strain curves for the 3 ksi specimens	23
3.13 Average stress-strain curves for the 6 ksi specimens	24
3.14 Volumetric curves for the 3 ksi specimens with 1 layer	25
3.15 Volumetric curves for the 3 ksi specimens with 2 layers	26
3.16 Volumetric curves for the 3 ksi specimens with 3 layers	27
3.17 Volumetric curves for the 3 ksi specimens with 4 layers	28
3.18 Volumetric curves for the 3 ksi specimens with 5 layers	29
3.19 Volumetric curves for the 6 ksi specimens with 1 layer	30
3.20 Volumetric curves for the 6 ksi specimens with 2 layers	31
3.21 Volumetric curves for the 6 ksi specimens with 3 layers	32
3.22 Volumetric curves for the 6 ksi specimens with 4 layers	33
3.23 Average volumetric curves for the 3 ksi specimens	34
3.24 Average volumetric curves for the 6 ksi specimens	35
3.25 Typical dilation response of carbon-wrapped concrete	37
3.26 Dilation curves for the 3 ksi specimens with 1 layer	38
3.27 Dilation curves for the 3 ksi specimens with 2 layers	39
3.28 Dilation curves for the 3 ksi specimens with 3 layers	40
3.29 Dilation curves for the 3 ksi specimens with 4 layers	41
3.30 Dilation curves for the 3 ksi specimens with 5 layers	42
3.31 Dilation curves for the 6 ksi specimens with 1 layer	43
3.32 Dilation curves for the 6 ksi specimens with 2 layers	44
3.33 Dilation curves for the 6 ksi specimens with 3 layers	45
3.34 Dilation curves for the 6 ksi specimens with 4 layers	46
3.35 Average dilation curves for the 3 ksi specimens	47
3.36 Average dilation curves for the 6 ksi specimens	48
4.1 Parameters of the confinement model	50
4.2 Comparison of model with carbon-wrapped specimens of Picher (1995)	53
4.3 Comparison of model with S-glass-wrapped specimens of Mastrapa (1997)	54

4.4 Comparison of confinement model with the 3 ksi, 1-layer specimens 56
4.5 Comparison of confinement model with the 3 ksi, 2-layer specimens 57
4.6 Comparison of confinement model with the 3 ksi, 3-layer specimens 58
4.7 Comparison of confinement model with the 3 ksi, 4-layer specimens 59
4.8 Comparison of confinement model with the 3 ksi, 5-layer specimens 60
4.9 Comparison of confinement model with the 6 ksi, 1-layer specimens 61
4.10 Comparison of confinement model with the 6 ksi, 2-layer specimens 62
4.11 Comparison of confinement model with the 6 ksi, 3-layer specimens 63
4.12 Comparison of confinement model with the 6 ksi, 4-layer specimens 64
5.1 Deformed shape of the discretized top quarter of the specimen 69
5.2 Contour of equivalent Von Mises total strains 70
5.3 Comparison of FE model with the 3 ksi, 1-layer specimens 72
5.4 Comparison of FE model with the 3 ksi, 2-layer specimens 73
5.5 Comparison of FE model with the 3 ksi, 3-layer specimens 74
5.6 Comparison of FE model with the 3 ksi, 4-layer specimens 75
5.7 Comparison of FE model with the 3 ksi, 5-layer'specimens 76
5.8 Comparison of FE model with the 6 ksi, 1-layer specimens 77
5.9 Comparison of FE model with the 6 ksi, 2-layer specimens 78
5.10 Comparison of FE model with the 6 ksi, 3-layer specimens 79
5.11 Comparison of FE model with the 6 ksi, 4-layer specimens 80

EXECUTIVE SUMMARY

Problem Statement

Fiber-wrapping offers a -high strength, low weight, and corrosion-resistant jacket which can be easily and quickly installed with negligible increase in the column's cross-section. Since the first application of fiber-wrapping technique to concrete chimneys in Japan (Katsumata and Yagi 1990), there has been an abundance of studies on the use of this technique. It has been put into practice in several states including California, Nevada, New York, and Vermont. Both carbon and glass fibers have been utilized, although carbon fibers are more expensive.

Since use of fiber composites for confinement of concrete is relatively new, theoretical work in this area is limited to the models that were originally developed for transverse steel reinforcement. However, it has been shown that concrete behaves very differently when confined by elasto-plastic materials such as steel as compared to linearly elastic materials such as fiber composites (Mirmiran and Shahawy 1997a). Applying the same models to fiber-wrapped concrete may result in overestimating the strength and unsafe design. In the absence of reliable models, construction industry may be forced to either avoid the use of advanced composites, or to incorporate high "factors of safety," making composite construction less economical. The PI has previously developed such a model for glass-wrapped concrete columns (Mirmiran 1997a&b). There is a need to extend the work to carbon-wrapped concrete columns.

Objectives

The objectives of this study were as follows:

1. Investigate the behavior of carbon-wrapped concrete specimens in uniaxial compression, based on the tests previously conducted by the Florida Department of Transportation.

2. Compare the experimental results with the confinement model of Samaan, Mirmiran and Shahawy (1998) which was developed for concrete-filled E-glass FRP tubes.

3. Compare the experimental results with a non-associative Drucker-Prager type plasticity model using the finite element analysis.

Findings

The experimental component of this study was conducted by the Florida Department of Transportation, Structural Research Laboratory, Tallahassee, FL. A total of 55 6" x 12" concrete cylinders including 45 carbon-wrapped and 10 control (unconfined) specimens were tested in uniaxial compression. Two parameters were considered in the experimental program; concrete strength (3 and 6 ksi), and number of layers of carbon fabric (1-Slayers). Typical failure of carbonwrapped specimens was marked by fiber fracture at or near the mid-height of the specimens. Since the fabric was uni-directional (at 0°), a band or ring was typically formed as a result of the shearing off and separation of the fabric in the hoop direction. The response of carbon-wrapped specimens

is generally bilinear, although more curvilinear than the response of glass-wrapped concrete. The first slope follows the modulus of elasticity of unconfined concrete, while the second slope depends on the number of layers and the stiffness of the jacket. As for volumetric response, the 6 ksi specimens behave very similar to the glass-wrapped concrete, in that the direction of dilation is reversed as the jacket takes over beyond the critical stage of concrete. However, the 3 ksi specimens do not even show any expansion, as the carbon wrap appears to be stiff enough to restrain any dilation tendency of concrete. For both concrete batches, thicker jackets show faster recovery of dilation as well as higher compaction rates. The dilation response of carbon-wrapped concrete appears to be generally the same as that of glass-wrapped concrete.

The confinement model that was developed for the glass-wrapped concrete predicted the response of carbon-wrapped specimens rather well. However; due to lack of accurate data on the properties of the jacket, it was not feasible to get better predictions, or to better evaluate the model. The finite element analysis with the non-associative Drucker-Prager type plasticity proved very effective for modeling of carbon-wrapped specimens. The differences were again attributed to the lack of accurate data on the properties of the jacket.

Conclusions

Carbon-wrapping of concrete column adds to its strength and ductility. The behavior of carbon-wrapped concrete is in general very similar to that of glass-wrapped concrete. The bilinear confinement that was developed- for glass-wrapped concrete can be applied to carbon-wrapped concrete. However, a better fit can be obtained by re-calibrating the model for an entire database that consists of both carbon-wrapped and glass-wrapped concrete. Such database needs to be accompanied by a set of accurate coupon tests on the properties of the jacket. The finite element modeling is also useful in predicting the response of carbon-wrapped concrete. A more accurate estimate of jacket properties make the analysis fit the test results better.

CHAPTER1

INTRODUCTION

1.1 Problem Statement

Deterioration of RC columns due to corrosion ofthe reinforcing steel and spalling of concrete cover has been a major problem for the aging infrastructure ("Florida" 1991). There are three methods of retrofitting for concrete columns; RC jacketing, steel jacketing, and fiber-wrapping. RC jacketing requires formwork and considerable increase in weight and cross-section of the column. Steel j ticketing is also labor intensive and costly. Fiber-wrapping offers a high strength, low weight, and corrosion-resistant jacket which can be easily and quickly installed with negligible increase in the column's cross-section. Since the first application of fiber-wrapping technique to concrete chimneys in Japan (Katsumata and Yagi 1990), there has_ been an abundance of studies on the use of this technique. It has been put into practice in several states including California, Nevada, New York, and Vermont. Both carbon and glass fibers have been utilized, although carbon fibers are more expensive. The hoop fibers enhance shear and axial strength as well as ductility of the column (Saadatmanesh et al. 1994). When an increase in the flexural strength is desired, fiber reinforced plastic (FRP) sheets are bonded to the column in the axial direction (Ballinger et al. 1993).

Since use of fiber composites for confinement of concrete is relatively new, theoretical work in this area is limited to the models that were originally developed for transverse steel reinforcement. However, it has been shown that concrete behaves very differently when confined by elasto-plastic materials such as steel as compared to linearly elastic materials such as fiber composites (Mirmiran and Shahawy 1997a). Applying the same models to fiber-wrapped concrete may result in overestimating the strength and unsafe design. In the absence of reliable models, construction industry may be forced to either avoid the use of advanced composites, or to incorporate high "factors of safety," making composite construction less economical. The PI has previously developed such a model for glass-wrapped concrete columns (Mirmiran 1997a&b). There is a need to extend the work to carbon-wrapped concrete columns.

1.2 Research Objectives

The objectives of this study were as follows:

1. Investigate the behavior of carbon-wrapped concrete specimens in uniaxial compression, based on the tests previously conducted by the Florida Department of Transportation.

2. Compare the experimental results with the confinement model of Samaan, Mirmiran and

Shahawy (1998) which was developed for concrete-filled E-glass FRP tubes.

3. Compare the experimental results with a non-associative Drucker-Prager type plasticity model using the finite element analysis.

1.3 Report Outline

This report consists of 6 chapters. Chapter 1 provides an introduction to the study. A brief review of the relevant literature is provided in Chapter 2. Chapter 3 documents the experimental work that was performed by the Florida Department of Transportation. Confinement model and the finite element modeling are discussed in Chapters 4 and 5, respectively. Chapter 6 summarizes the conclusions and discusses various recommendations.

CHAPTER 2

LITERATURE REVIEW

2.1 Fiber-Wrapping Applications .

Although most studies on fiber-wrapped columns have been conducted in the past five years (Bavarian et al. 1996), the first attempt at such confinement mechanism was made in late 1970's. Kurt (1978) suggested using commercially available plastic pipes (PVC or ABS) filled with concrete. His experimental studies indicated that plastic pipes were more effective than steel pipes in confining concrete. For a slenderness ratio of less than 20, plastic-encased concrete showed a 45° shear failure, both in the concrete core and in the plastic pipe, resulting from the combination of axial compression and hoop tension in the pipe. Since the plastic used by Kurt was weak, the enhancement in column's strength was not significant. Later, Fardis and Khalili (1981, 1982) from MIT wrapped bi-directional FRP on 3 "x6" and 4"x8" concrete cylinders under uniaxial compression tests, and on 3 "x6"x48" beams under third-point loading. They achieved considerable strength and ductility enhancements. In early 1990's, as part of an investigation on the effect of confinement on high strength concrete, Lahlou et al. (1992) tested two 2"x4" glass fiber tubes filled with concrete. However, since the fibers were axially oriented (pultruted), they did not observe any significant enhancement in concrete strength.

Fiber-wrapping technology was first used in practice for concrete chimneys in Japan (Katsumata and Yagi 1990). The concept was then extended to the retrofitting of concrete columns (Ballinger et al. 1993). In the U.S., Hexcel Fyfe has installed field demonstration wraps for Caltrans (Fyfe 1995). It adopted a method called "active wrapping," in which pressurized cement grout is pumped between the original column and the composite wrap.. few of the columns thus wrapped have since failed by fiber fracture, which is now attributed to the wrapping mechanism. This method is replaced with a "passive wrap," i.e., without pressurized grouting. In an effort to minimize the onsite installation time and cost, an approach similar to steel jacketing was taken by the researchers at the Penn State University who investigated a system of pre-formed FRP shells. The two half cylinder shells are joined on site by applying adhesives. Tests at Penn State indicated that such systems fail by separation of the shells along the joint (Nanni and Bradford 1995). Similar approaches have also been introduced at the University of Southern California (Xiao et al. 1996). Another jacketing method includes wrapping thick FRP cables/tapes around concrete columns (Nanni and Bradford 1995). Researchers at the University of Arizona have used precured E-glass and polyester straps (tapes) with 0.03 to 0.04 inch thickness to wrap around existing columns with an epoxy adhesive (Saadatmanesh et al. 1994). Testing quarter-scale columns, they achieved ductilities of up to five times the as-built columns, and with no shear failure up to twice the stroke

limit of control columns (Jin et al. 1994). Durability of fiberglass wraps has been investigated under the individual effect of ultra-violet rays, salt water, moisture, alkaline soil, hot temperatures up to 140°F, freeze-thaw conditions, cold temperatures up to -40°F, and ozone gas for one thousand hours, with no significant loss of strength or failure, although the exact results and methods of experiments are not disclosed by the manufacturer (Fyfe 1995).

2.2 Modeling Procedures

Since the early years of development of the fiber-wrapping technology, three distinct modeling techniques have been suggested; (a) using (and extending) steel-based confinement models, (b) developing new FRP-based empirical models, and (c) using finite element with plasticity approach. A brief description of each method follows:

Steel-Based Confinement Models

Of the models for steel-confined concrete, the one that has been repeatedly mentioned and used by far the most, is that of Mander et al. (1988). They developed a stress-strain model for concrete subjected to uniaxial compression, and confined by transverse reinforcement. The concrete section may contain any type of confining steel; either spiral or circular hoops, or rectangular stirrups with or without supplementary cross ties. A single equation defines the entire stress-strain curve. The model allows for cyclic loading, and includes the effect of strain-rate. The influence of various types of confinement*is taken into account by defining an effective lateral confining stress, which is dependent on the configuration of the transverse and longitudinal reinforcement. An energy balance approach is used to predict the axial compressive strain in concrete corresponding to the first fracture of transverse reinforcement. The method involves balancing the strain energy capacity of transverse reinforcement to the strain energy stored in concrete as the result of confinement.

This model was used directly for fiber-wrapped specimens by Saadatmanesh et al. (1994). They generated moment-thrust interaction diagrams based on those stress-strain results. Later, studies by Mirmiran and Shahawy (1997b) and Nanni and Bradford (1995) showed that Mander's model overestimates the strength while grossly underestimating the ductility of confined concrete.

Variation of steel-based models have also been applied to FRP-confined concrete. Mirmiran and Shahawy (1995) adapted Madas and Elnashai (1992) for fiber composites. The model attempted to enforce strain compatibility between the jacket and the core. This was done by using a thirddegree polynomial suggested by Elwi and Murray (1979). However, it was later shown that dilation characteristics ofFRP-confined concrete are considerably different (Mirmiran and Shahawy 1997b). Another modification of Mander's model was performed by Priestley and Seible (1996). They developed an empirical relationship for the ultimate strain of FRP-confined concrete rather than using Mander's energy-balanced approach. Most recently, Monti and Spoelstra (1997) proposed a confinement model for fiber-wrapped circular columns. They used a model similar to Ahmad and Shah (1982). However, they used Mander's stress-strain relationship, and Pantazopoulou's model (1995) for lateral strains and strain compatibility. They showed their model to compare reasonably well with the data of Picher et al. (1996).

FRP-Based Empirical Models

Perhaps the first attempt at developing FRP-specific models can be credited to Fardis and Khaiili (1982). They suggested a hyperbolic equation for the stress-strain relation. However, Nanni and Bradford (1995) showed the model to grossly underestimate the ductility of fiber-wrapped columns, while comparing reasonably well for the strength. Ahmad, Khaloo and Irshaid (1991) conducted an investigation of the confinement effectiveness of fiberglass spirals as transverse reinforcement for concrete columns. They related the peak stress of confined concrete to the spacing of the spirals. The only FRP-based empirical model, to date, is that of Samaan, Mirmiran and Shahawy (1998) which uses a bilinear stress-strain relationship and incorporates the stiffness of the jacket in calculating the lateral strains.

Finite Element Analysis (Plasticity Approach)

Rochette and Labossi6re (1996) have used an incremental finite element technique to evaluate the response of fiber-wrapped square concrete columns. They modeled concrete as an elastic-perfectly plastic material, and adopted the Drucker-Prager failure criterion. The model favorably compared with the results of their own uniaxial compression tests (Picher et al. 1996). They concluded, however, that a more complex elasto-plastic formulation of concrete behavior is needed to enhance the model for various cross sections, fiber orientations, and load combinations. Earlier, Karabinis and Kiousis (1994) had used the same approach for modeling of steel-confined concrete. However, Mirmiran and Shahawy (1997a) reported that the model of Karabinis and Kiousis can not predict the strength or ductility of FRP-confined concrete. More recently, Zagers (1998) at UCF has applied anon-associative Drucker-Prager plasticity model with 0° dilatancy angle using ANSYS® Version 5.3. Results are in close agreement with the tests on fiberglass tubes. More details on this approach can be found in Chapter 5.

CHAPTER 3
EXPERIMENTAL WORK

3.1 Uniaxial Compression Tests

In order to develop an analytical model for carbon-wrapped concrete columns, it is necessary to conduct a detailed experimental program. This program has already been conducted by Tom Beitelman at the Florida Department of Transportation, Structural Research Laboratory, Tallahassee, FL. The reduced data was provided to the PI by FDOT. This chapter offers a brief description of the experimental program, and a detailed analysis of test results.

Specimen Layout

A total of 55 6" x 12" concrete cylinders including 45 carbon-wrapped and 10 control (unconfined) specimens were tested. Two parameters were considered in the experimental program; concrete strength, and number of layers of carbon fabric. Two concrete target strengths were used in the study; 3000 and 6000 psi. It should be noted that the actual strength of the 6 ksi batch was about 7000 psi. However, throughout this report, for consistency, all references are made to the target strength of 6 ksi. The concrete was mixed on site with the following proportions:

Table 3.1 Concrete mix design

Description	3000 psi target strength	6000 psi target strength
Water	65.56 lbs.	65.56 lbs.
Cement	96.40 lbs.	159.89 lbs.
Coarse aggregate[1]	372.00 lbs.	372.00 lbs.
Fine aggregate	348.00 lbs.	295.20 lbs.
W/C ratio	0.68	0.41

[1] ¾" max. aggregate size, river rock.

No additive was used in any of the mixes. Of each strength, two different batches were prepared due to the size limit of the concrete mixer. The batches were identified by the letters a and b in the specimen designations. The concrete cylinders were wrapped with a unidirectional stitched 'This chapter documents the work that was conducted by the Florida Department of Transportation.

carbon fabric using epoxy resin. Details of the material properties for the carbon and epoxy are reported elsewhere (Garmestani 1997). Table 3.2 shows the manufacturer's data and the FDOT's suggested values for the mechanical, properties of the wrap.

Table 3.2 Material properties of carbon wraps

Description	Manufacturer's data[1]	FDOT's suggested values[2]
Tensile strength	530 ksi	330 ksi
Tensile modulus of elasticity	33,500 ksi	12,000 ksi
Ultimate tensile elongation	1.4%	2.2 %

[1] Reported for the carbon fabric only (11 yarns/inch, 70 x 10.5 in^2/yarn).

[2] Based on split-disk tests and finite element analysis by Tom Beitelman of FDOT.

The 3000 psi specimens were wrapped with 1, 2, 3, 4, or 5 layers of fabric. The 6000 psi specimens were wrapped with 1, 2, 3, or 4 layers of fabric. For each concrete strength and number of layers, 4 or 5 samples were made for repeatability verification. The fabric was epoxy bonded to the concrete cylinder. Regardless of number of layers, the entire jacket was made of one continuous sheet.of fabric that was cut to the proper length and width. An additional 2" of overlap splice was provided. No groove was slit into the jacket for these specimens (as compared to the glass-wrapped concrete of Mirmiran 1997a&b). All specimens were capped with sulfur mortar.

Instrumentation

All specimens were fitted with three LVDTs that were mounted on two round sleeves around the specimens. The sleeves were attached to the specimen with pin-type support that would not affect the dilation of the specimen. Figure 3.1 shows the LVDTs placed at 120° apart around the specimen. To measure the lateral strains, two surface gages were mounted at the mid-height of each specimen, 180' apart. The surface gages were attached to the jacket after sanding and cleaning the contact surface of the specimen. In addition to surface gages, some of the specimens were fitted with an embedded strain gage inside concrete to measure the axial (longitudinal) strains in concrete. However, axial strains were calculated from the LVDTs, since it was observed that for all practical purposes, the

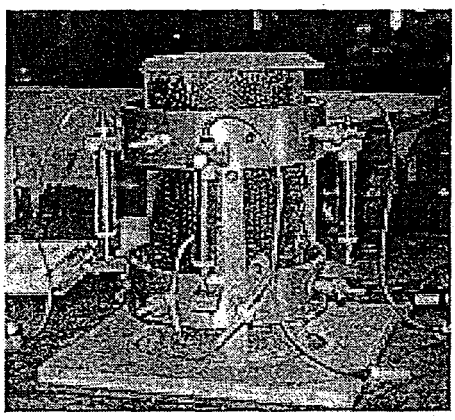

Figure 3.1 Instrumentation

average axial strains measured by LVDTs were as accurate as the measurements made with the embedded gages.

Test Procedure

All specimens were tested using a 550-kip MTS compression machine and a Mega DAQ data acquisition system. Specimens were loaded monotonically under a displacement control mode with a constant rate of 0.22 in. per minute.

Observed Behavior

Typical failure of carbon-wrapped specimens was marked by fiber fracture at- or near the mid-height of the specimens. Failure near the top and bottom surfaces was not of consequence due to friction between the platens and the specimen. However, it was noticed that if the capping was not level at the top or bottom, the failure point would shift away from the mid-height of the specimen. Since the fabric was uni-directional (at 0°), a band or ring was typically formed as a result of the shearing off and separation of the fabric in the hoop direction. No delamination was observed at the splice. Once the jacket was removed, it became clear that shear cones were formed at the top and bottom of some specimens. Failure was generally sudden. Unlike the glass-wrapped concrete, no white patches were developed to help detecting the distressed concrete core. However, popping noises 'heard during various stages of loading were the same as those reported for glass-wrapped concrete. The sounds were attributed to the micro cracking of concrete and shifting of aggregates. Those specimens that were fitted with an embedded strain gage showed a weak spot at the wire interface, since the strain gage wire was inserted very close to the edge. Such defects are noted in the next section under test results.

Figure 3.2 Typical failure of carbon-wrapped concrete

Test Results

Results are summarized in Tables 3.3 and 3.4 for the 3000 and 6000 psi concrete strengths, respectively. In these tables, f'_{cu} and ϵ_{cu} are the ultimate strength and strain of the specimen, E_c is the initial modulus of elasticity of concrete, and $y_{ave.}$ is the Poisson's ratio based on the average axial and lateral strains. For each tested specimen, the presence of any defect is also noted. Data for these tables was provided by Tom Beitelman of FDOT.

Table 3.3 Test results for 3 ksi specimens

	Sample No.	f'_{cu} (ksi)	ϵ_{cu}	E_c (ksi)	$\gamma_{ave.}$	Defects
Control	1 (Batch b)	2.80	0.0031	2300	0.15	None
	2 (Batch a)	2.50	0.0045	3100	0.45	LVDT No. 2 unusable
	3 (Batch a)	2.80	0.0032	2400	-	None
	4 (Batch b)	2.80	0.0028	2400	-	None
	5 (Batch b)	3.00	0.0030	2400	-	None
	Average	2.82	0.0033	2580	0.30	
	Sample No.	f'_{cu} (ksi)	ϵ_{cu}	E_c (ksi)	$\gamma_{ave.}$	Defects
1 layer	1 (Batch a)	4.50	0.0165	2700	0.06	Small pockets at wire interface
	2 (Batch b)	5.40	0.0135	3300	0.22	Air bubble at wire
	3 (Batch a)	-	-	-	-	Not tested
	4 (Batch b)	4.83	0.0145	3400	0.12	None
	5 (Batch b)	5.15	0.0191	1900	0.01	None
	Average	4.90	0.0159	3730	0.1025	
	Sample No.	f'_{cu} (ksi)	ϵ_{cu}	E_c (ksi)	$\gamma_{ave.}$	Defects
2 layers	1 (Batch b)	6.90	0.0273	1700	0.08	None
	2 (Batch a)	6.50	0.0200	2470	0.07	End buckled
	3 (Batch a)	7.43	0.0230	3100	0.17	None
	4 (Batch a)	6.02	0.0190	2000	0.05	Bubble in carbon at the top of the cylinder
	5 (Batch b)	6.80	0.0214	2000	0.06	None
	Average	6.73	0.0221	2230	0.086	
	Sample No.	f'_{cu} (ksi)	ϵ_{cu}	E_c (ksi)	$\gamma_{ave.}$	Defects
3 layers	1 (Batch a)	7.88	0.0205	2000	0.013	None
	2 (Batch a)	10.87	0.0320	2550	0.150	None
	3 (Batch b)	9.40	0.0210	2000	0.085	Crooked cap
	4 (Batch b)	9.15	0.0285	1900	0.095	None
	5 (Batch b)	8.09	0.0270	2000	0.080	None
	Average	9.08	0.0258	2100	0.0846	

Table 3.3 Continued

	Sample No.	f'_{cu} (ksi)	ϵ_{cu}	E_c (ksi)	$\gamma_{ave.}$	Defects
4 layers	1 (Batch a)	10.51	0.0335	1630	0.005	None
	2 (Batch b)	10.45	0.0250	2400	0.125	None
	3 (Batch a)	10.21	0.0325	1700	0.080	None
	4 (Batch b)	11.54	0.0460	3000	0.005	Crooked cap
	5 (Batch b)	12.21	0.0410	1700	0.035	LVDT rig loose in places
	Average	10.98	0.0356	2090	0.050	
	Sample No.	f'_{cu} (ksi)	ϵ_{cu}	E_c (ksi)	$\gamma_{ave.}$	Defects
5 layers	1 (Batch a)	6.94	0.0180	2400	0.14	Chip in the cap, end collapsed
	2 (Batch a)	13.15	0.0450	1500	0.08	None
	3 (Batch b)	13.18	0.0340	2600	0.14	Crooked cap
	4 (Batch b)	11.70	0.0360	1600	0.08	None
	5 (Batch b)	13.18	0.0380	2000	0.10	None
	Average	11.63	0.0342	2020	0.108	

Table 3.4 Test results for 6 ksi specimens

	Sample No.	f'_{cu} (ksi)	ϵ_{cu}	E_c (ksi)	$\gamma_{ave.}$	Defects
Control	1 (Batch b)	7.45	0.00265	3700	0.20	None
	2 (Batch a)	7.08	0.00275	3550	0.10	None
	3 (Batch b)	7.15	0.00200	3300	-	Only one transverse gage
	4 (Batch a)	7.13	0.00430	2200	-	None
	5 (Batch a)	6.75	0.00260	3500	-	None
	Average	7.11	0.00286	3250	0.15	
	Sample No.	f'_{cu} (ksi)	ϵ_{cu}	E_c (ksi)	$\gamma_{ave.}$	Defects
1 layer	1 (Batch b)	8.15	0.0058	3000	0.01	Chip missing in corner; Crooked cap
	2 (Batch b)	8.36	0.0060	3800	0.05	None
	3 (Batch b)	8.61	0.0051	4000	0.10	None
	4 (Batch a)	9.34	0.0080	3100	0.08	None
	5 (Batch a)	8.39	0.0063	3100	0.09	Uneven cap
	Average	8.57	0.00624	3400	0.066	
	Sample No.	f'_{cu} (ksi)	ϵ_{cu}	E_c (ksi)	$\gamma_{ave.}$	Defects
2 layers	1 (Batch b)	11.16	0.0100	3900	0.12	None
	2 (Batch a)	10.80	0.0088	3500	0.27	None
	3 (Batch a)	11.75	0.0105	3800	0.08	None
	4 (Batch a)	10.50	0.0080	3600	0.12	Kink in fabric
	5 (Batch a)	11.26	0.0110	4000	0.14	None
	Average	11.09	0.00966	3760	0.146	
	Sample No.	f'_{cu} (ksi)	ϵ_{cu}	E_c (ksi)	$\gamma_{ave.}$	Defects
3 layers	1 (Batch b)	13.84	0.0059	5000	0.10	None
	2 (Batch a)	13.23	0.0115	4500	0.07	None
	3 (Batch a)	-	-	-	-	
	4 (Batch b)	15.20	0.0170	3200	0.11	None
	5 (Batch b)	15.04	0.0160	3500	0.11	None
	Average	14.33	0.0126	4050	0.0975	

Table 3.4 Continued

	Sample No.	f'_{cu} (ksi)	ϵ_{cu}	E_c (ksi)	$\gamma_{ave.}$	Defects
4 layers	1 (Batch a)	16.30	0.0185	2900	0.07	None
	2 (Batch a)	16.35	0.0185	3300	0.12	None
	3 (Batch b)	15.80	-	5300	-	Pins not removed before testing
	4 (Batch a)	16.40	0.0210	3100	-	No failure
	5 (Batch b)	16.30	0.0180	3700	0.07	No failure
	Average	16.34	0.0190	3250	0.087	

3.2 Analysis of Results

The data was first reduced for the ASTM toe compensation (see Mirmiran 1997a) and the balance loads. Most adjustments were already made by FDOT, and only a few specimens needed further adjustment for the toe compensation. Three aspects of response were studied as follows; stress-strain, volumetric strains, and dilatancy.

Stress .Strain Response

The stress-strain plots for the tested specimens are grouped together by the concrete strength and number of layers. Figures 3.3-3.7 show the stress-strain diagrams for the 3 ksi specimens with 1-5 layers, and Figures 3.8-3.11 show the stress-strain diagrams for the 6 ksi specimens with 1-4 layers. Each plot shows the axial stress versus axial and radial strains. Radial strains are negative (tensile). Results for multiple samples are shown on each graph for comparison. The average stressstrain curves are plotted in Figures 3.12 and 3.13 for the 3 ksi and 6 ksi specimens, respectively. The response is generally bilinear, although more curvilinear than the response of glass-wrapped concrete. The first slope generally follows the modulus of elasticity of unconfined concrete, while the second slope depends on the number of layers and the stiffness ofthe jacket. The transition zone between the two slopes is indicative of FRP jacket taking the role of dilation restraint for the concrete core..

Volumetric Strains

Axial stress versus change in volume curves are grouped together by the concrete strength and number of layers. Figures 3.14-3.18 show the volumetric curves for the 3 ksi specimens with 1-5 layers, and Figures 3.19-3.22 show the response for the 6 ksi specimens with 1-4 layers. The average volumetric curves are plotted in Figures 3.23 and 3.24 for the 3 ksi and 6 ksi specimens, respectively. In each figure, the horizontal axis represents the change in volume per unit volume of concrete core. This can be calculated as the sum of axial and lateral (radial) strains as below:

$$\frac{\Delta V}{V} = \varepsilon_v = \varepsilon_1 + \varepsilon_2 + \varepsilon_3 = \varepsilon_1 + 2\varepsilon_r \qquad (3.1)$$

where E_v = volumetric strain, E_i = axial strain, and $E,$ = radial strain. Note that radial strains are negative (tensile). As shown in the figures, the 6 ksi specimens behave very similar to the glass wrapped concrete, in that the direction of dilation is reversed as the jacket take's over beyond the critical stage of concrete. However, the 3 ksi specimens do not even show any expansion, as the carbon wrap appears to be stiff enough to restrain any dilation tendency. For both concrete batches, thicker jackets show faster recovery of dilation as well as higher compaction rates.

Dilatancy

Dilation rate of concrete is defined as the tangent Poisson's ratio or the first derivative of the radial-axial strain curves. The experimental dilation rate is calculated for every two consecutive readings as below:

$$\mu_{\exp} = \frac{\Delta\varepsilon_r}{\Delta\varepsilon_l} = \frac{\varepsilon_{rnew} - \varepsilon_{rold}}{\varepsilon_{1new} - \varepsilon_{1old}} \qquad (3.2)$$

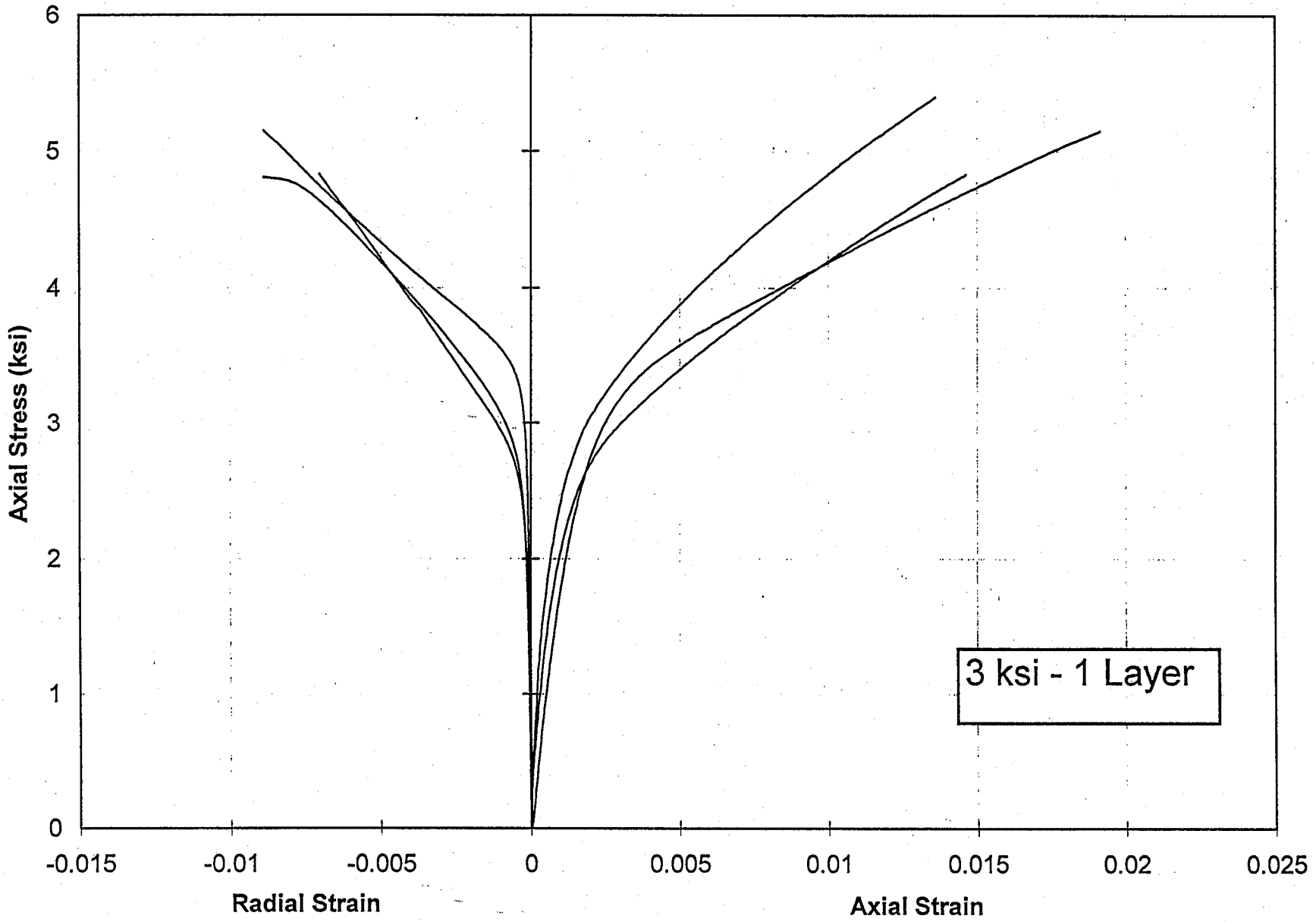

Figure 3.3 Stress-strain curves for the 3 ksi specimens with 1 layer

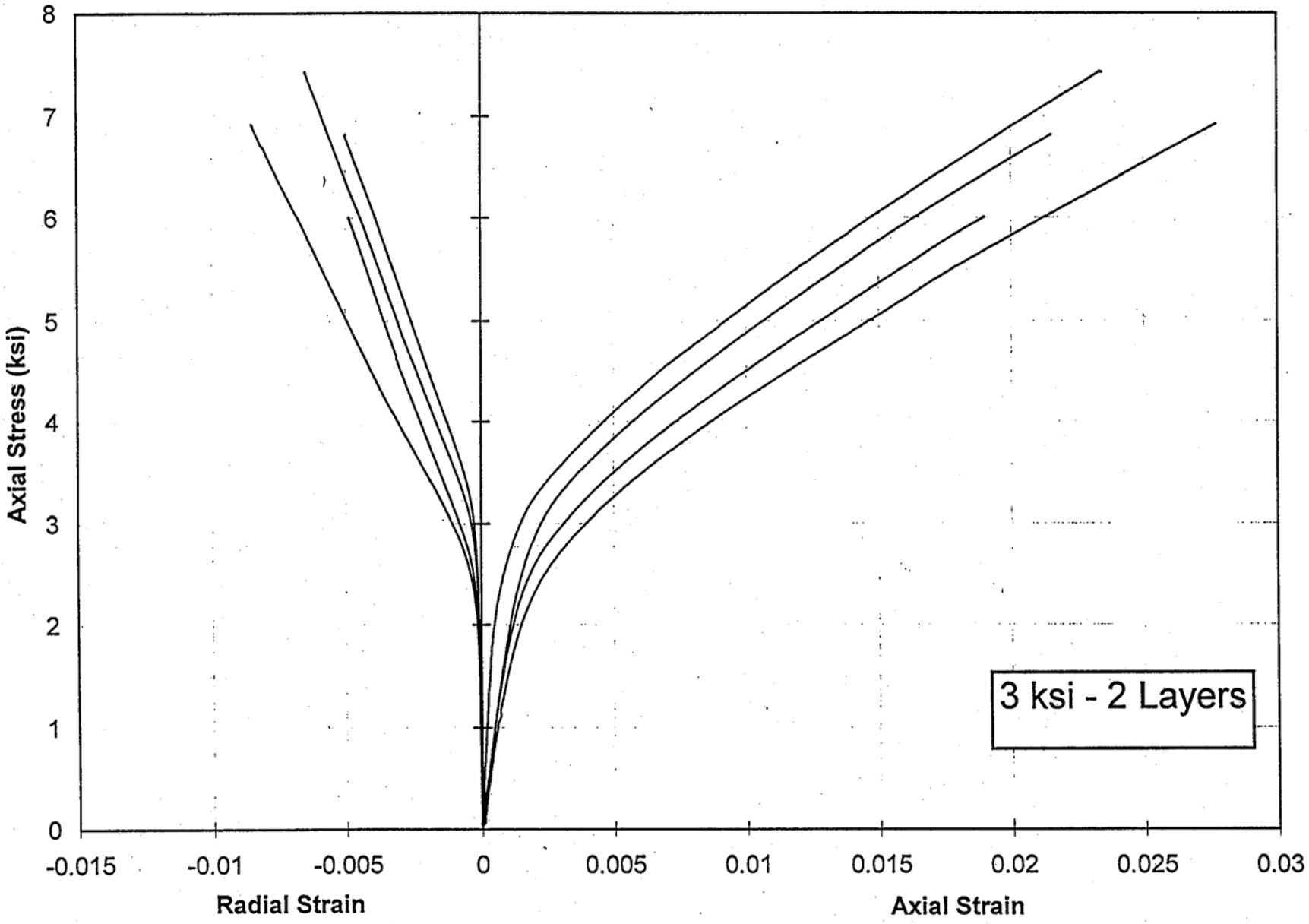

Figure 3.4 Stress-strain curves for the 3 ksi specimens with 2 layers

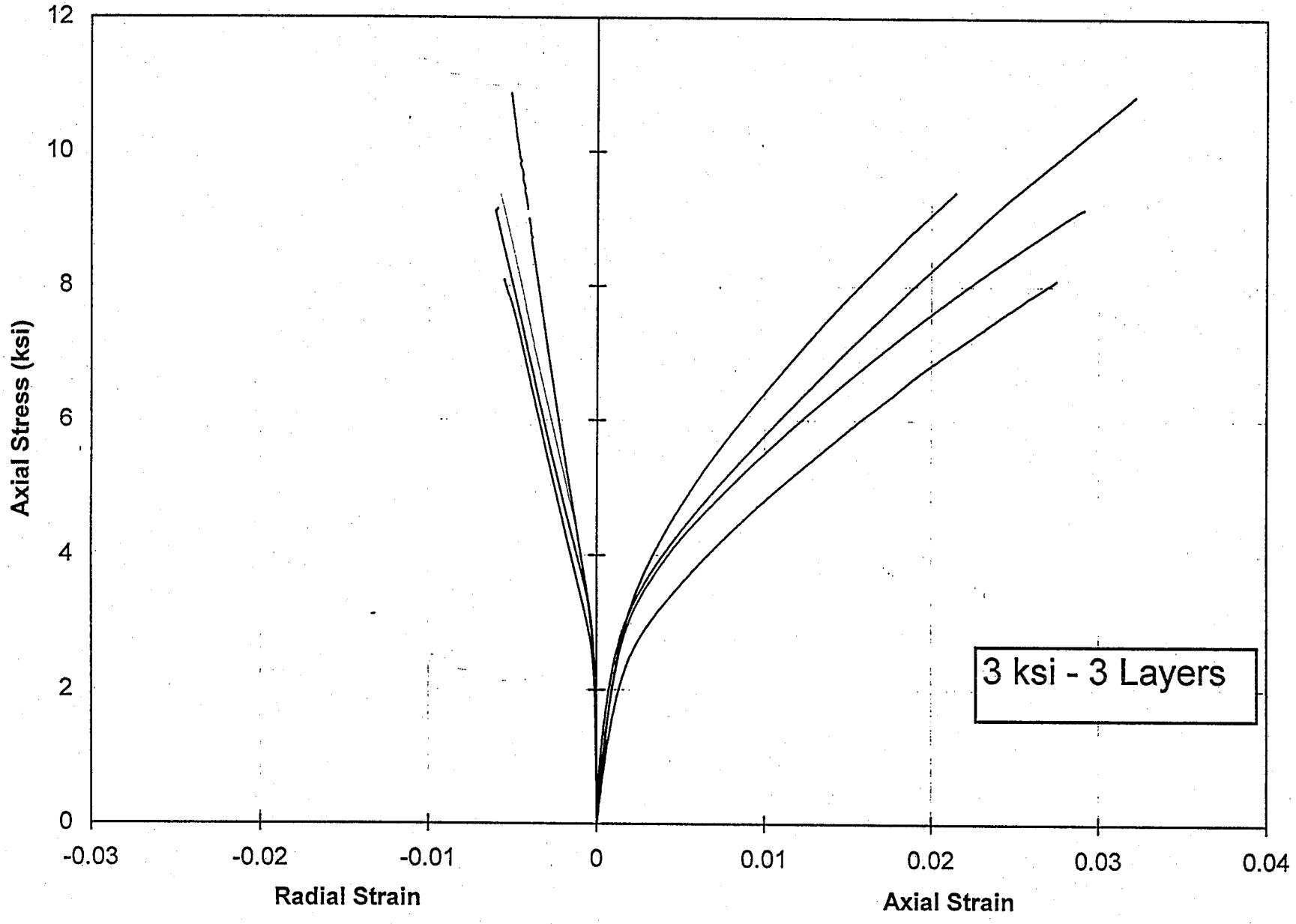

Figure 3.5 Stress-strain curves for the 3 ksi specimens with 3 layers

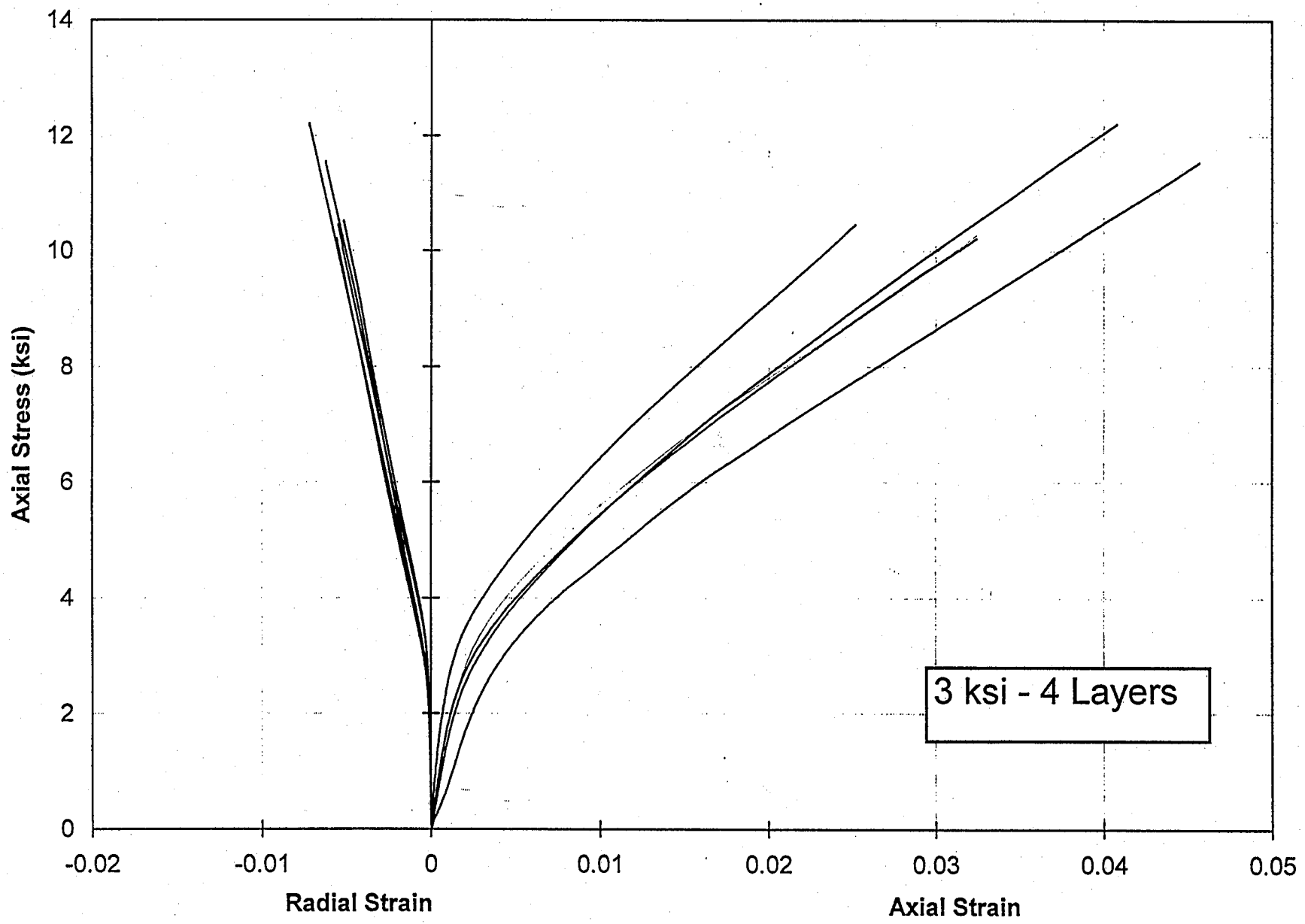

Figure 3.6 Stress-strain curves for the 3 ksi specimens with 4 layers

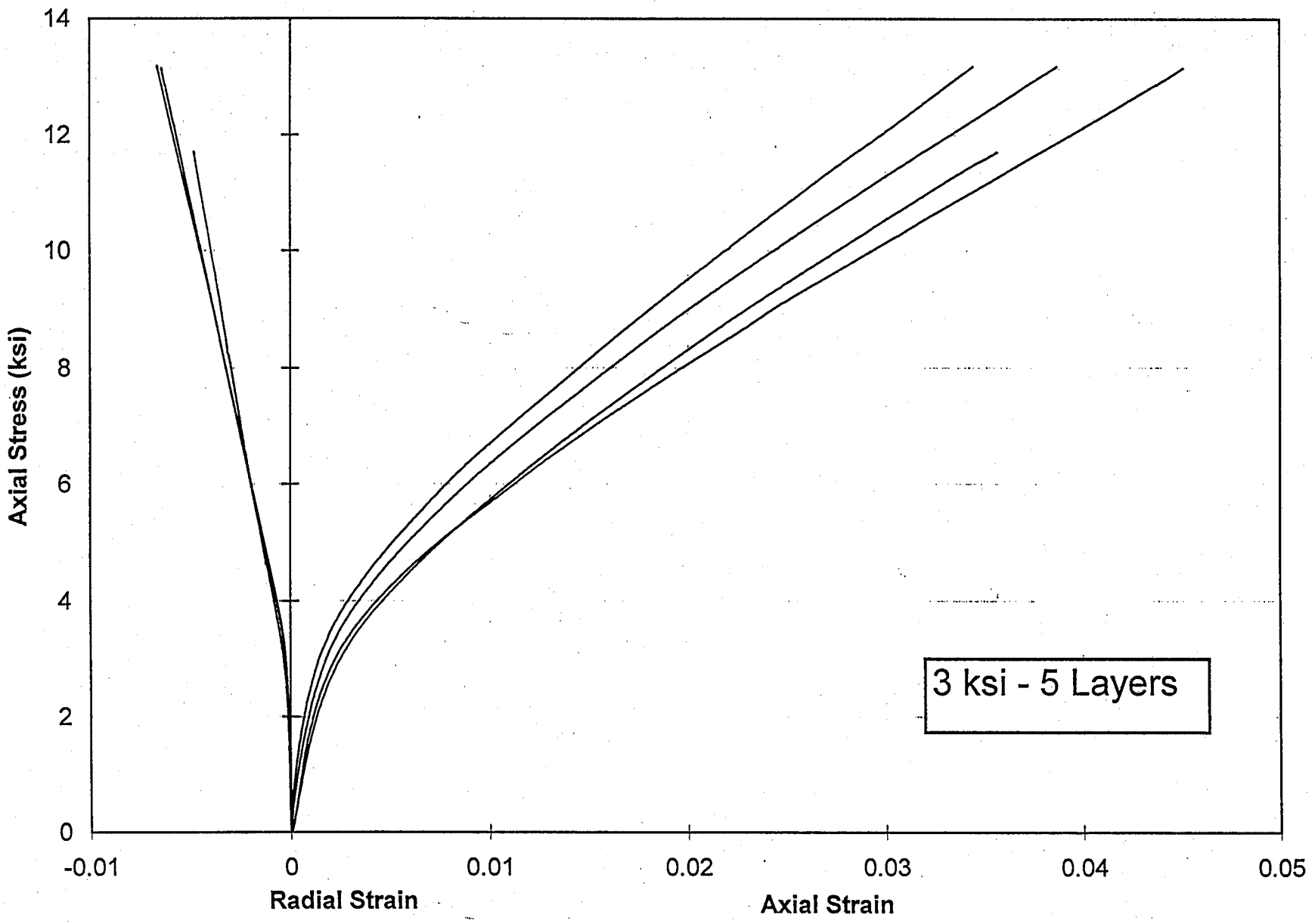

Figure 3.7 Stress-strain curves for the 3 ksi specimens with 5 layers

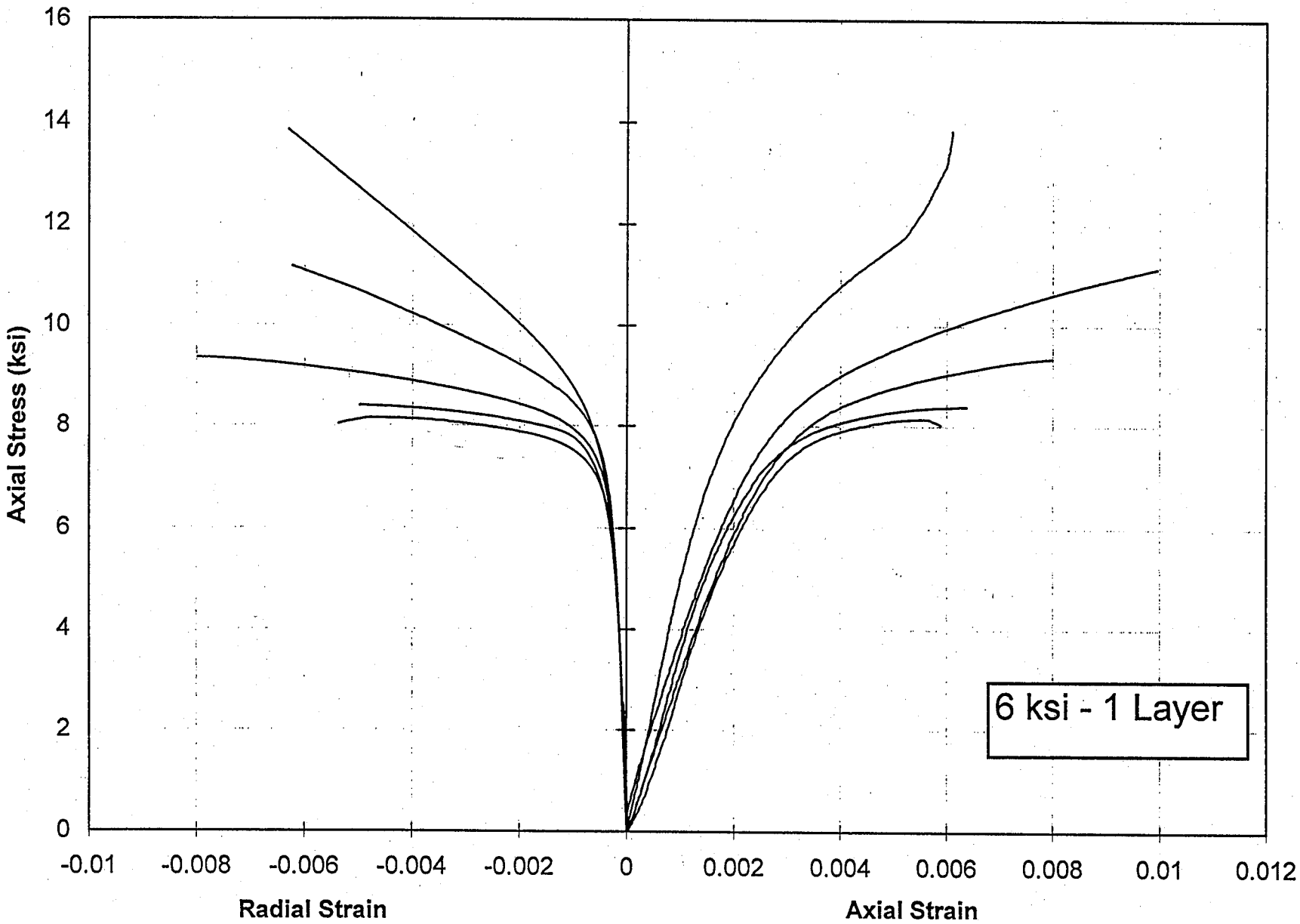

Figure 3.8 Stress-strain curves for the 6 ksi specimens with 1 layer

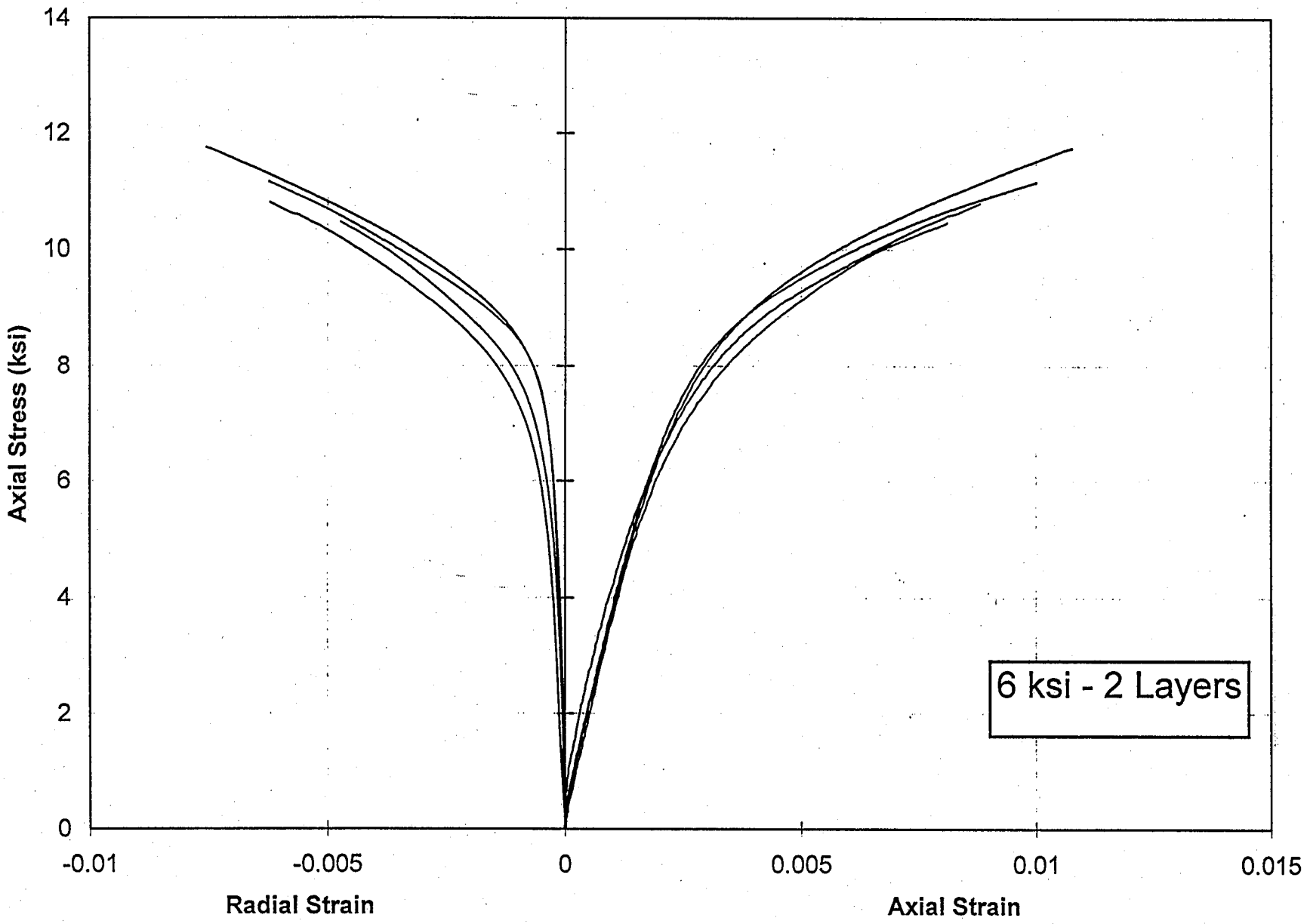

Figure 3.9 Stress-strain curves for the 6 ksi specimens with 2 layers

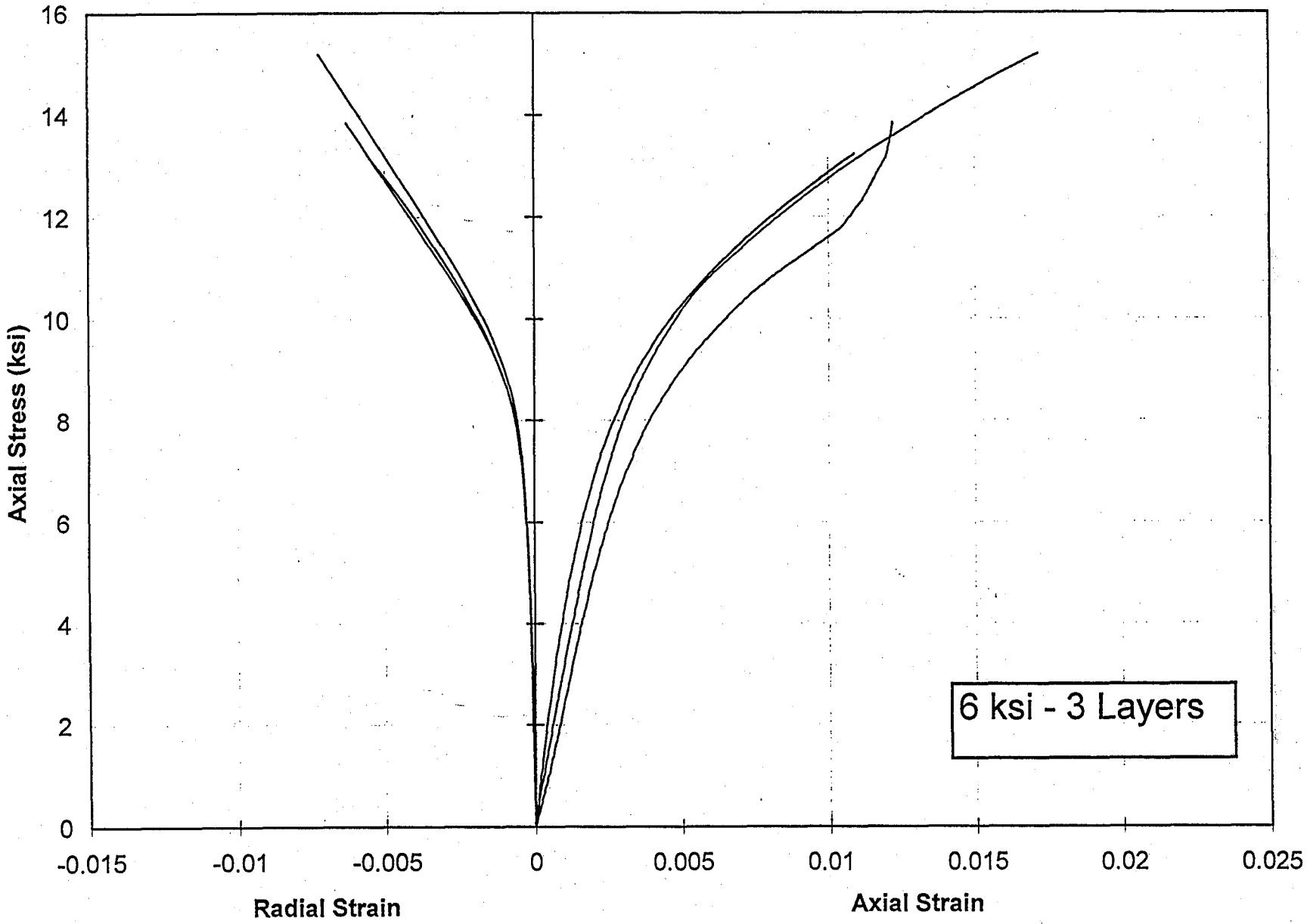

Figure 3.10 Stress-strain curves for the 6 ksi specimens with 3 layers

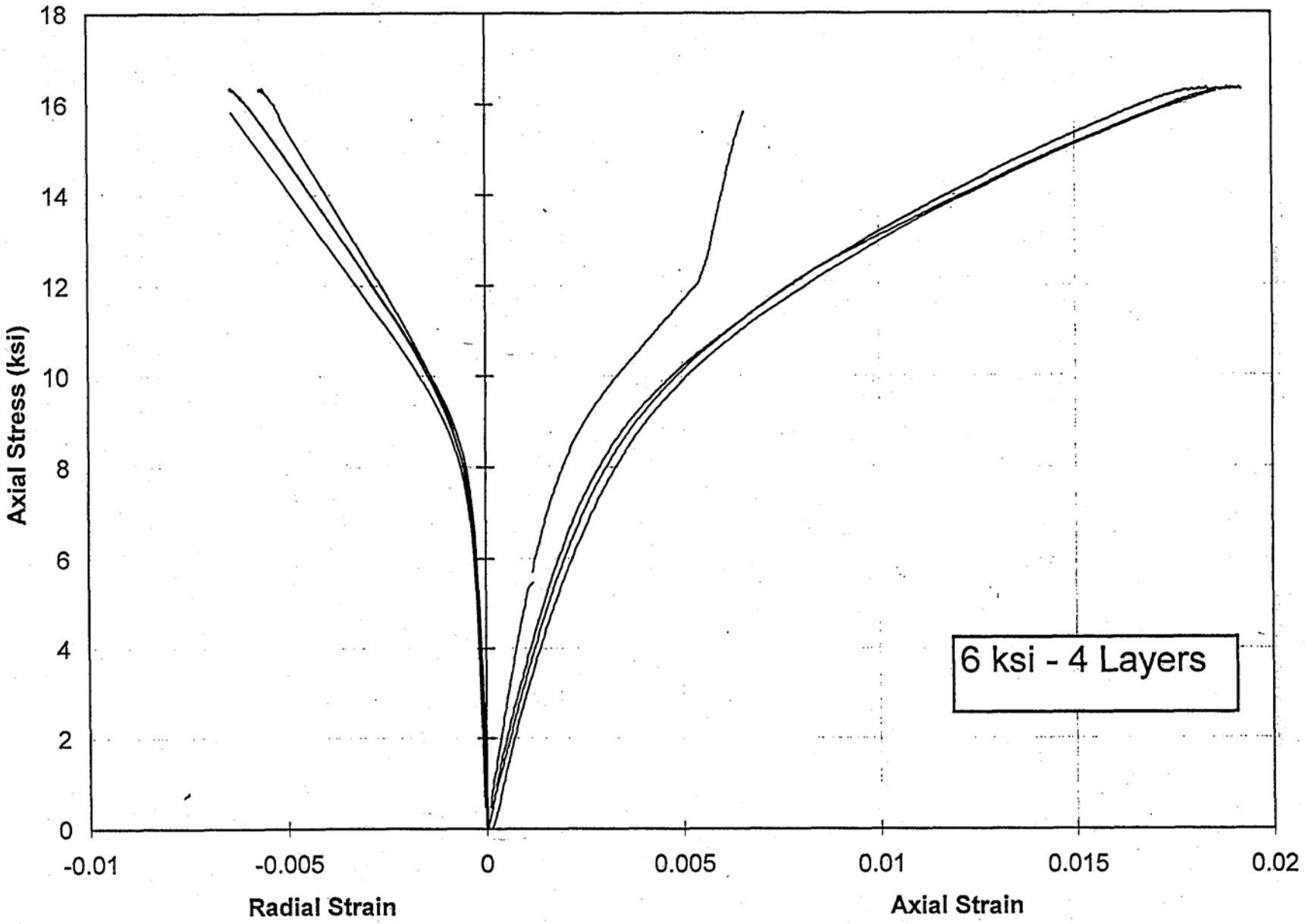

Figure 3.11 Stress-strain curves for the 6 ksi specimens with 4 layers

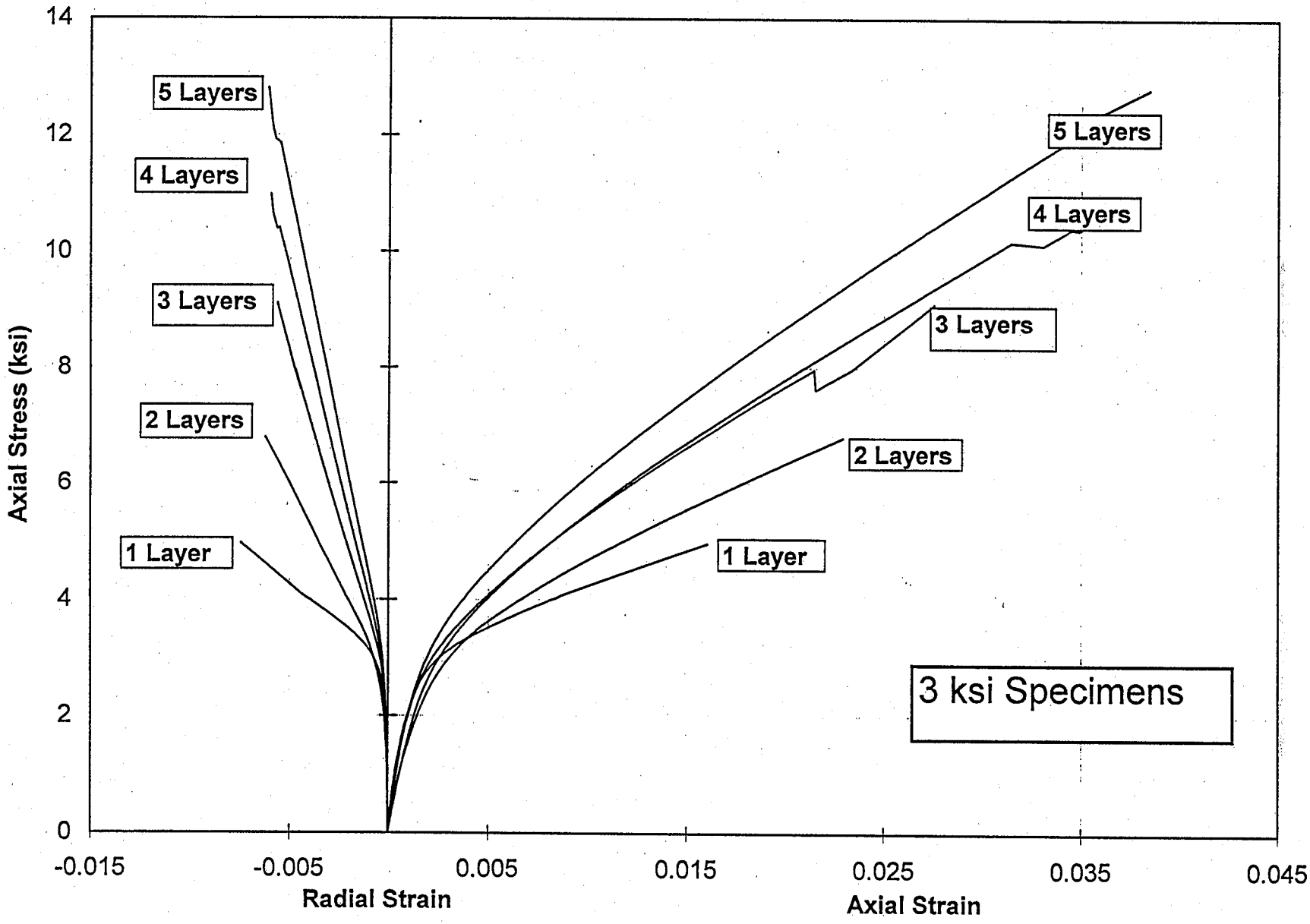

Figure 3.12 Average stress-strain curves for the 3 ksi specimens

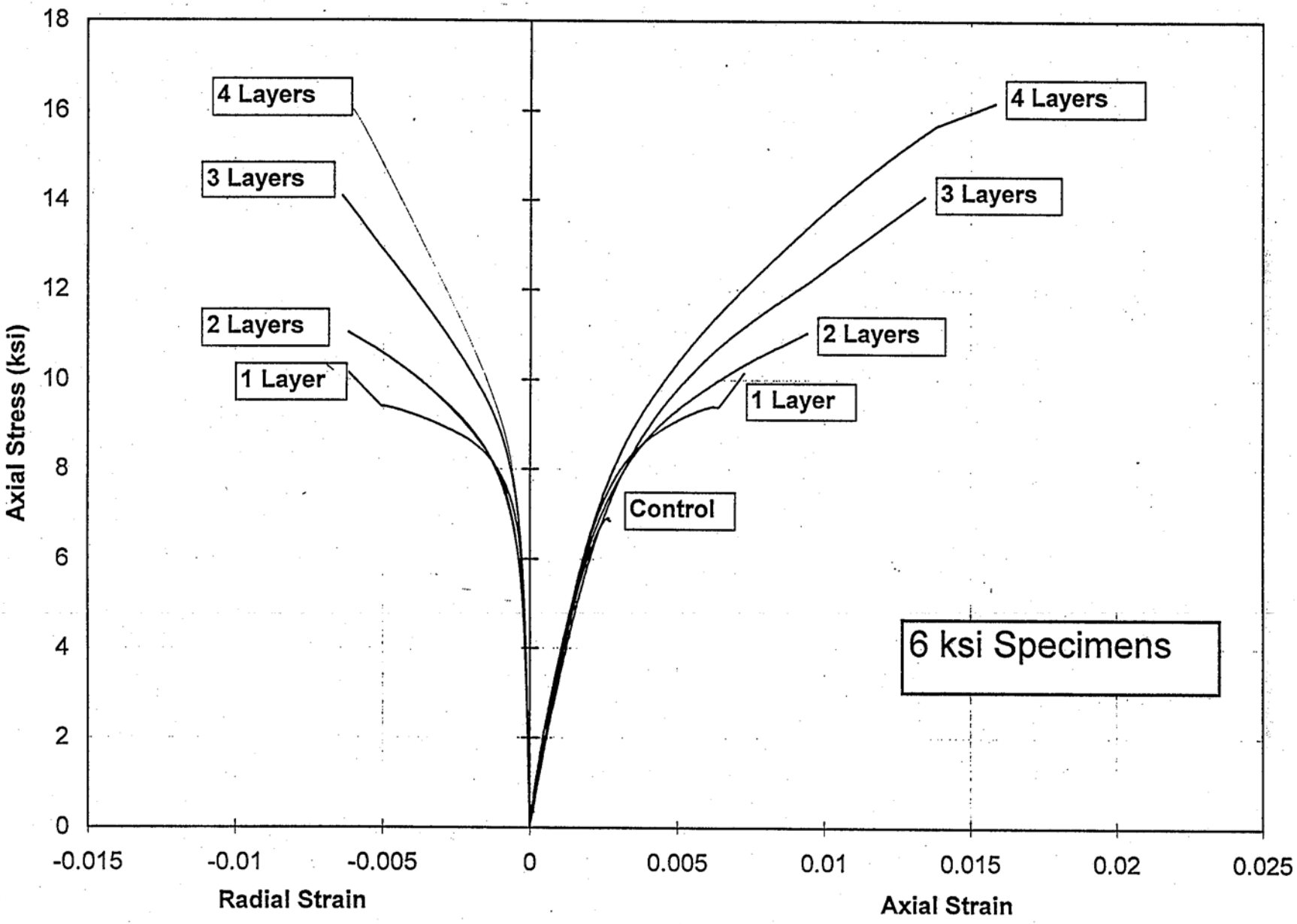

Figure 3.13 Average stress-strain curves for the 6 ksi specimens

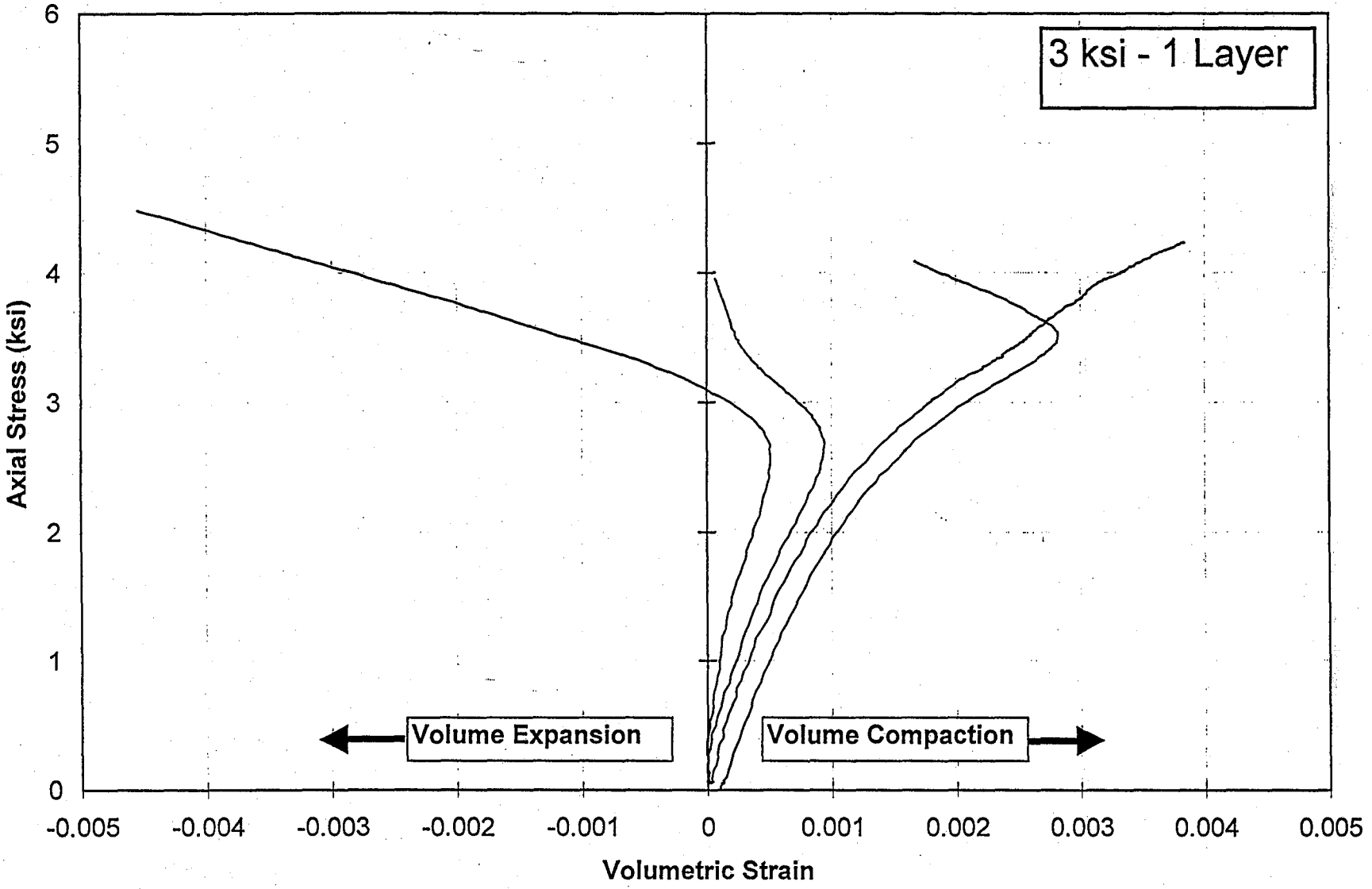

Figure 3.14 Volumetric curves for the 3 ksi specimens with 1 layer

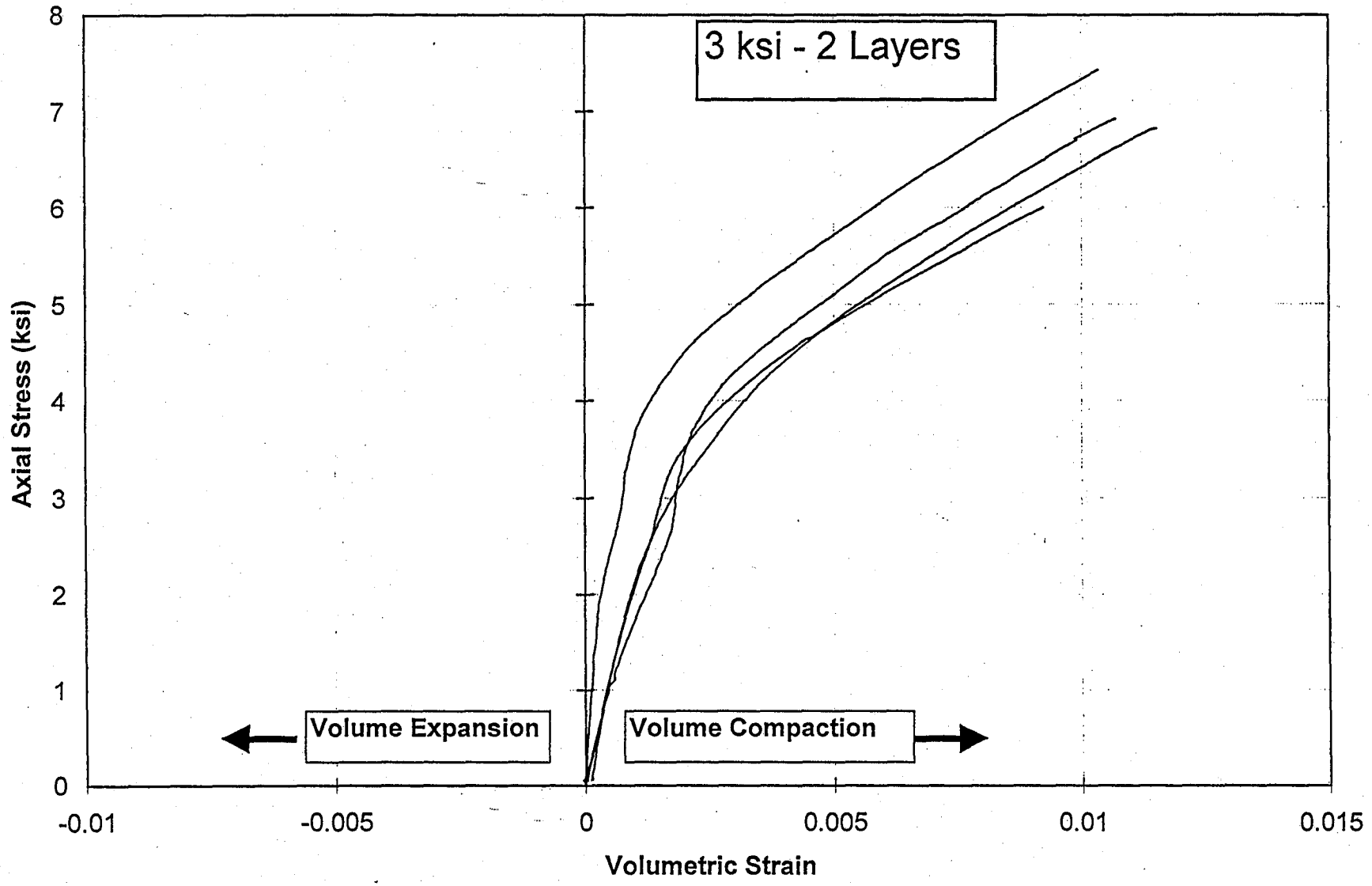

Figure 3.15 Volumetric curves of the 3 ksi specimens with 2 layers

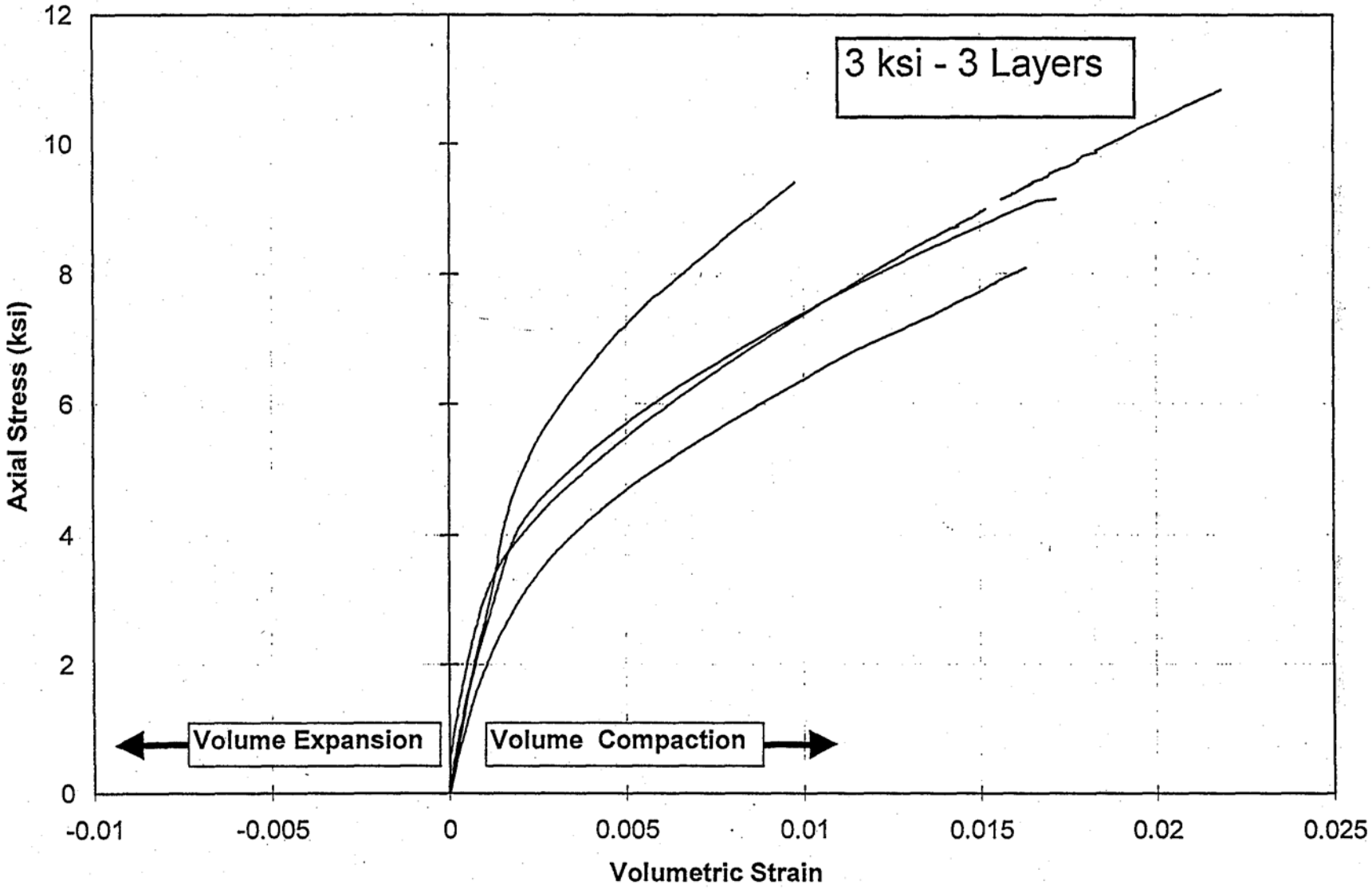

Figure 3.16 Volumetric curves for the 3 ksi specimens with 3 layers

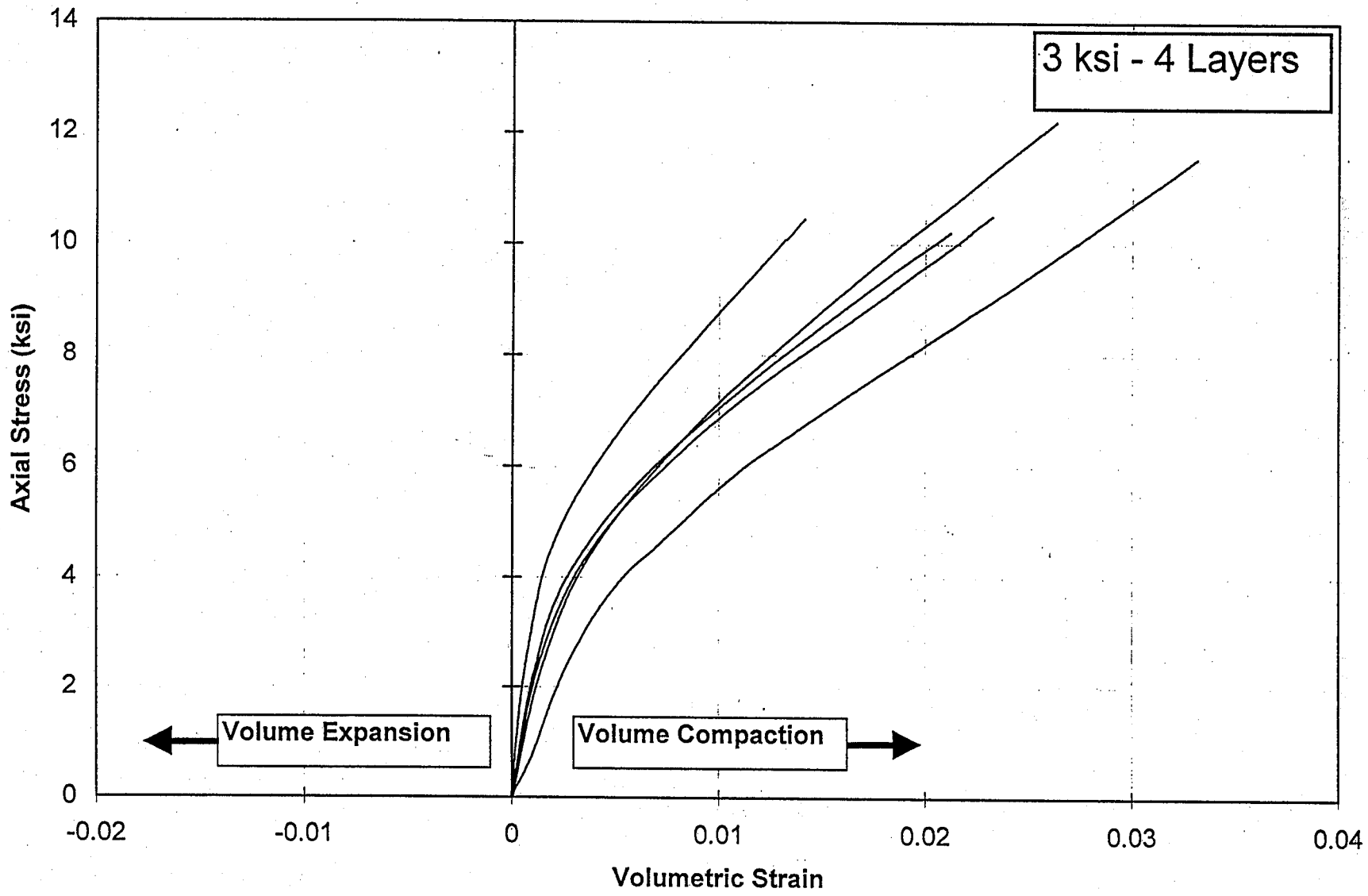

Figure 3.17 Volumetric curves for the 3 ksi specimens with 4 layers

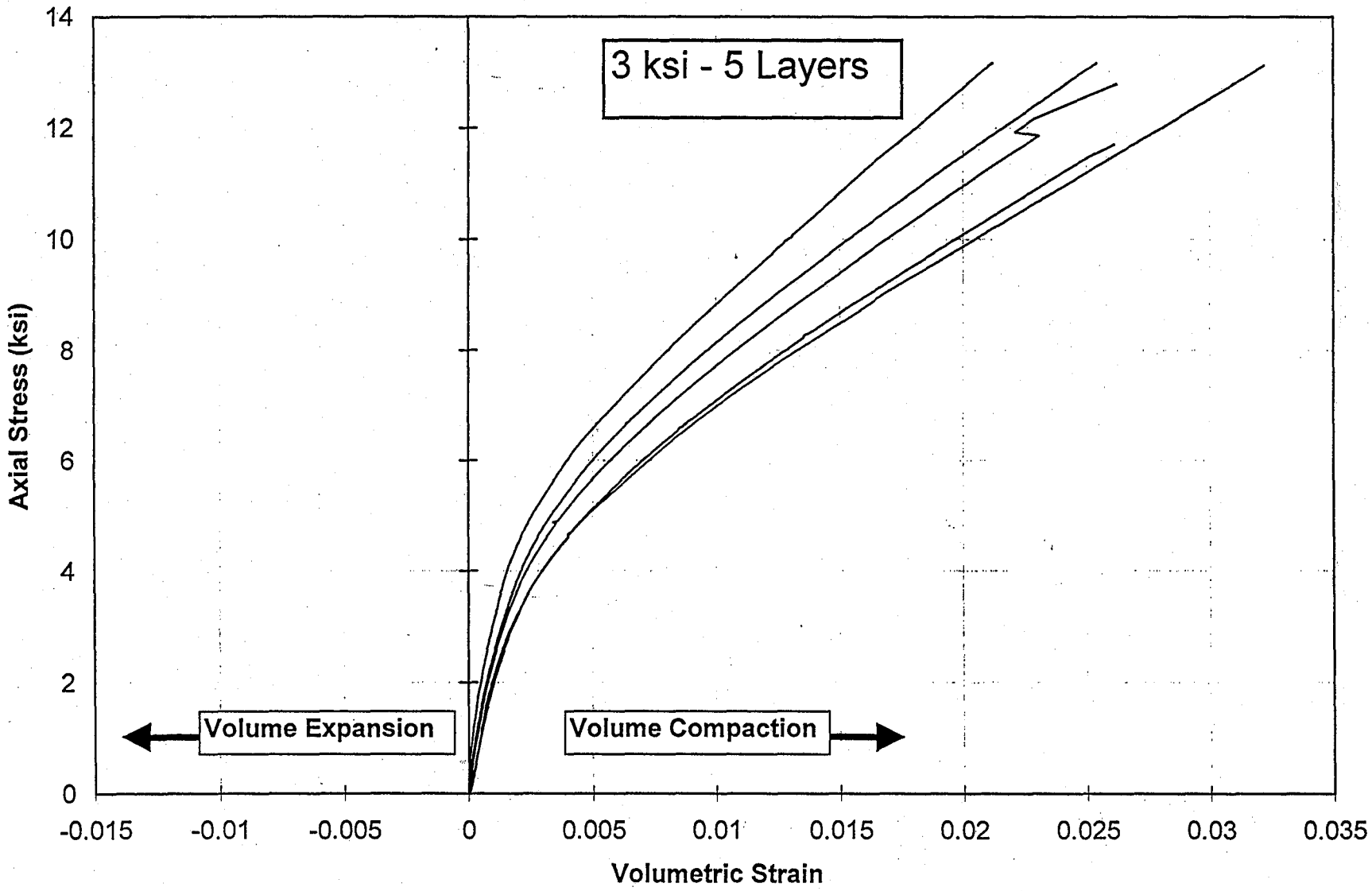

Figure 3.18 Volumetric curves for the 3 ksi specimens with 5 layers

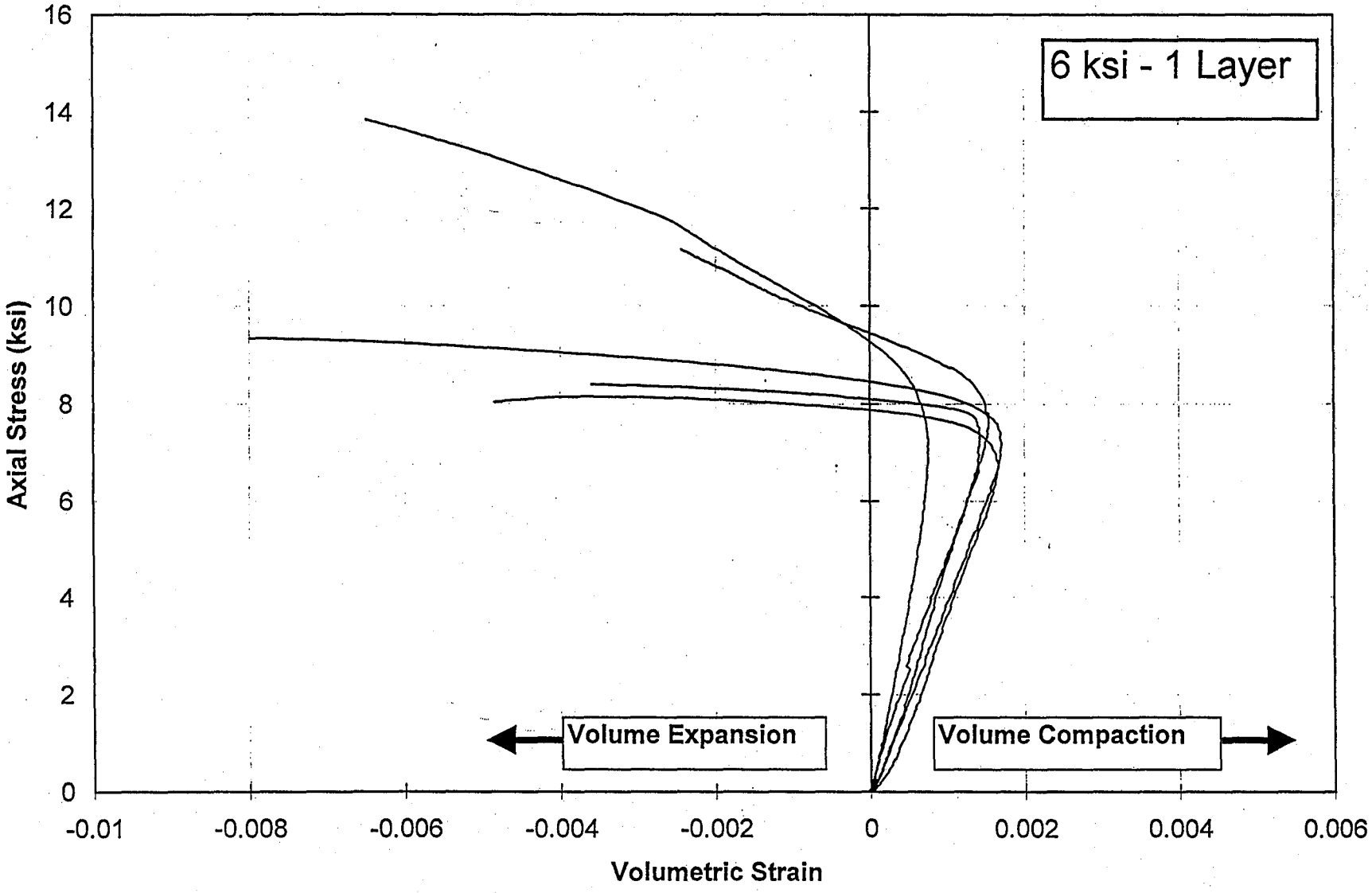

Figure 3.19 Volumetric curves for the 6 ksi specimens with 1 layer

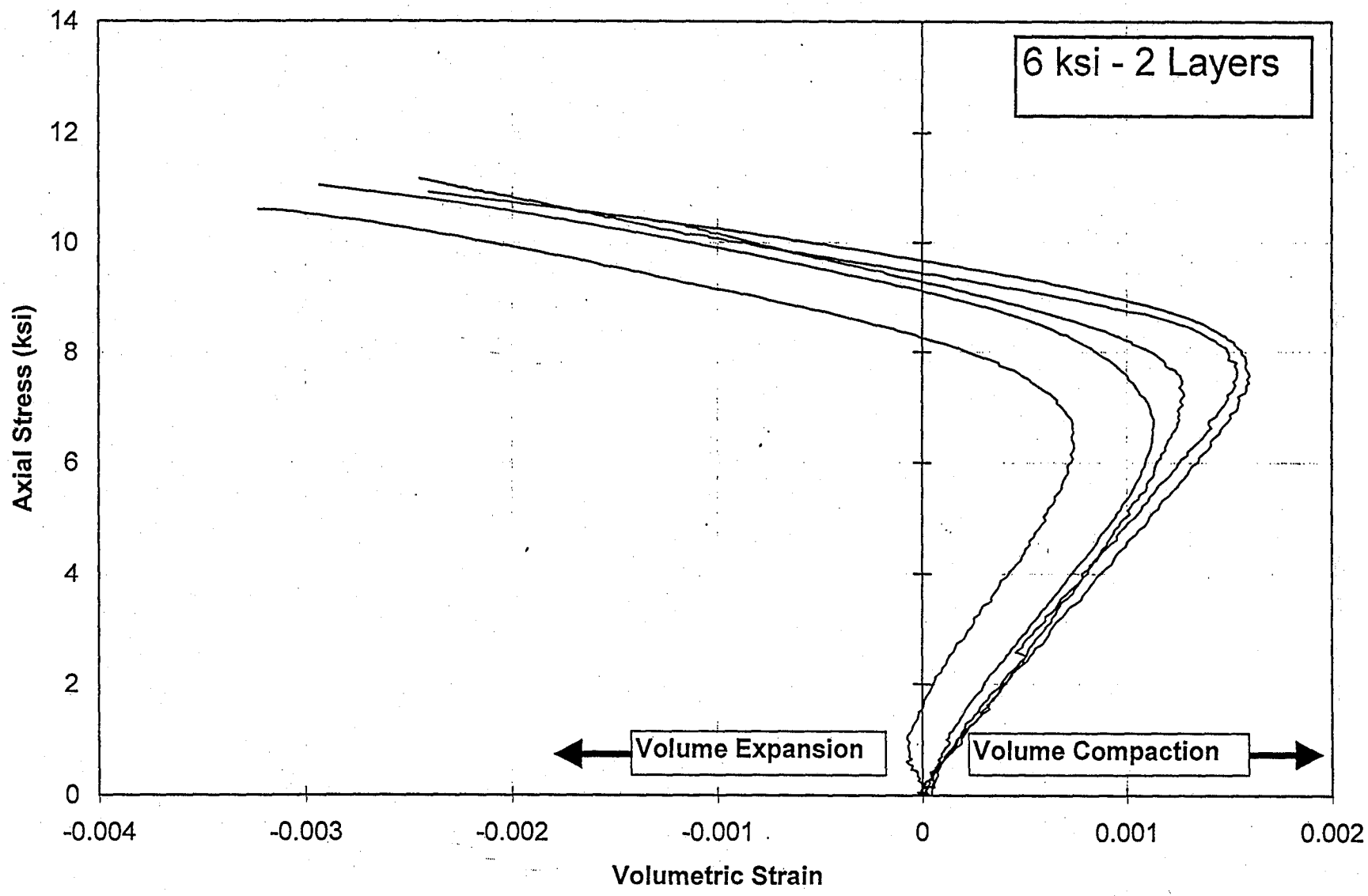

Figure 3.20 Volumetric curves for the 6 ksi specimens with 2 layers

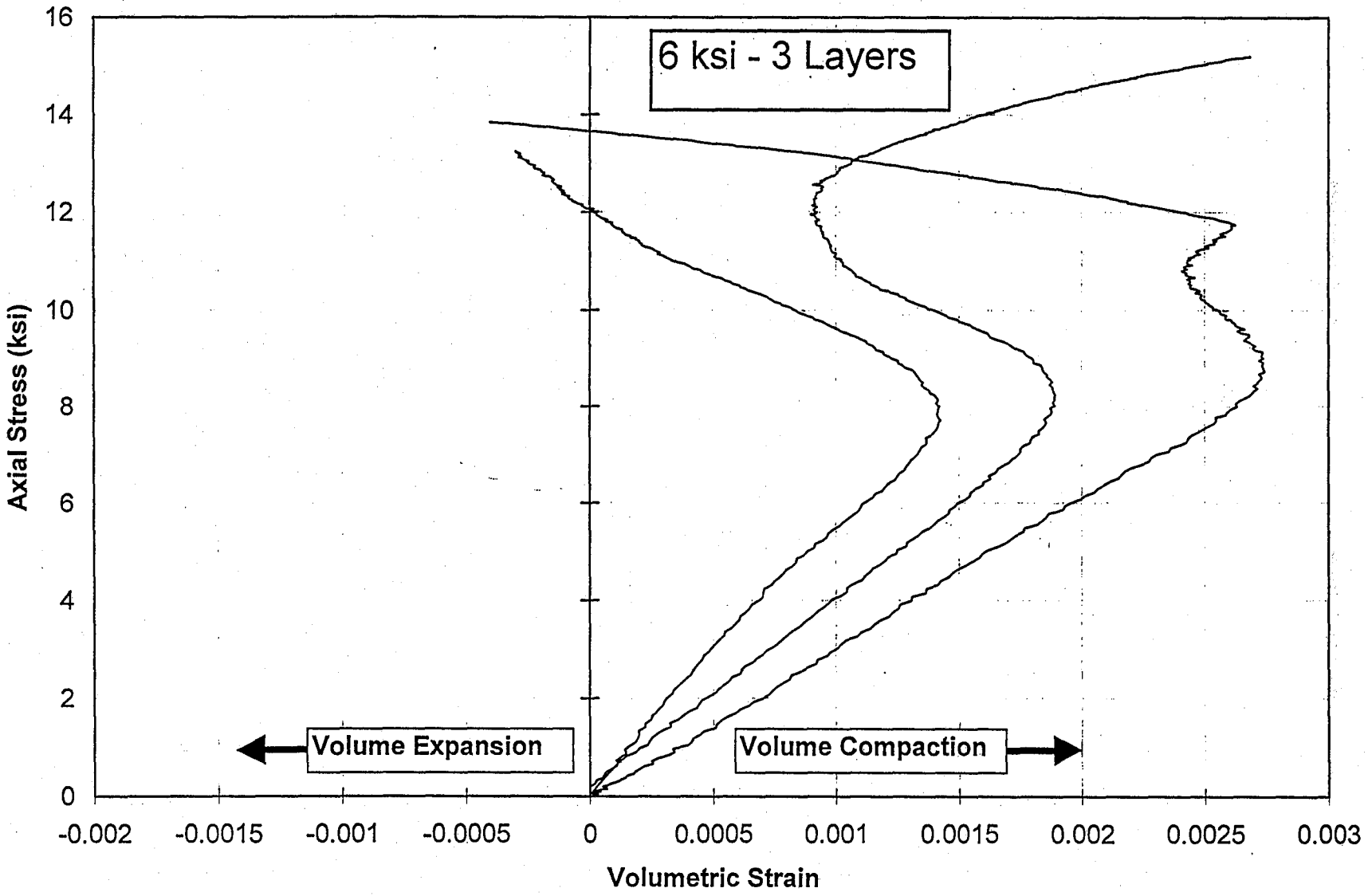

Figure 3.21 Volumetric curves for the 6 ksi specimens with 3 layers

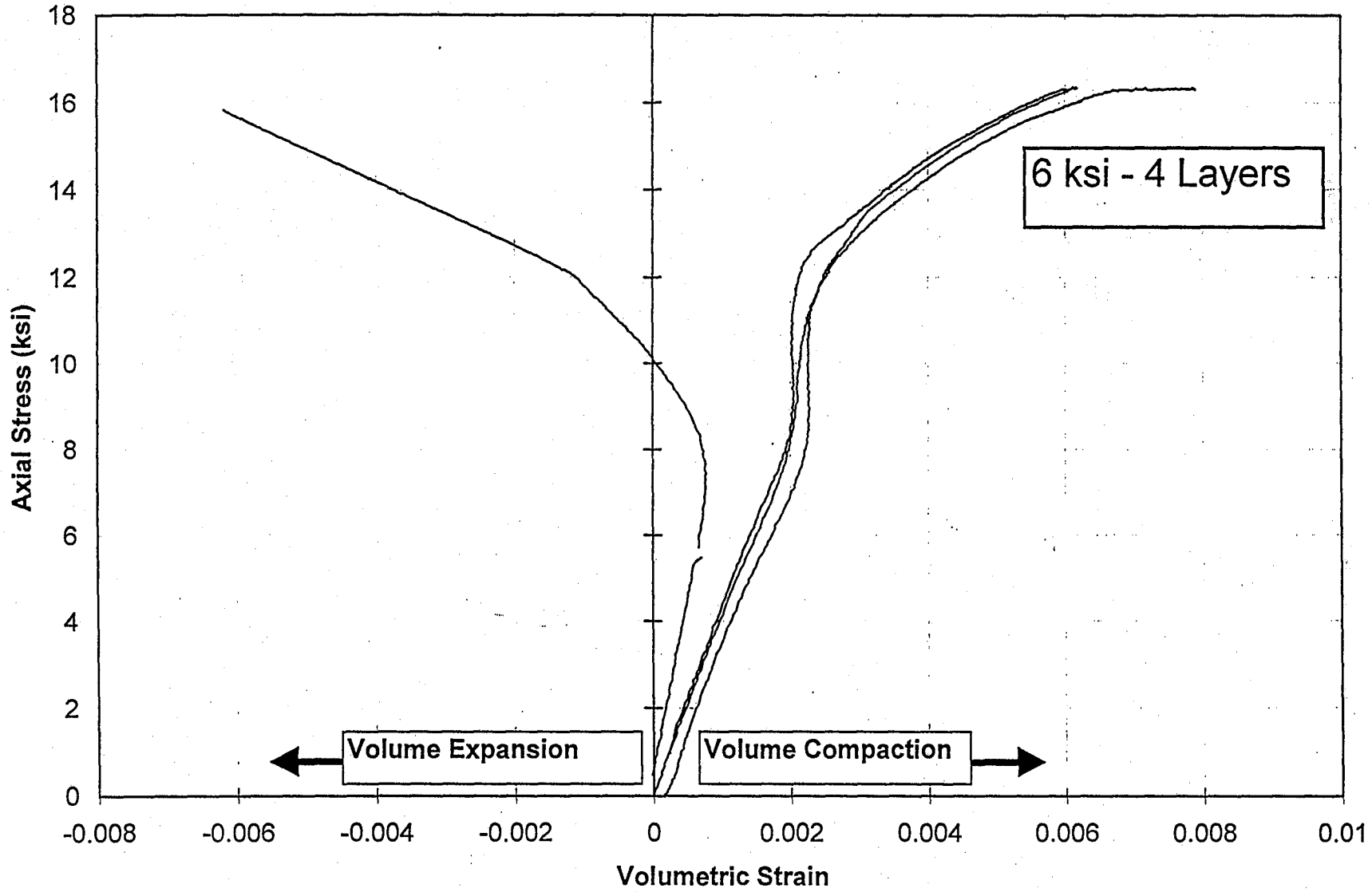

Figure 3.22 Volumetric curves for the 6 ksi specimens with 4 layers

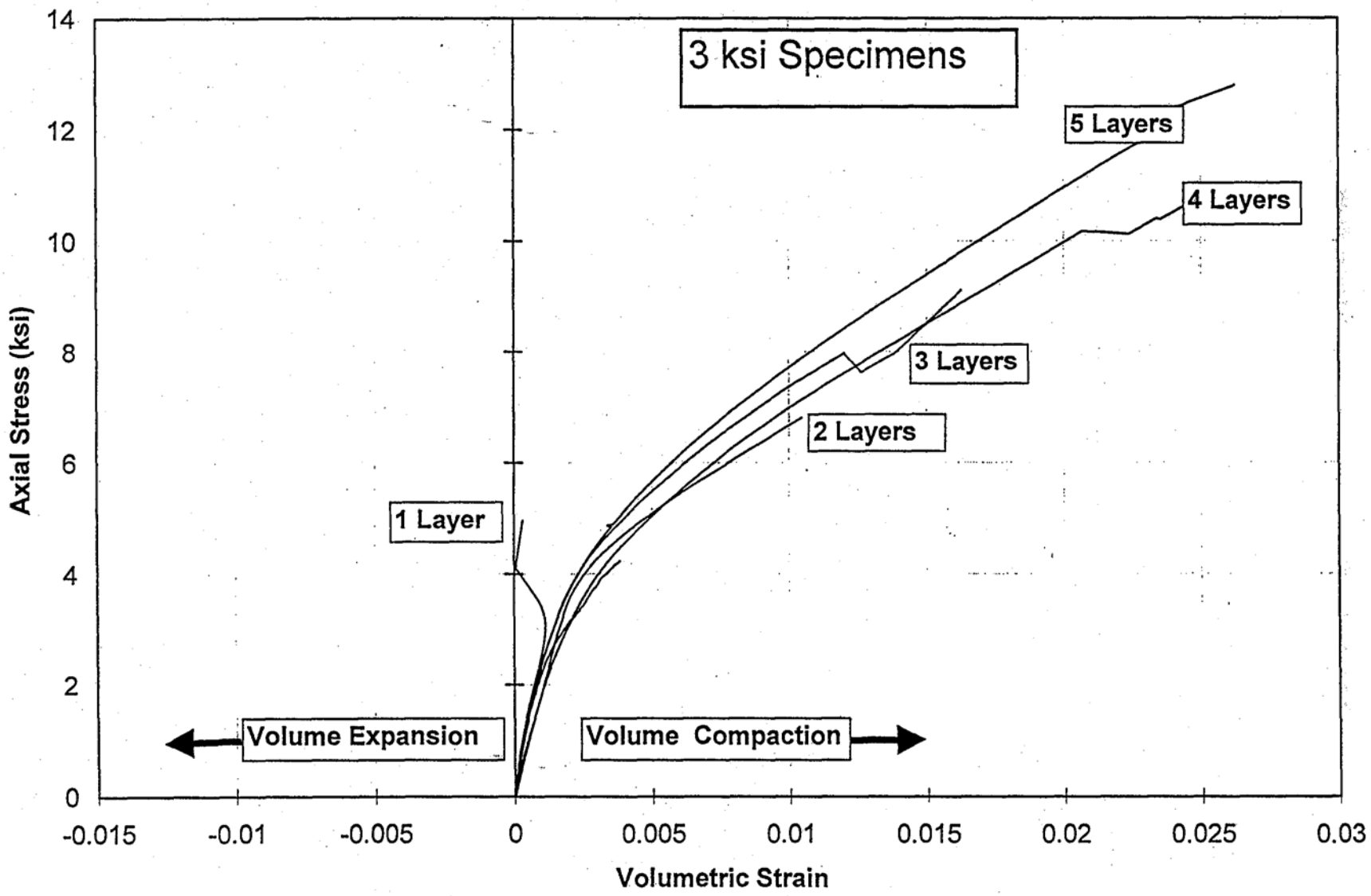

Figure 3.23 Average volumetric curves for the 3 ksi specimens

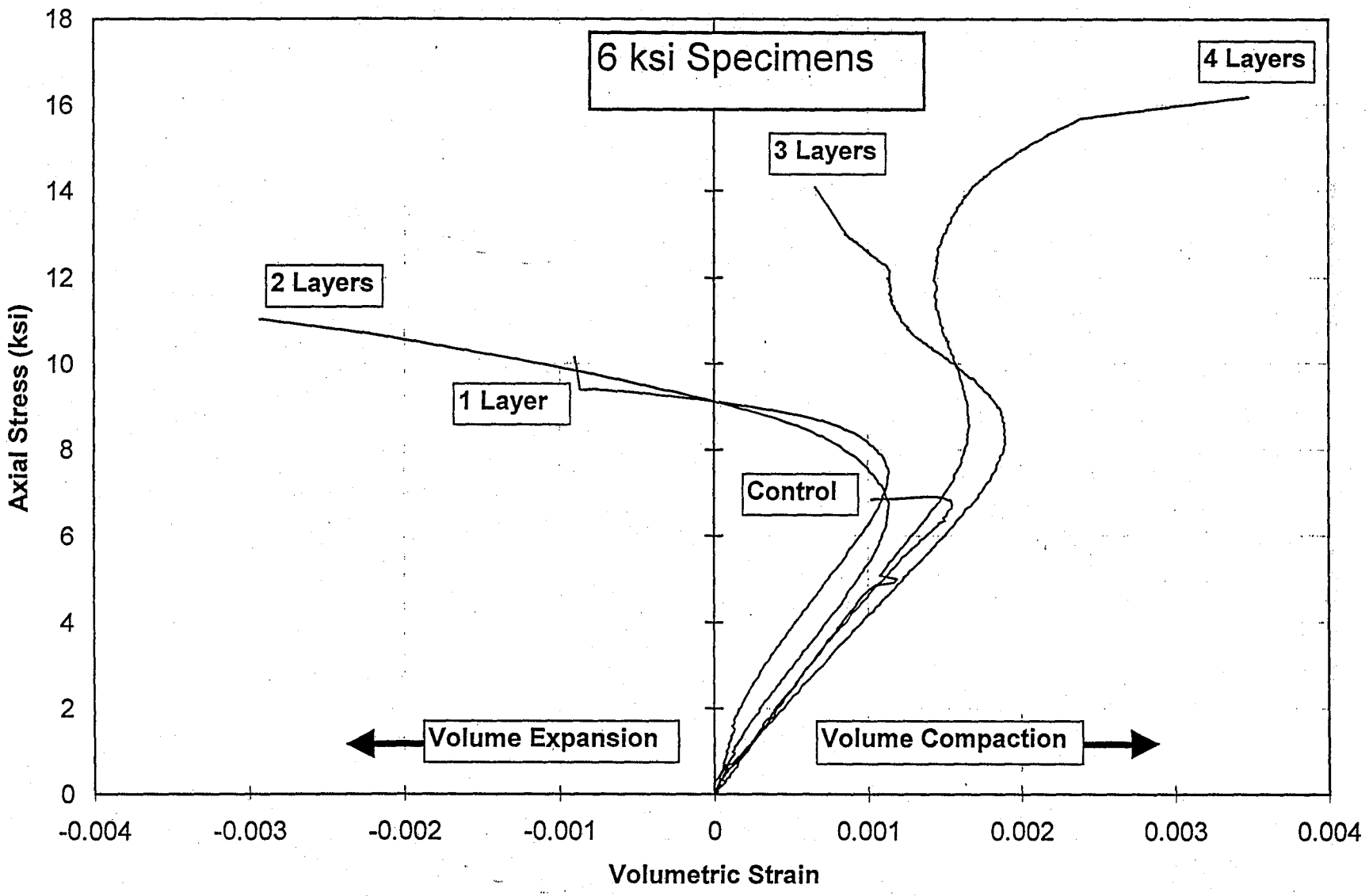

Figure 3.24 Average volumetric curves for the 6 ksi specimens

A typical plot of dilation rate versus axial strain (p.-E,) is shown in Figure 3.25. The scatter or noise observed in the diagram is due to the close readings. A moving average can reduce the noise level in the figure. It was noticed, however, that all dilation curves follow a fractional. form as follows:

$$\mu = \frac{\mu_o + a\varepsilon_1 + b\varepsilon_1^{\,2}}{1 + c\varepsilon_1 + d\varepsilon_1^{\,2}} \qquad (3.3)$$

where $\mu_{.o}$ = initial dilation rate, ϵ_1 = axial strain, and a, b, c, and d are constants. The initial dilation rate (μ_0) is the same as the initial Poisson ratio (v.) which is typically between 0.10 and 0.20. A regression analysis was performed to fit the best fractional curve for each specimen. This was performed via the Microsoft Excel Solver tool by minimizing the sum of the squares of individual errors; i.e., (Test Data - Fitted Data)^{r}. The results are grouped together by the concrete strength and number of layers. Figures 3.26-3.30 show the dilation curves for the 3 ksi specimens with 1-5 layers, and Figures 3.31-3.34 show the dilation curves for the 6 ksi specimens with l-4 layers. The average dilation curves are plotted in Figures 3.35 and 3.36 for the 3 ksi and 6 ksi specimens, respectively. The dilation response of carbon-wrapped concrete appears to be generally the same as that of glass wrapped concrete, with three distinct regions. The first region corresponds to micro-cracking of concrete and rapid increase of lateral expansion. The peak of lateral expansion coincides with the ultimate failure strain of unconfined concrete, signifying that concrete has lain itself completely onto the jacket. At that point, the jacket takes over and consistently reduces the lateral expansion rate, until it stabilizes it at a constant rate just before failure. It appears that generally thinner jackets have higher peak and ultimate dilation rates than do thicker jackets.

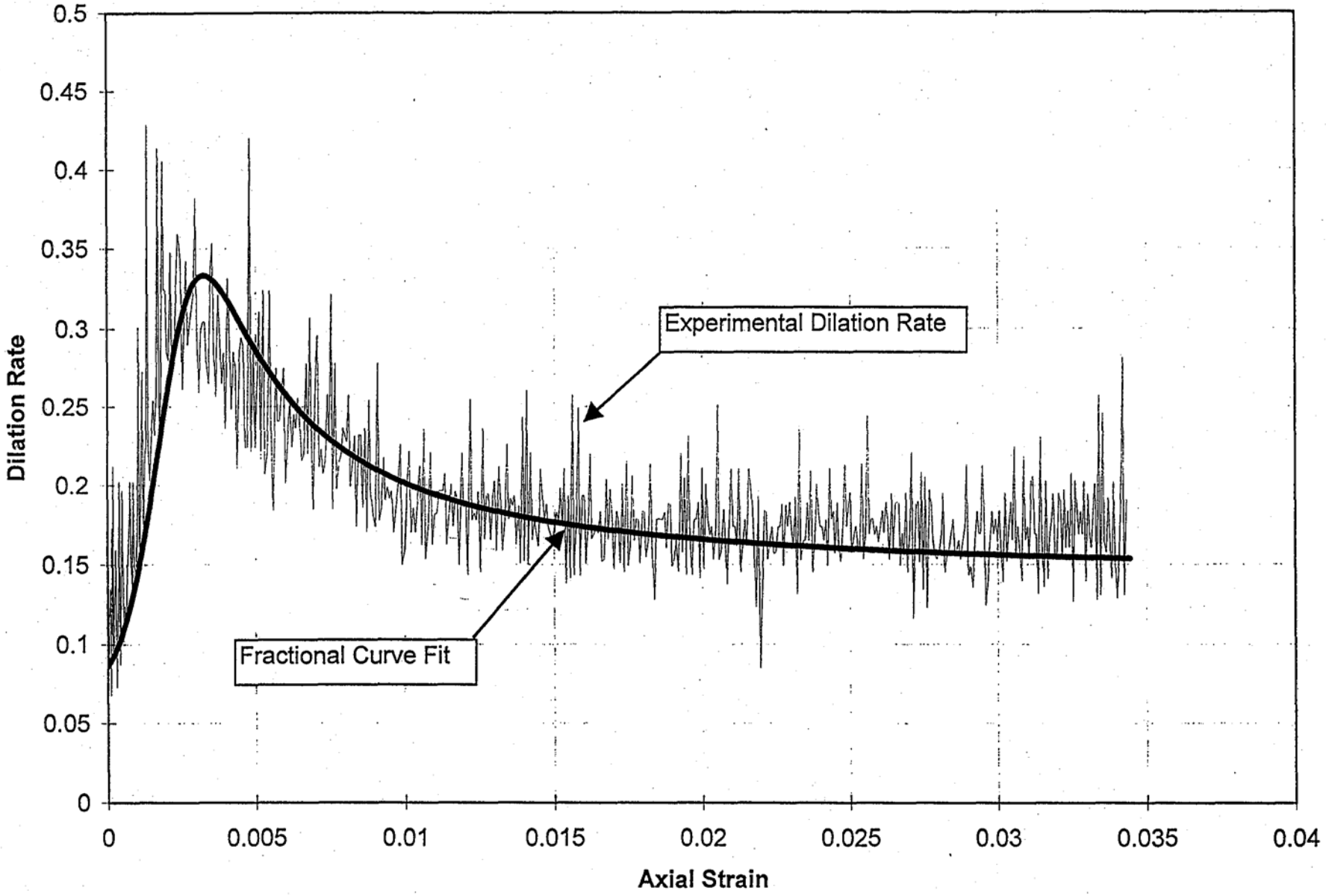

Figure 3.25 Typical dilation response of carbon-wrapped concrete

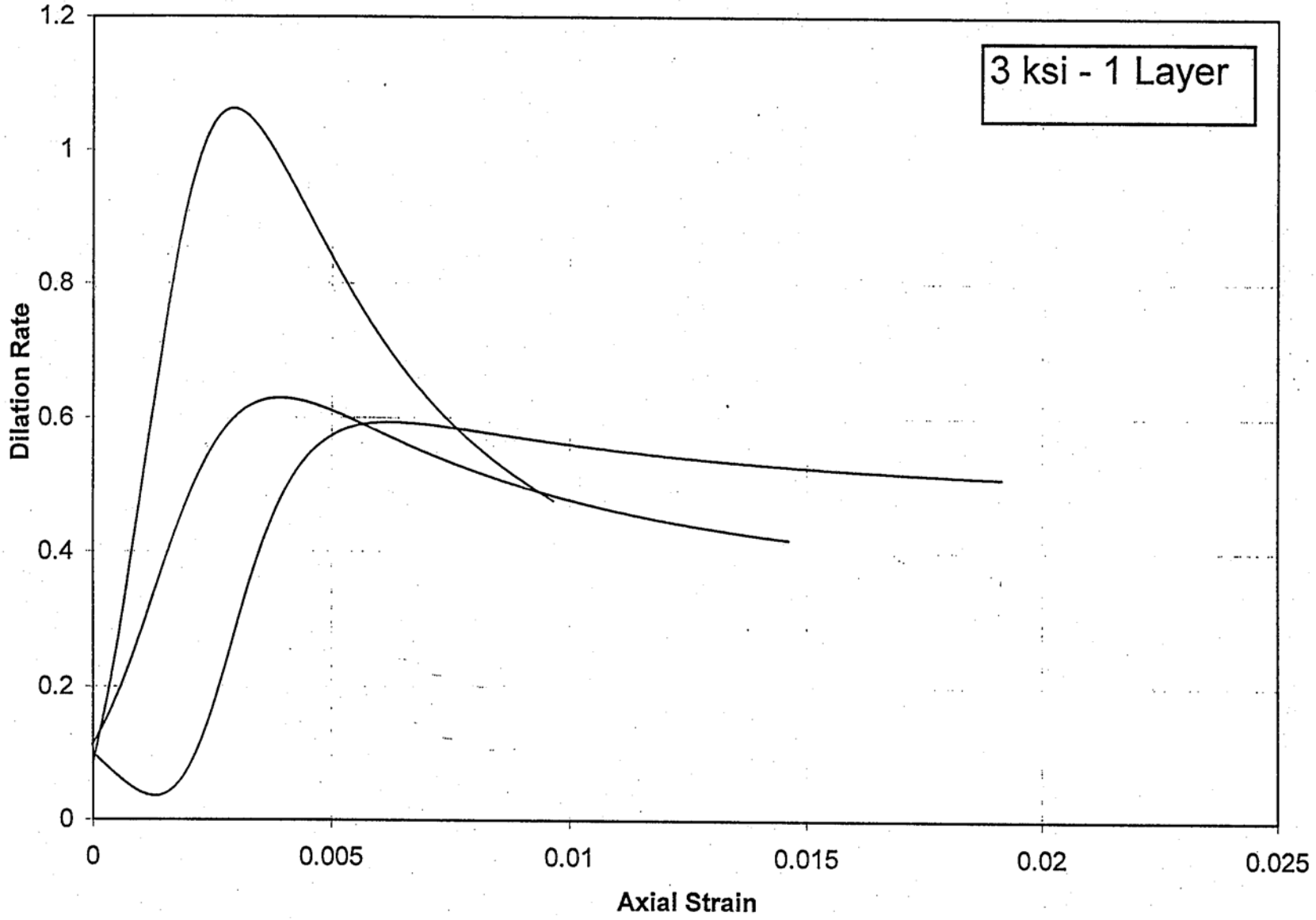

Figure 3.26 Dilation curves for the 3 ksi specimens with 1 layer

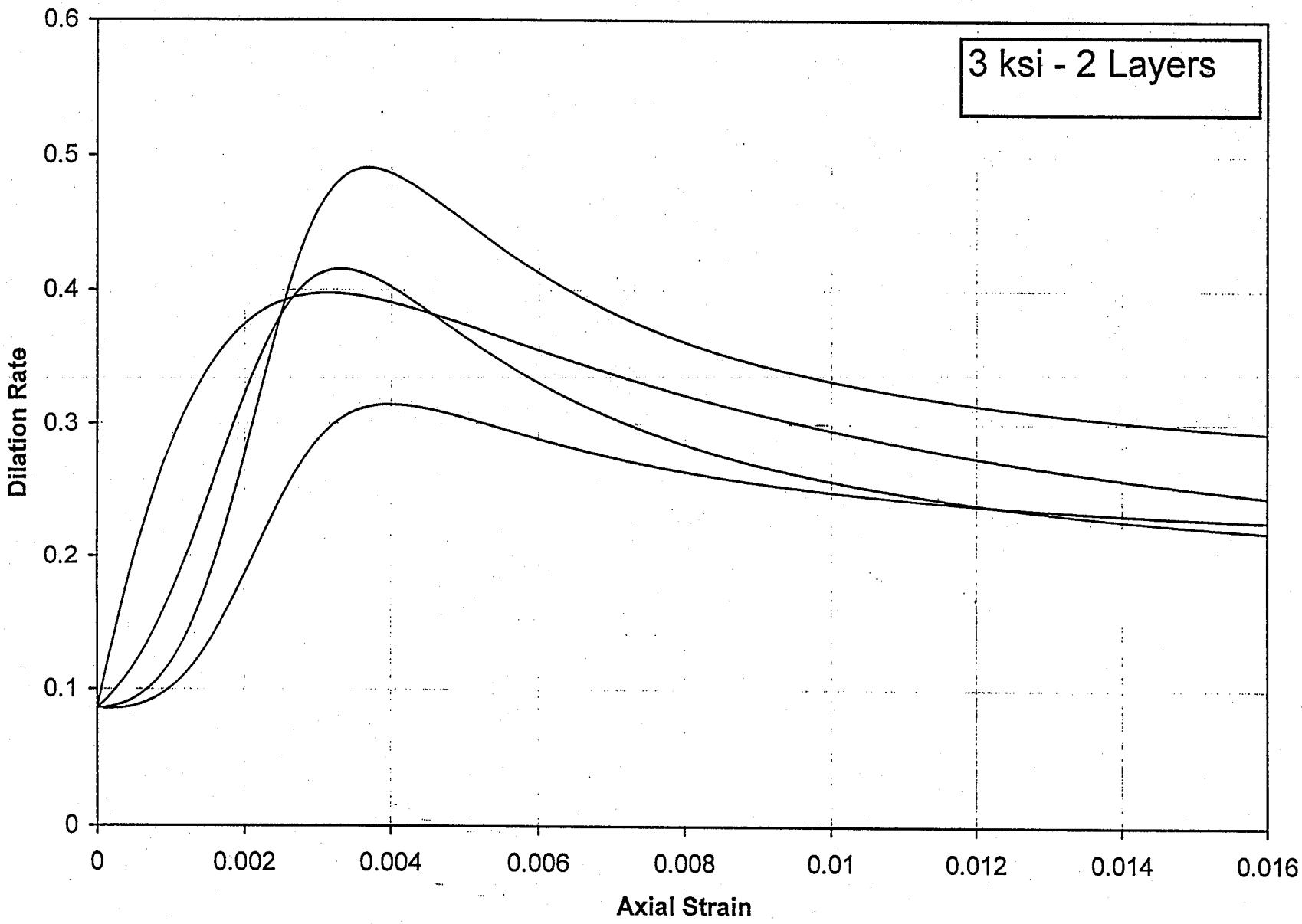

Figure 3.27 Dilation curves for the 3 ksi specimens with 2 layers

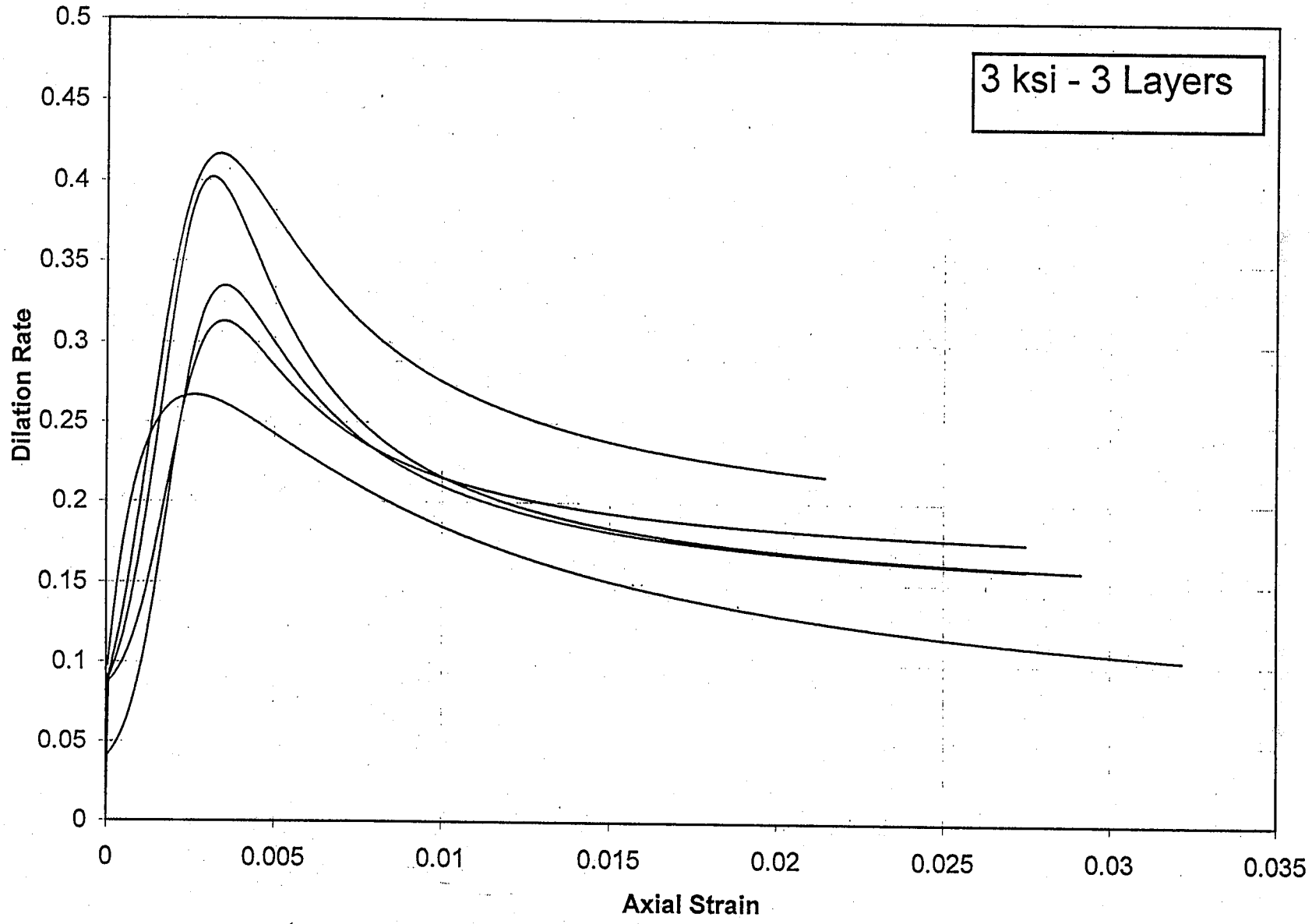

Figure 3.28 Dilation curves for the 3 ksi specimens with 3 layers

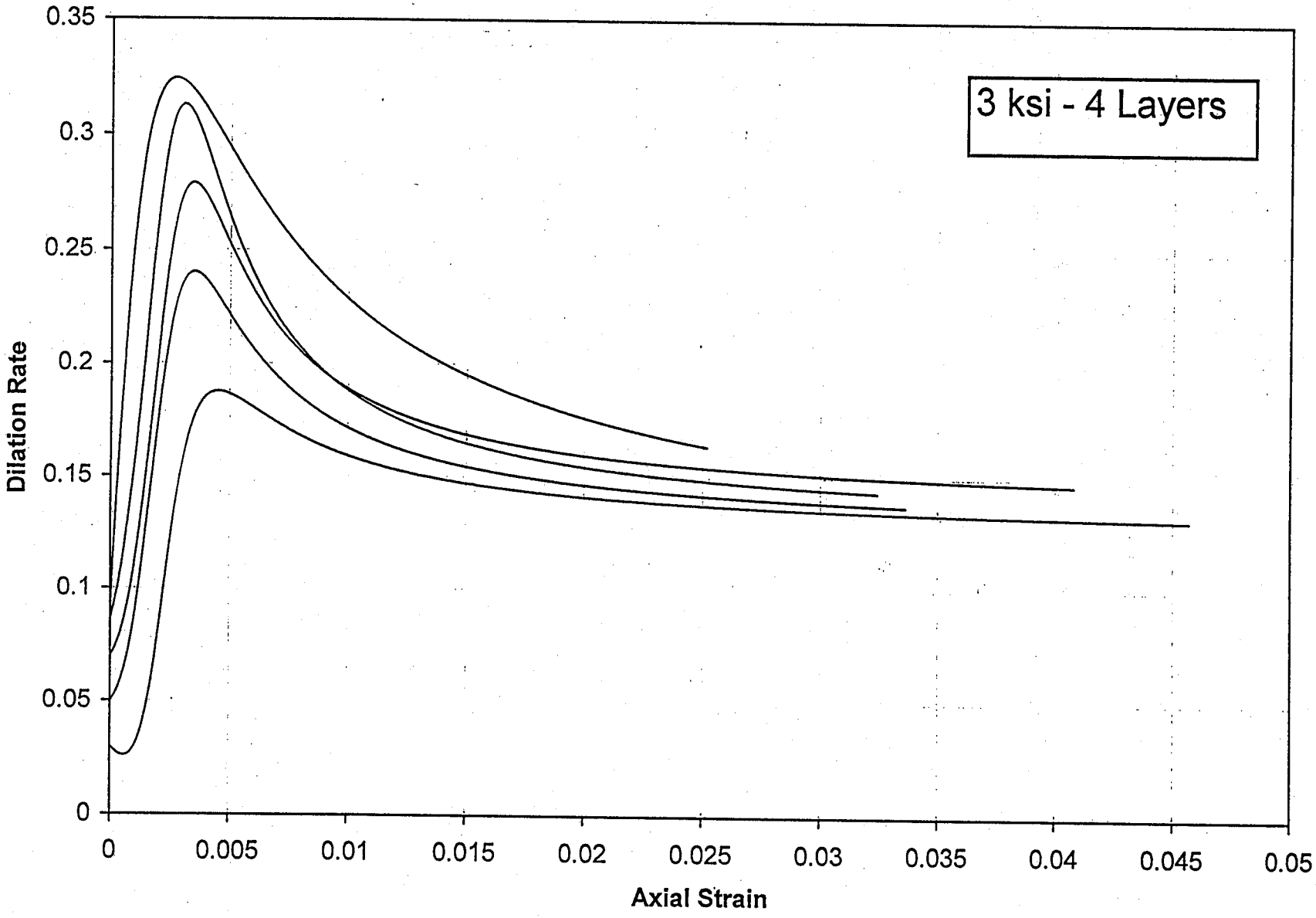

Figure 3.29 Dilation curves for the 3 ksi specimens with 4 layers

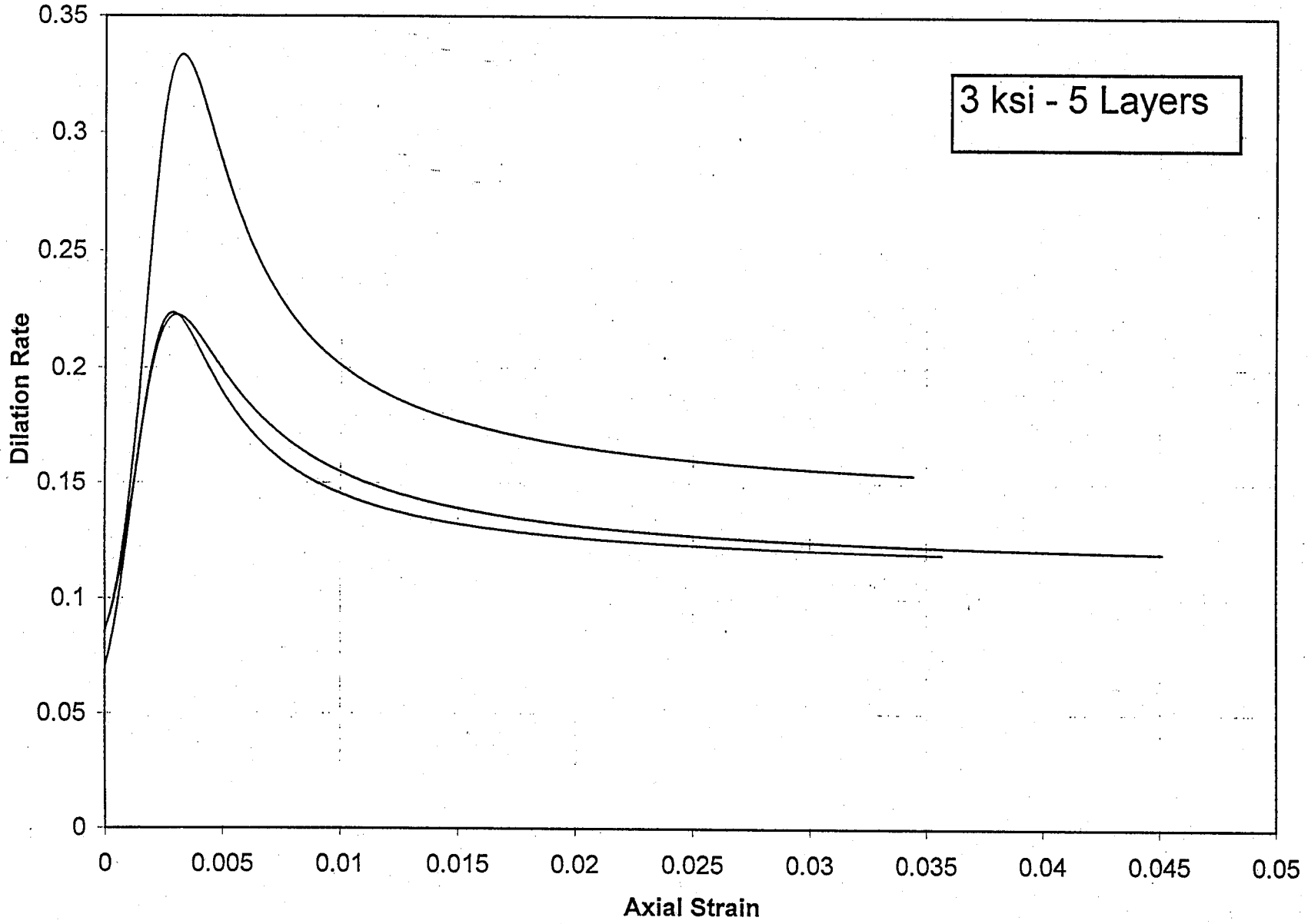

Figure 3.30 Dilation curves for the 3 ksi specimens with 5 layers

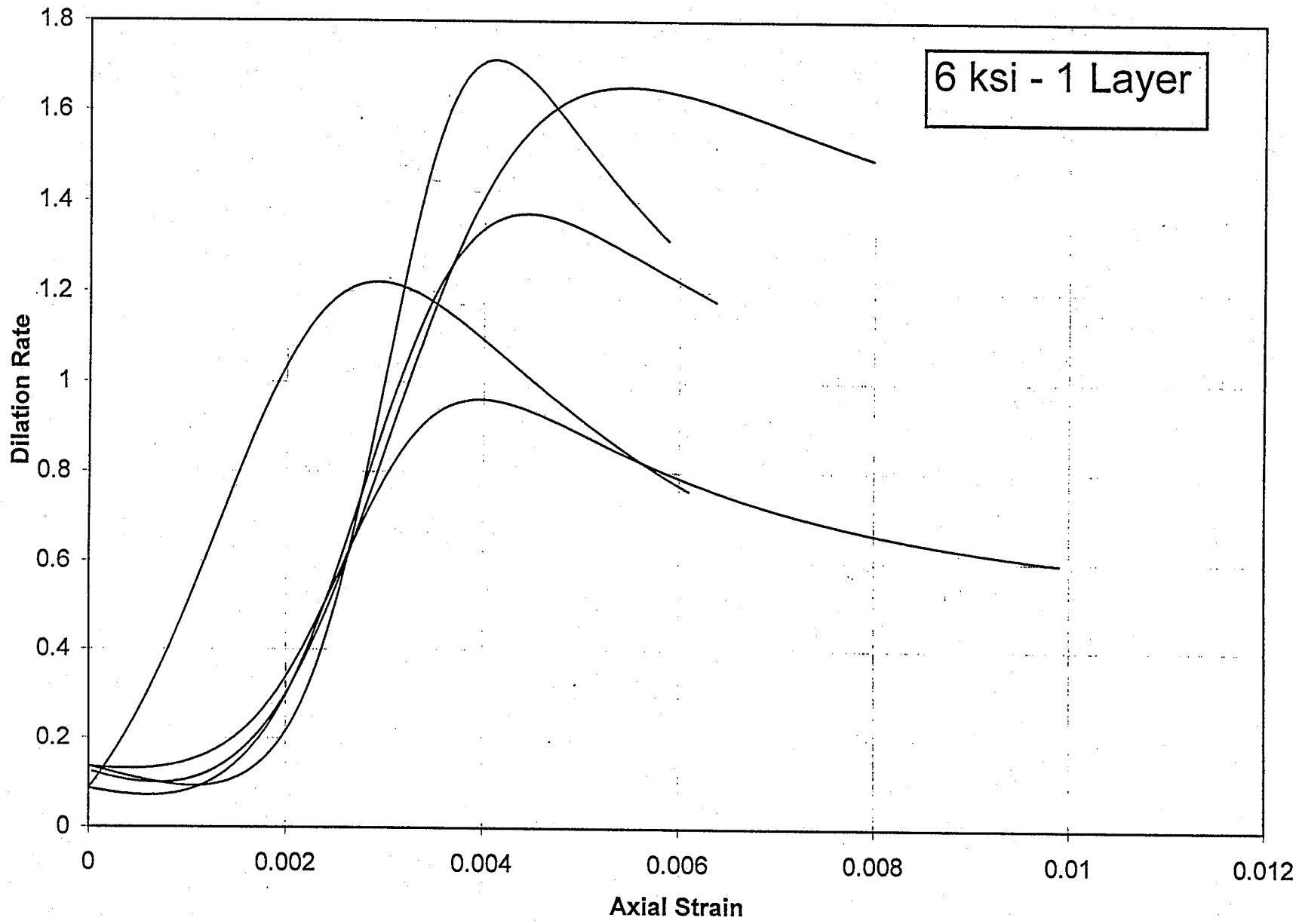

Figure 3.31 Dilation curves for the 6 ksi specimens with 1 layer

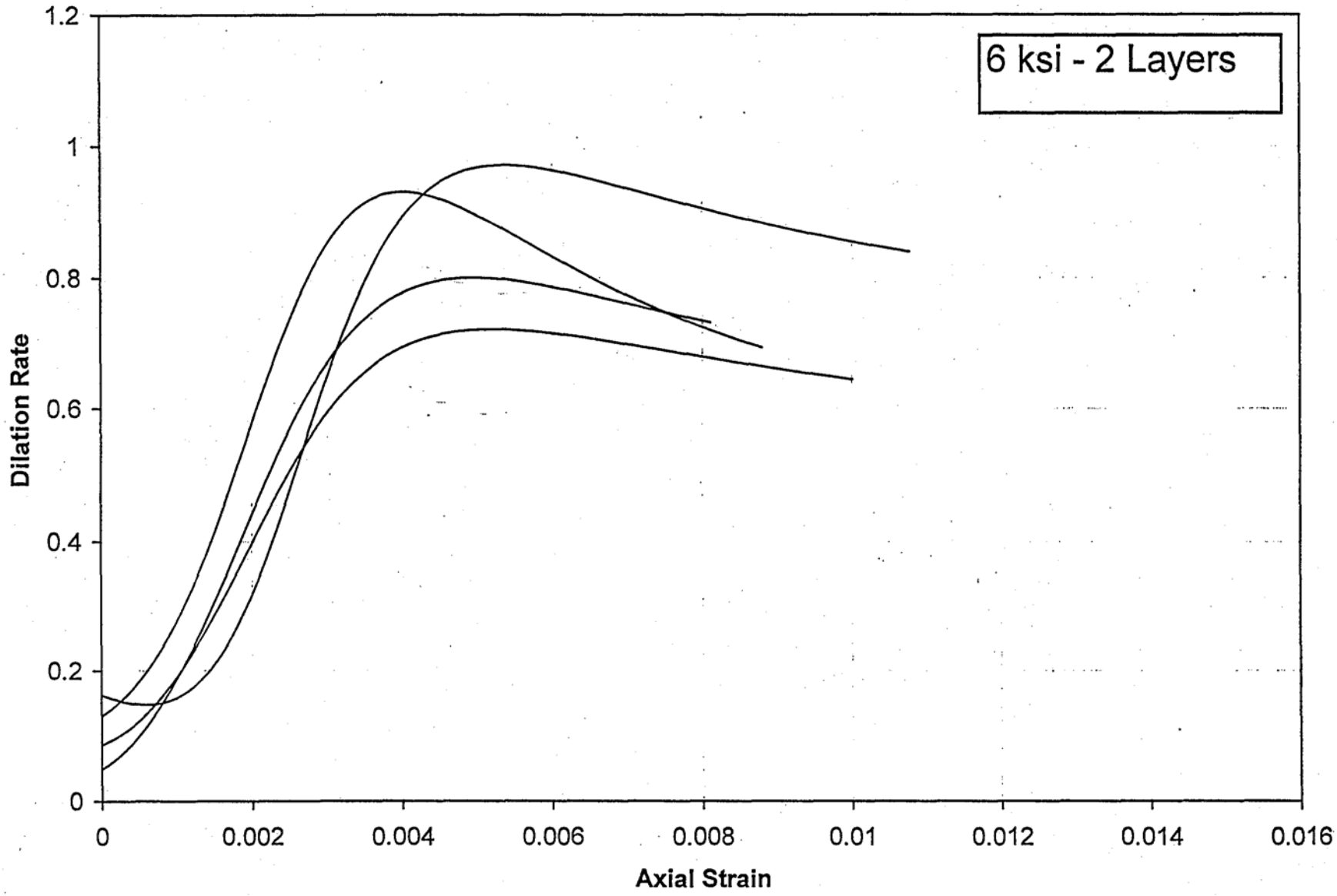

Figure 3.32 Dilation curves for the 6 ksi specimens with 2 layers

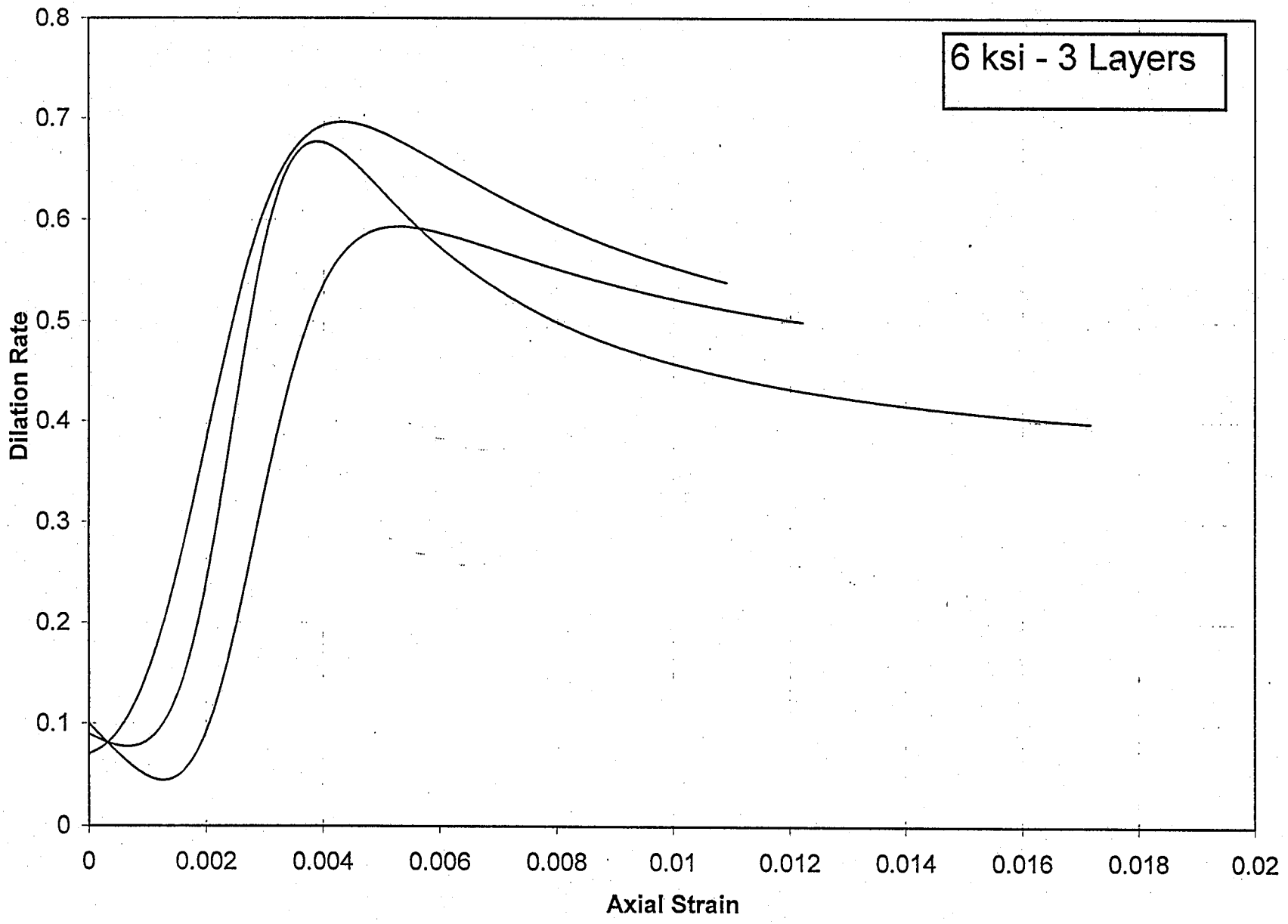

Figure 3.33 Dilation curves for the 6 ksi specimens with 3 layers

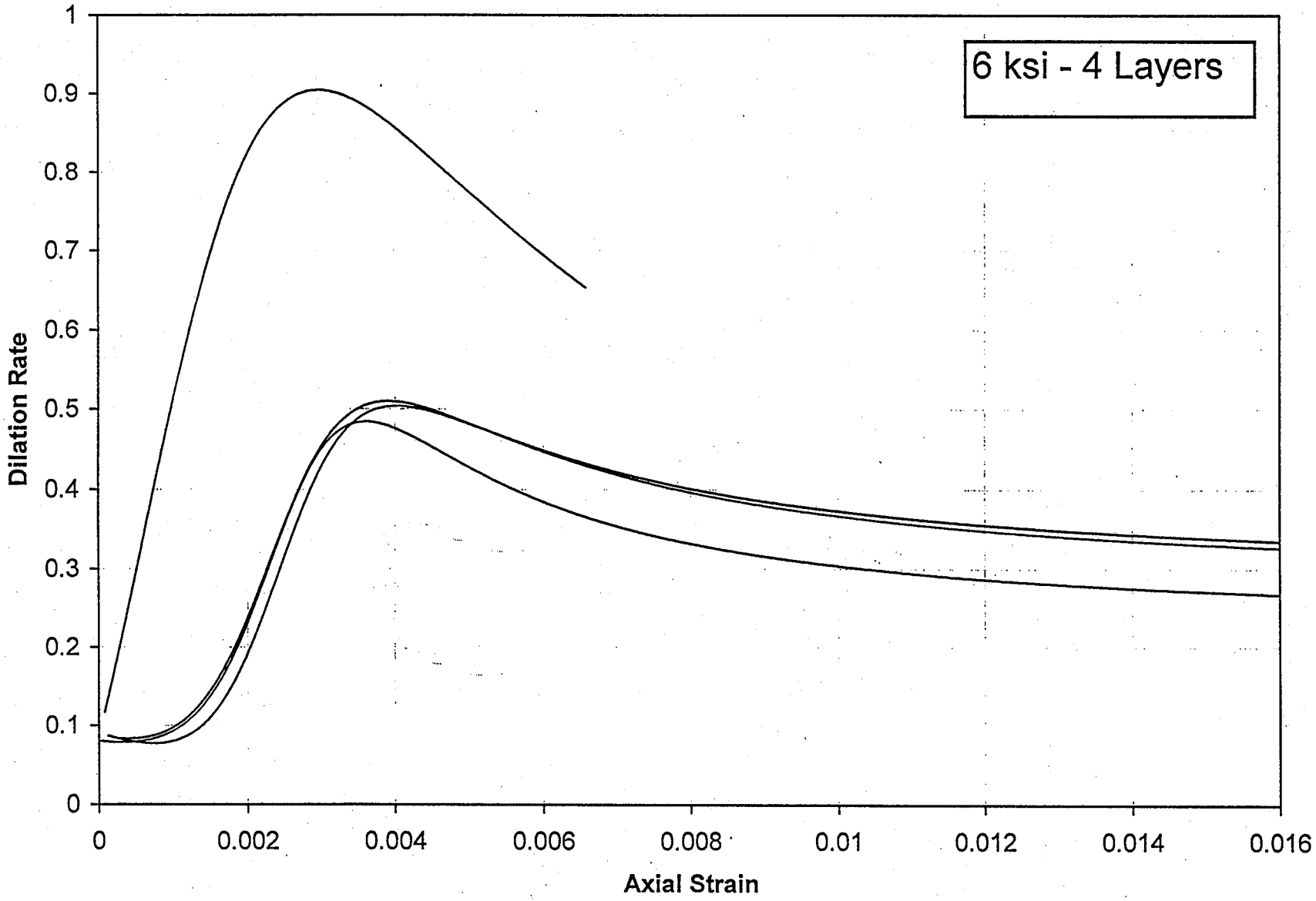

Figure 3.34 Dilation curves for the 6 ksi specimens with 4 layers

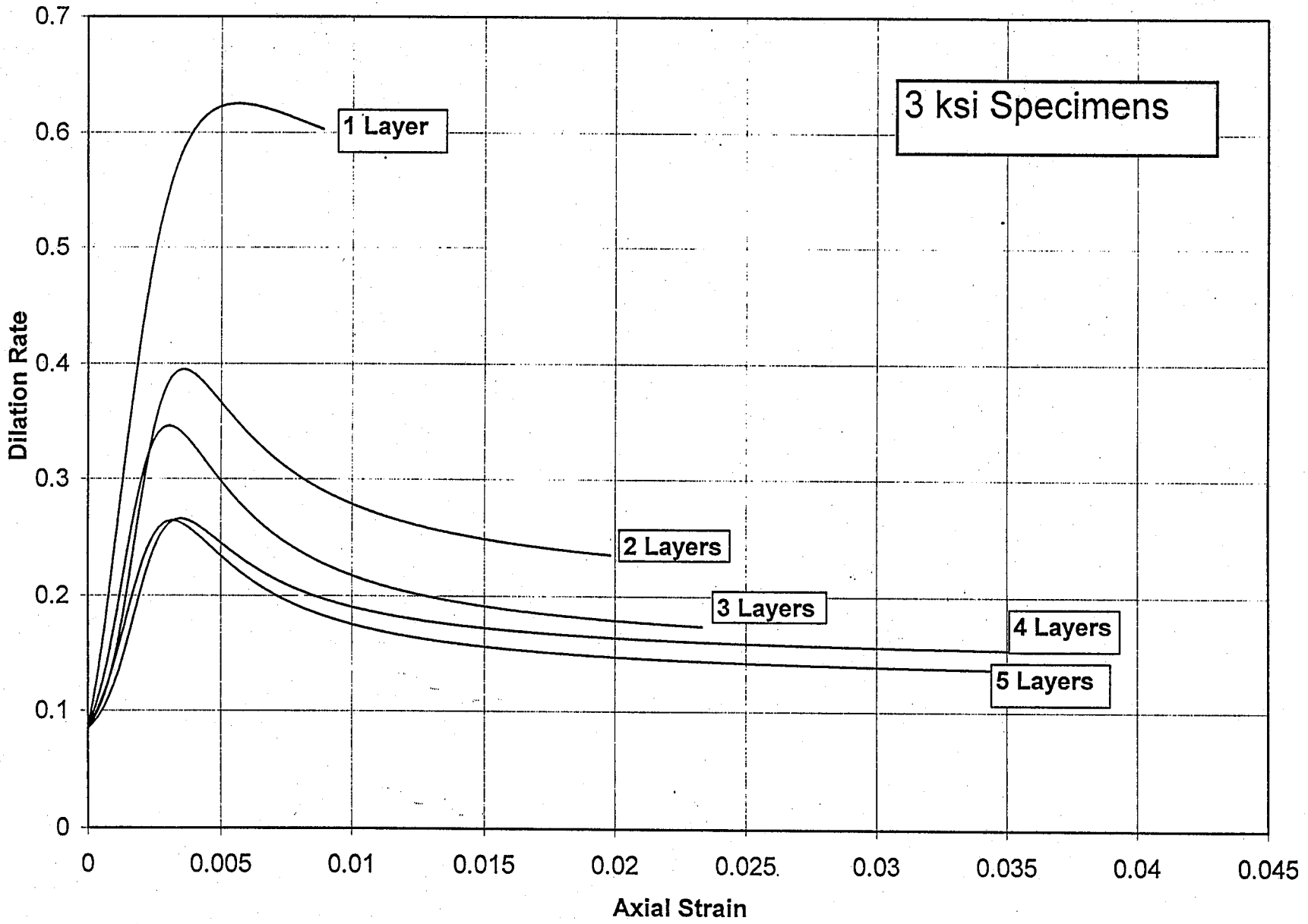

Figure 3.35 Average dilation curves for the 3 ksi specimens

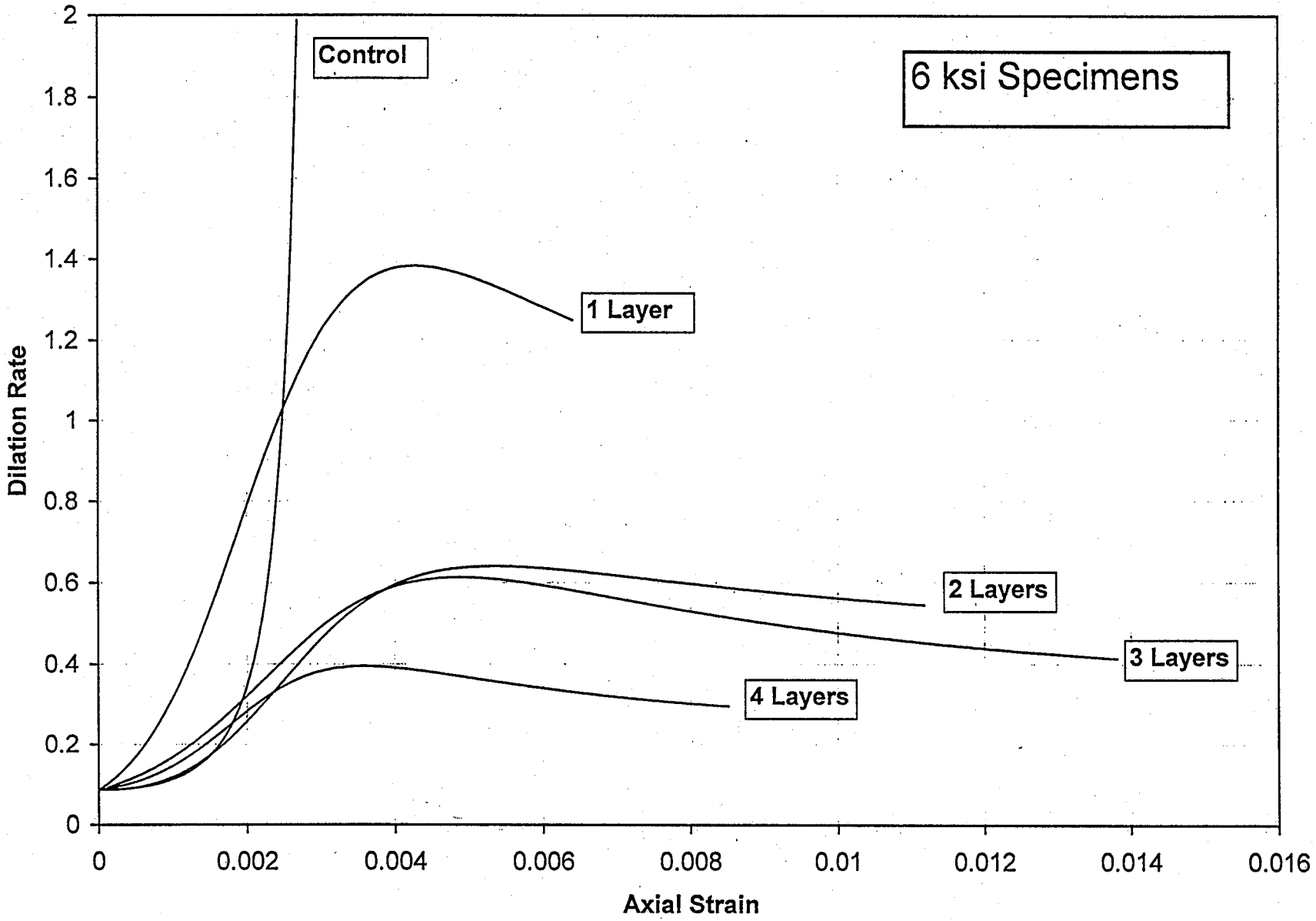

Figure 3.36 Average dilation curves for the 6 ksi specimens

CHAPTER 4

CONFINEMENT MODELING

4.1 Proposed Model .

Based on results from tests of concrete-filled glass FRP tubes, *a* confinement model was developed by Samaan, Mirmiran and Shahawy (1998). The model represents the bilinear response of FRP-confined concrete by *a* four-parameter relationship (Richard and Abbott 1975) *a s* below:

$$f_c = \frac{(E_1 - E_2)\varepsilon_c}{\left[1 + \left(\frac{(E_1 - E_2)\varepsilon_c}{f_o}\right)^n\right]^{\frac{1}{n}}} + E_2\varepsilon_c \tag{4.1}$$

where ϵ_c and f_c = axial strain and stress of concrete, E_1 and E_2= first and second slopes, f_o = reference plastic stress at the intercept of the second slope with the stress axis, and n = a curve-shape parameter which mainly controls the curvature in the transition zone. Figure 4.1 shows the basic parameters of this expression. The confined strength of concrete (f'_{cu}) is calculated as below (ksi):

$$f'_{cu} = f'_c + 3.38 f_r^{0.7} \tag{4.2}$$

where f C is the unconfined strength, and f,. is the confinement pressure which is calculated

$$f_r = \frac{2 f_j t_j}{D} \tag{4.3}$$

where f is the hoop strength of the jacket, t_j is jacket thickness, and D is the core diameter. The first slope (E,) is the same as the initial modulus of elasticity of concrete as estimated below (in ksi):

$$E_1 = 47.586\sqrt{1{,}000 f'_c} \tag{4.4}$$

The second slope (E_2) is a function of the stiffness of the confining jacket, and to a lesser extent, the unconfined strength of concrete core, as below:

$$E_2 = 52.411 f'^{0.2}_c + 1.3456 \frac{E_j t_j}{D} \tag{4.5}$$

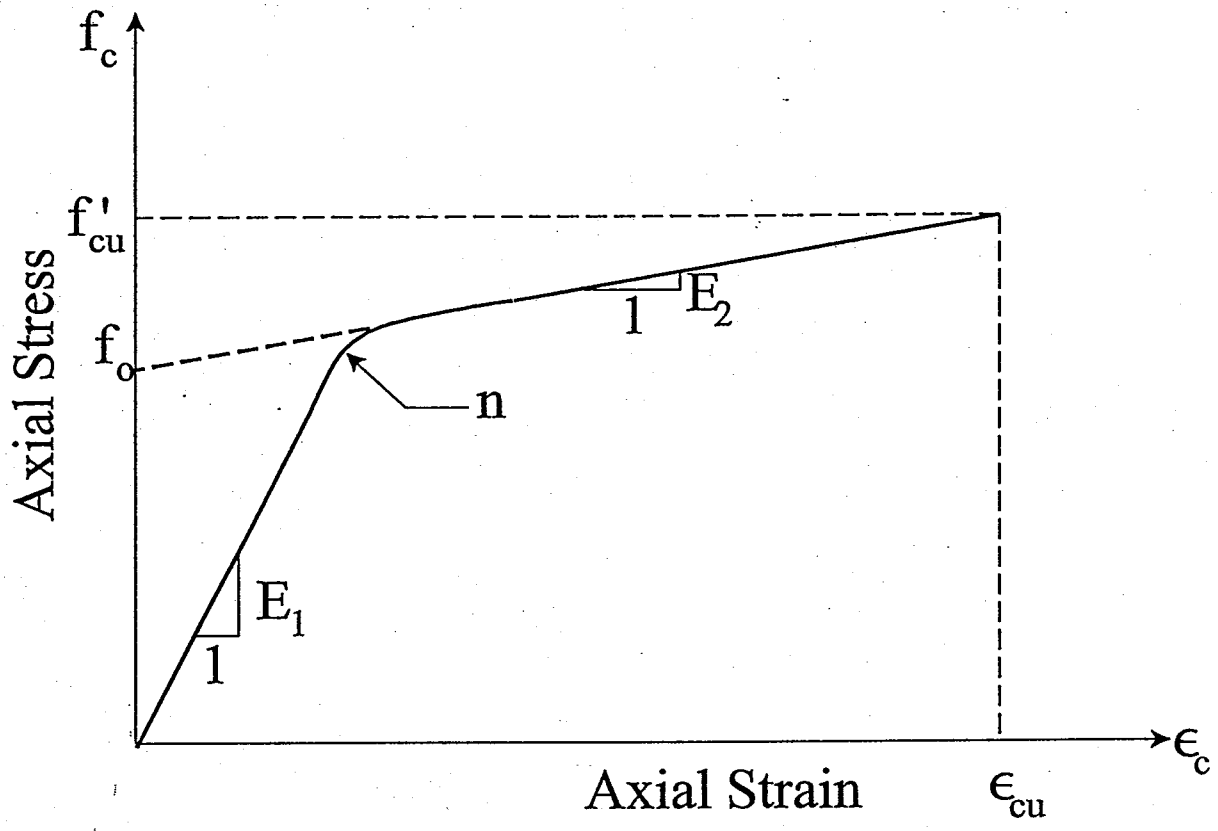

Figure 4.1 Parameters of the confinement model

where E_j = effective modulus of elasticity of the jacket in the hoop direction. The intercept stress f_o is a function of the strength of unconfined concrete and the confining pressure provided by the jacket, and was estimated as (in ksi)

$$f_o = 0.872f'_c + 0.371f_r + 0.908 \tag{4.6}$$

The ultimate strain ϵ_{cu} is determined from the geometry of the bilinear curve as

$$\varepsilon_{cu} = \frac{f'_{cu} - f_o}{E_2} \tag{4.7}$$

The curve-shape parameter n is set at a constant value of 1.5.

Modeling of Lateral Strains

Since the axial stress-lateral strain curve is also bilinear, and the transition zone occurs at the same axial stress level, the model is extended to the lateral direction, as

$$f_c = \frac{\left(E_{1r} - E_{2r}\right)\varepsilon_r}{\left[1 + \left(\frac{\left(E_{1r} - E_{2r}\right)\varepsilon_r}{f_{or}}\right)^{n_r}\right]^{\frac{1}{n_r}}} + E_{2r}\varepsilon_r \tag{4.8}$$

where subscript r denotes the lateral (radial) direction. The first slope E_{1r} is given by

$$E_{1r} = \frac{E_1}{\nu} \tag{4.9}$$

where ν = Poisson's ratio of concrete which usually varies between 0.15 and 0.22. The remaining parameters are found using the dilation rate μ which is defined as

$$\mu = -\frac{d\varepsilon_r}{d\varepsilon_c} \tag{4.10}$$

The values of μ_u was related to the stiffness of the confining jacket as below:

$$\mu_u = -0.187Ln\left(\frac{2E_j t_j}{f'_c D}\right) + 0.881 \tag{4.11}$$

Then, E_{2r} is calculated as

$$E_{2r} = \frac{E_2}{\mu_u} \tag{4.12}$$

and the curve-shape parameter as

$$n_r = \frac{n}{\mu_u} \tag{4.13}$$

The reference plastic stress, f_{or}, is calibrated in a form similar to f_o as (in ksi)

$$f_{or} = 0.636\, f'_c + 0.233\, f_r + 0.661 \tag{4.14}$$

Finally, the ultimate radial strain is calculated as:

$$\varepsilon_{ru} = \frac{f'_{cu} - f'_{cr}}{E_{2r}} \tag{4.15}$$

4.2 Verification of the Model

The model was validated against the results of two separate experiments, as follows:

Carbon Fiber-Wrapped Concrete Cylinders

Picher (1995) tested a total of 44 6" x 12" concrete cylinders wrapped in 2, 3, 4, or 5 layers of carbon fibers with different orientation angles. Most specimens, however, were made with three layers of carbon fibers. Fiber orientations of 0°, ±6°, ±9°, ±12°, ±18°, and ±24°, or a combination of these were used. Two different types of unidirectional carbon fabrics, namely Mitsubishi and Autocon, were used. The unconfined strength of concrete for all specimens was 5.76 ksi. Figure 4.2 shows the experimental versus predicted stress-strain curves for one of the 3-layer Autocon fiber wrapped specimens with a [+9°/-9°/0°] lay up, and one of the 5-layer Autocon specimens with a [0°/0°/+24°/-24°/0°] lay up. A very good agreement with the proposed model is evident.

S-Glass Fiber-Wrapped Concrete Cylinders

Mastrapa (1997) tested a total of 32 6" x 12" composite cylinders, half of which were wrapped in 1, 3, 5, or 7 layers of S-glass fabric, while for the other half, concrete of the same batch was poured in tubes made of the same S-glass fabric and with the same number of layers. The objective of the study was to determine the effect of construction bond on FRP-confined concrete. Tests were done in two series. In Series l, multi-layer jackets were made layer-by-layer with a splice length of about -17% of the perimeter of the cylinders, while in Series 2, the jacket was made of a continuous wrap of fabric with an overlap of about 32% of the perimeter of the cylinder. The average unconfined strength of concrete for specimens of Series 1 was 5.4 ksi. The hoop strength and modulus of the FRP jacket were 85 ksi and 2,984 ksi, respectively. Figure 4.3 shows the experimental versus predicted stress-strain curves for one of the 5-layer fiber-wrapped specimens of Series 1. A very good correlation is noted.

4.3 Results and Discussion

The predicted stress-strain curves of the model are plotted in Figures 4.4-4.8 for the 3 ksi specimens with 1-5 layers, and in Figures 4.9-4.12 for the 6 ksi specimens with 1-4 layers. The data used for generating these curves is listed in Table 4.1. It should be noted that the actual strength of the 6-ksi specimens was about 7-9 ksi from the bend point of the confined specimens. Therefore, a core strength of 8 ksi was used. It should also be noted that the average thickness of all jackets was given by the FDOT as 0.02" per layer, which results in a 0.10" thickness for the 5-layer specimens. However, thickness of a multi-layer jacket is nova multiple of the thickness of a single-layer jacket,

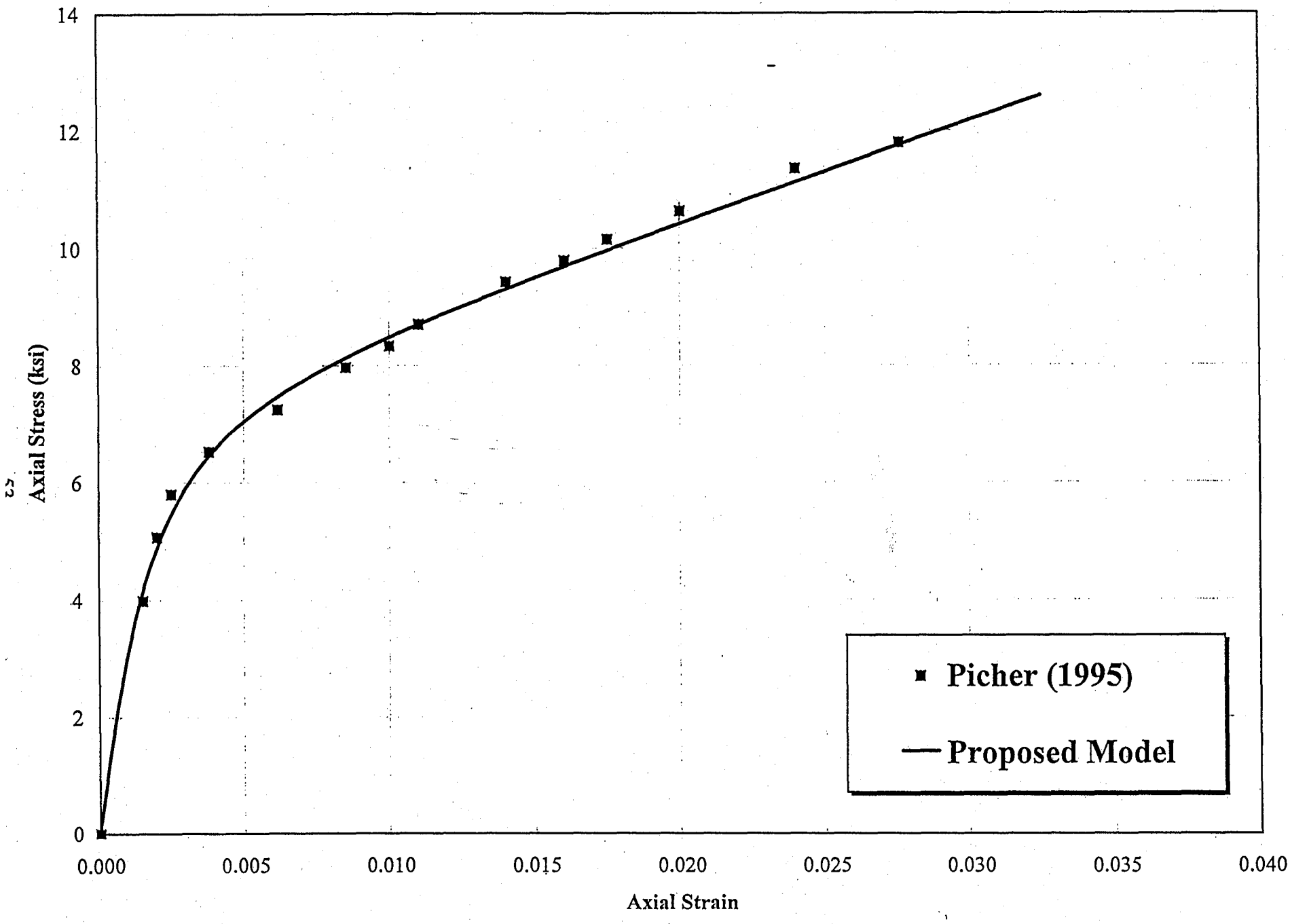

Figure 4.2 Comparison of model with carbon-wrapped specimens of Picher (1995)

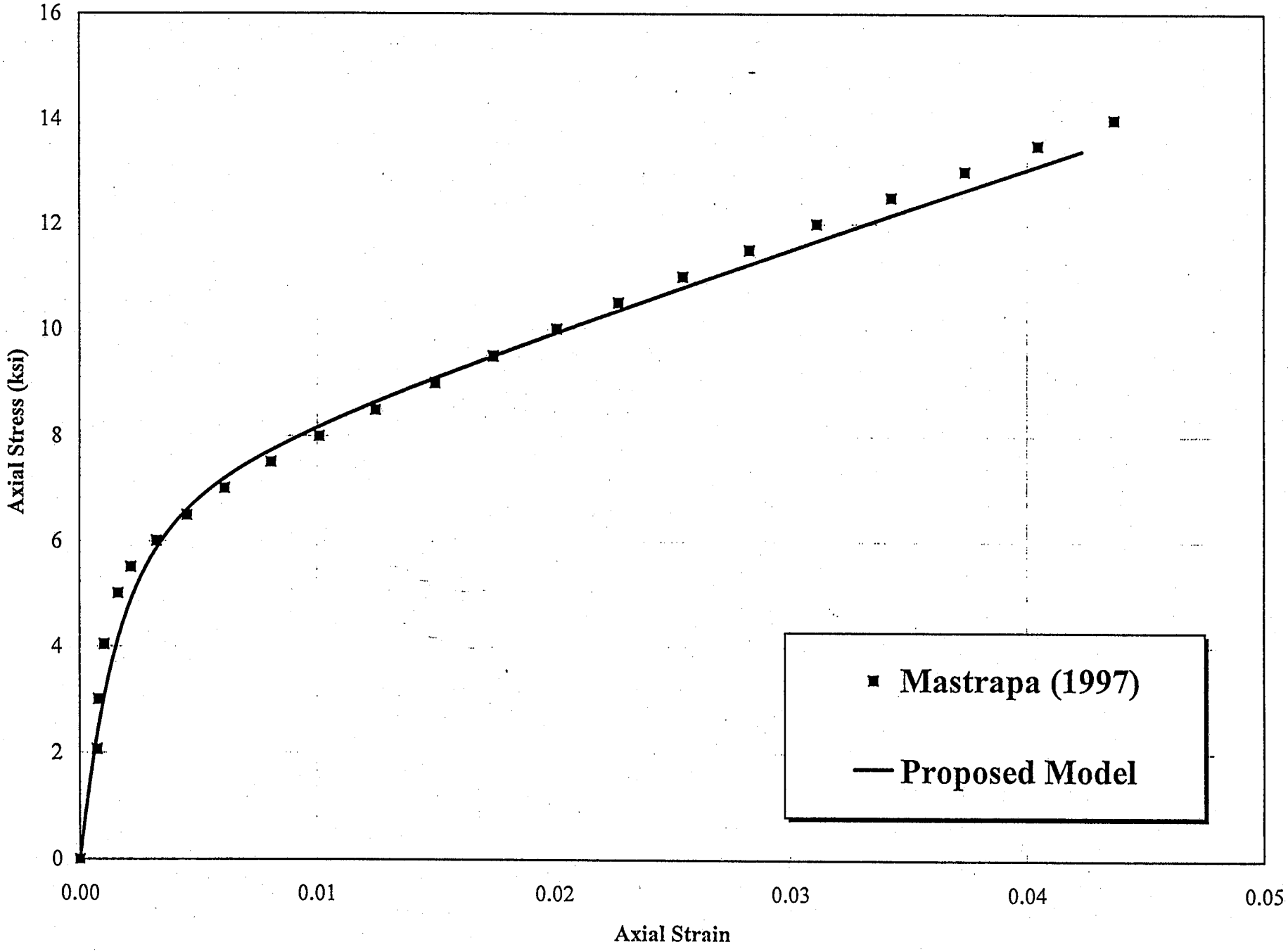

Figure 4.3 Comparison of model with S-glass-wrapped specimens of Mastrapa (1997)

because the resin is often squeezed out more by placing multiple layers. Therefore, with the increase in number of layers, the thickness per layer is reduced, while the strength and modulus are increased. However, since there was not enough data on the thickness and strength of the jacket, the thicknesses were selected based on the estimated fiber volume fraction which ranged between 70% for the 1layer specimens (0.014" per layer), down to 50% (0.010" per layer) for the 5-layer specimens. The modulus and strength were kept the same for all specimens.

It appears that the model predicts the response of the 3 ksi specimens better than the 6 ksi specimens. It should be noted here that direct application of Equation (4.2) would have resulted in a much higher ultimate strength. However, since it was clear that none of the specimens reached the hoop fracture strain of the jacket (f/E_j= 330112000 = 0.0275), the actual fracture strain of the jacket was used in cutting off the stress-strain curves of the model. Even though the model was equally validated against glass and carbon wraps (see Section 4.2), the database for the model was only made up of E-glass tubes. This indicates that the effect of modulus of elasticity- of the jacket may not have been fully incorporated, since only one type of material was used in calibrating the model. An attempt was made to re-calibrate the model (Equations 4.1-4.15) by including the carbon-wrapped specimens in the database. The results, even though not shown here, proved to be generally more accurate. However, due to the fact that the properties of the jacket (strength, modulus, thickness, and fiber volume fraction) are not known with any certainty, it did not seem appropriate to re-calibrate the model at this time. Once such data becomes available in a carefully controlled series of tests, which includes accurate coupon tests, a re-calibration of the model will be beneficial.

Table 4.1 Input values for the confinement model

Description of the item	Type of specimen	Input value
Unconfined strength of concrete (f'_c)	3 ksi specimens	3 ksi
	6 ksi specimens	8 ksi
Concrete Poisson's ratio	All specimens	0.12
Core diameter	All specimens	6 in.
Hoop strength of the jacket (f_j)	All specimens	330 ksi
Hoop modulus of elasticity of the jacket (E_j)	All specimens	12000 ksi
Jacket thickness	1-layer specimens	0.014 in.
	2-layer specimens	0.023 in.
	3-layer specimens	0.032 in.
	4-layer specimens	0.041 in.
	5-layer specimens	0.050 in.

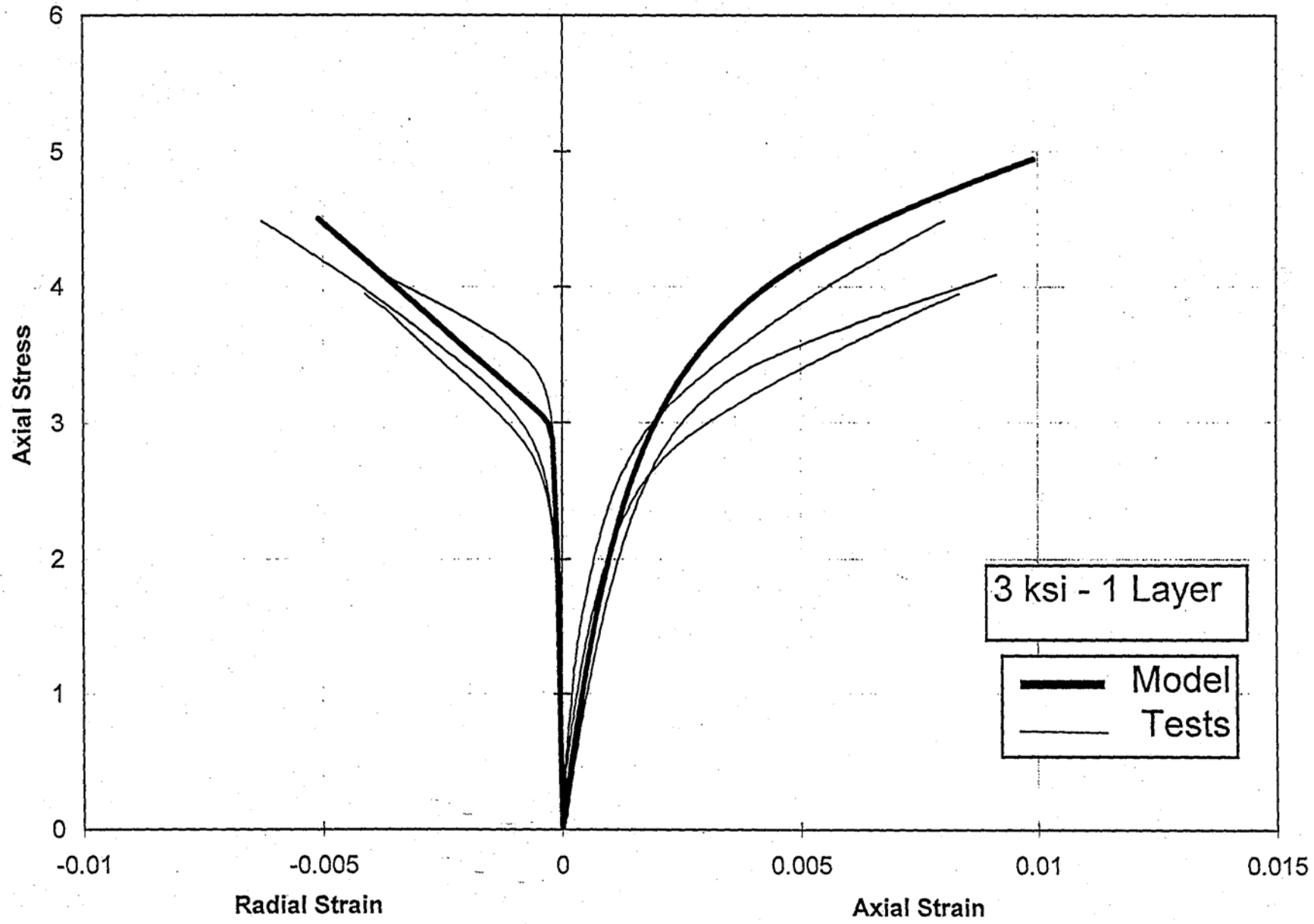

Figure 4.4 Comparison of confinement model with the 3 ksi, 1-layer specimens

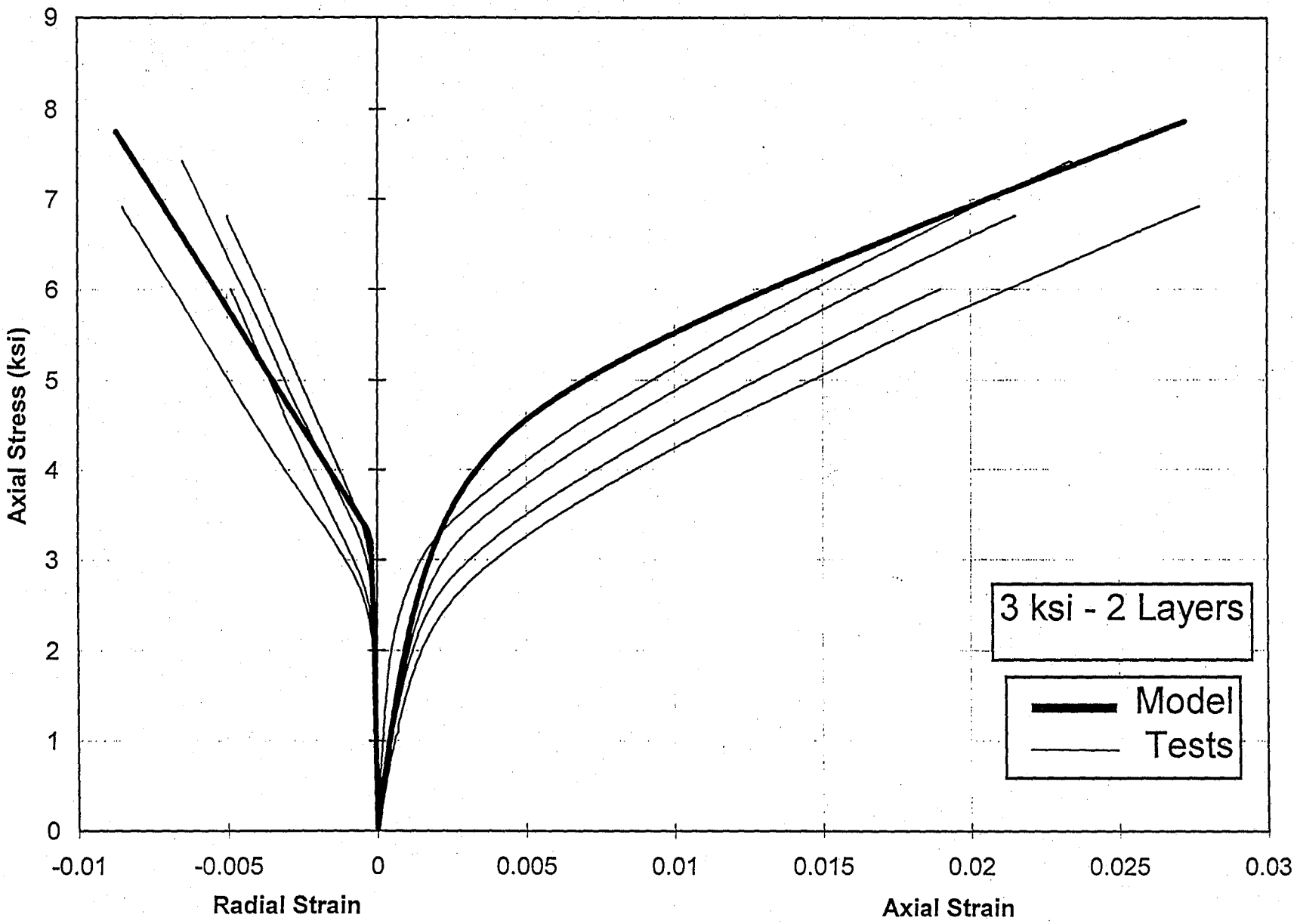

Figure 4.5 Comparison of confinement model with the 3 ksi, 2-layer specimens

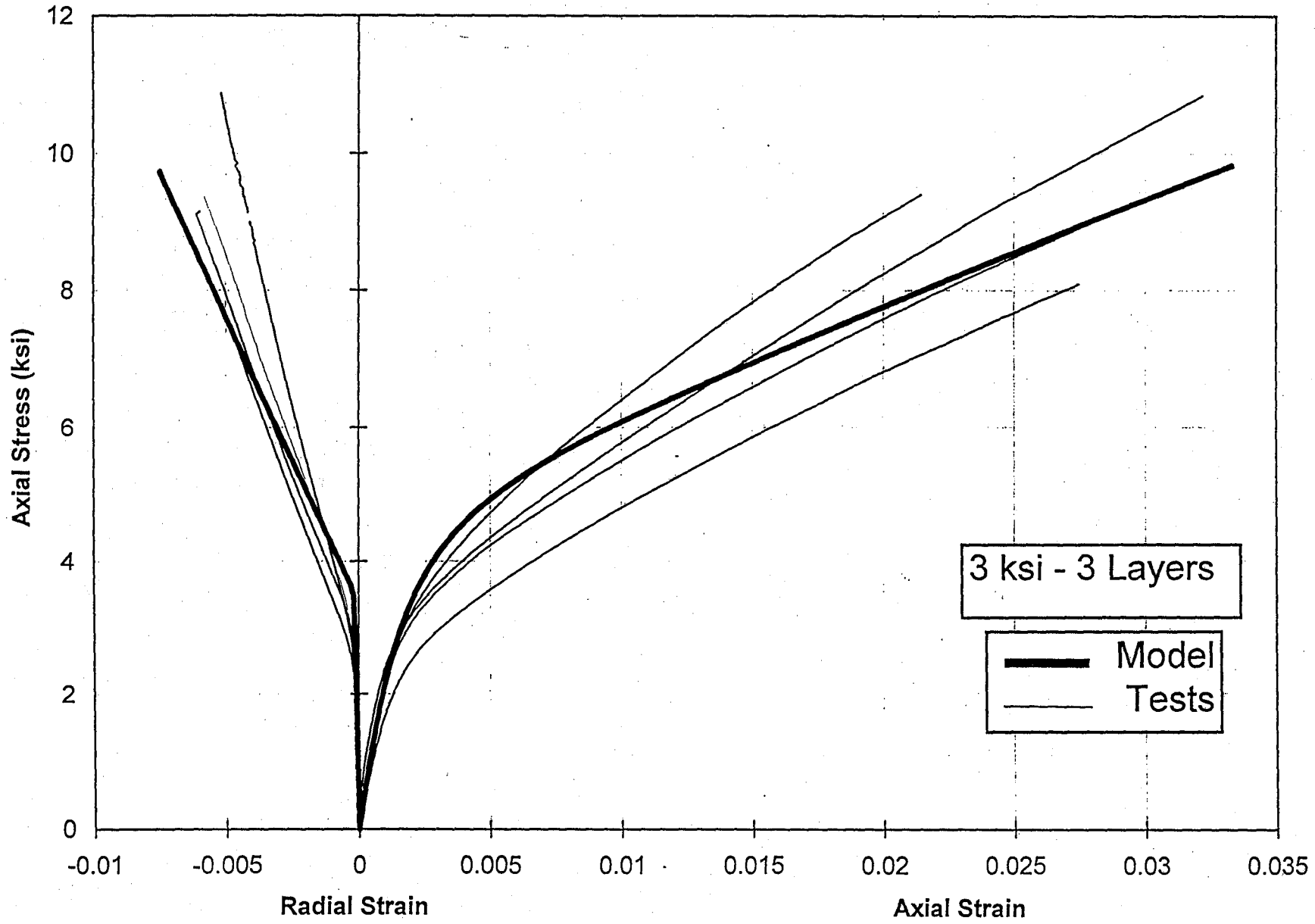

Figure 4.6 Comparison of confinement model with the 3 ksi, 3-layer specimens

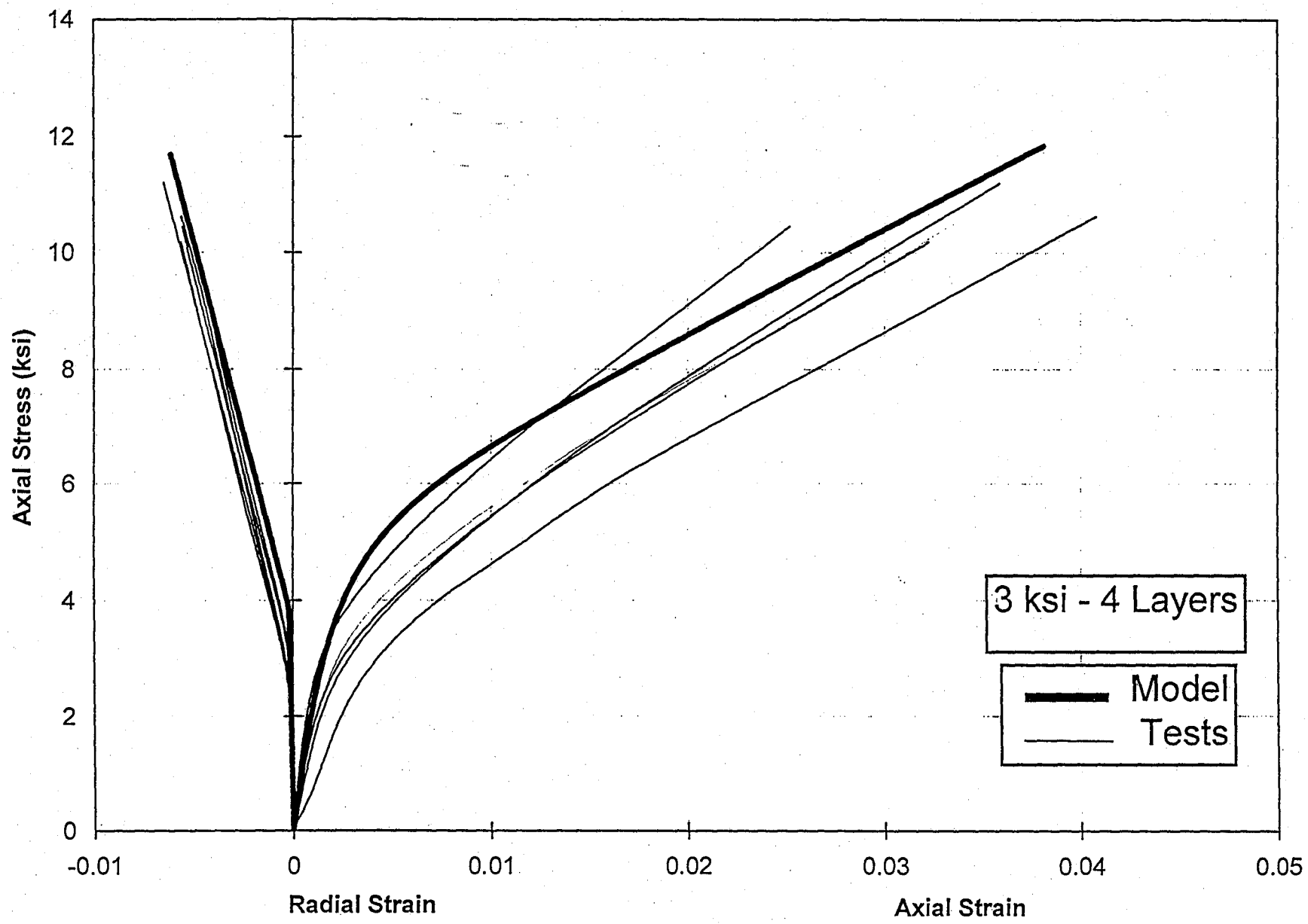

Figure 4.7 Comparison of confinement model with the 3 ksi, 4-layer specimens

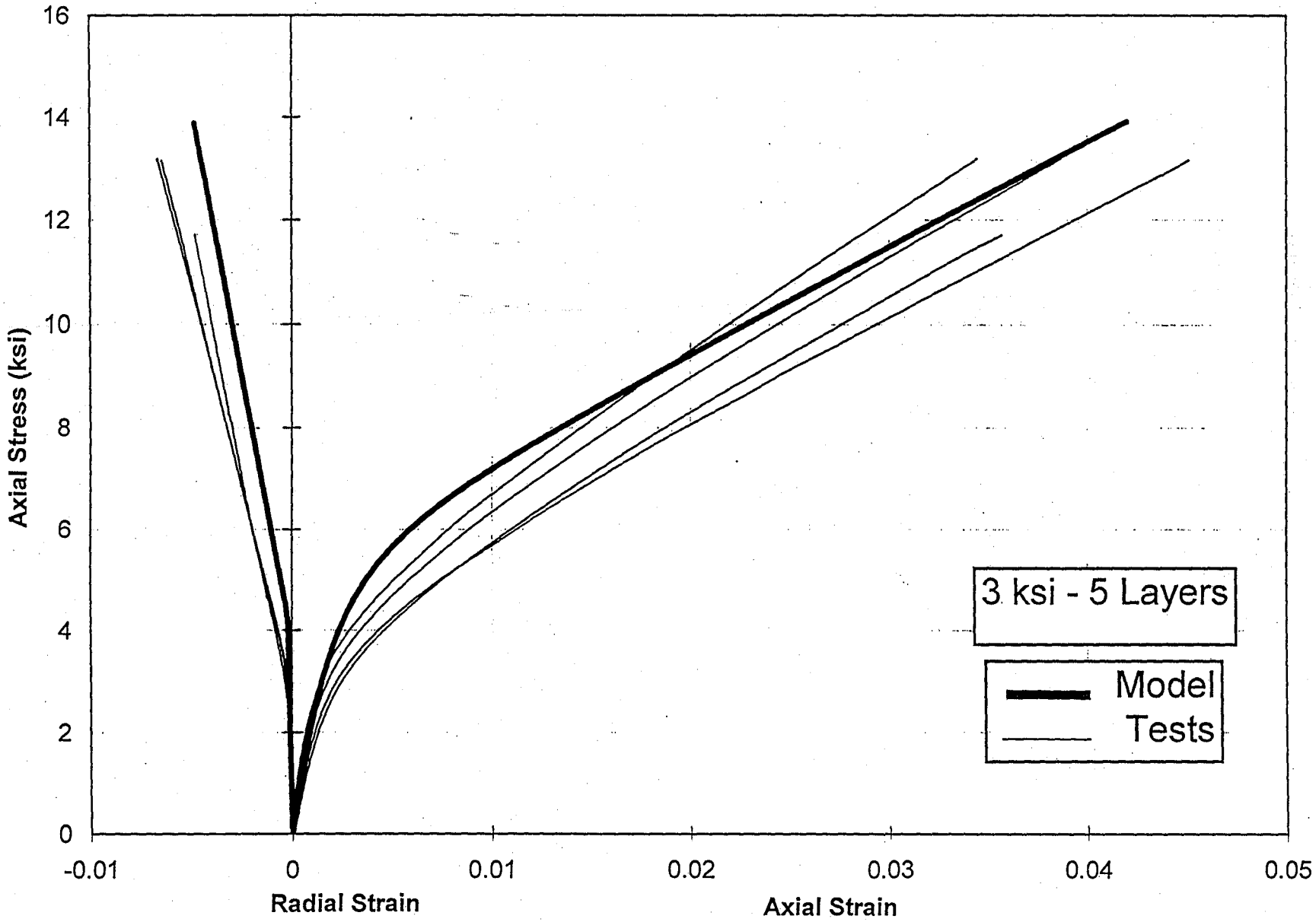

Figure 4.8 Comparison of confinement model with the 3 ksi, 5-layer specimens

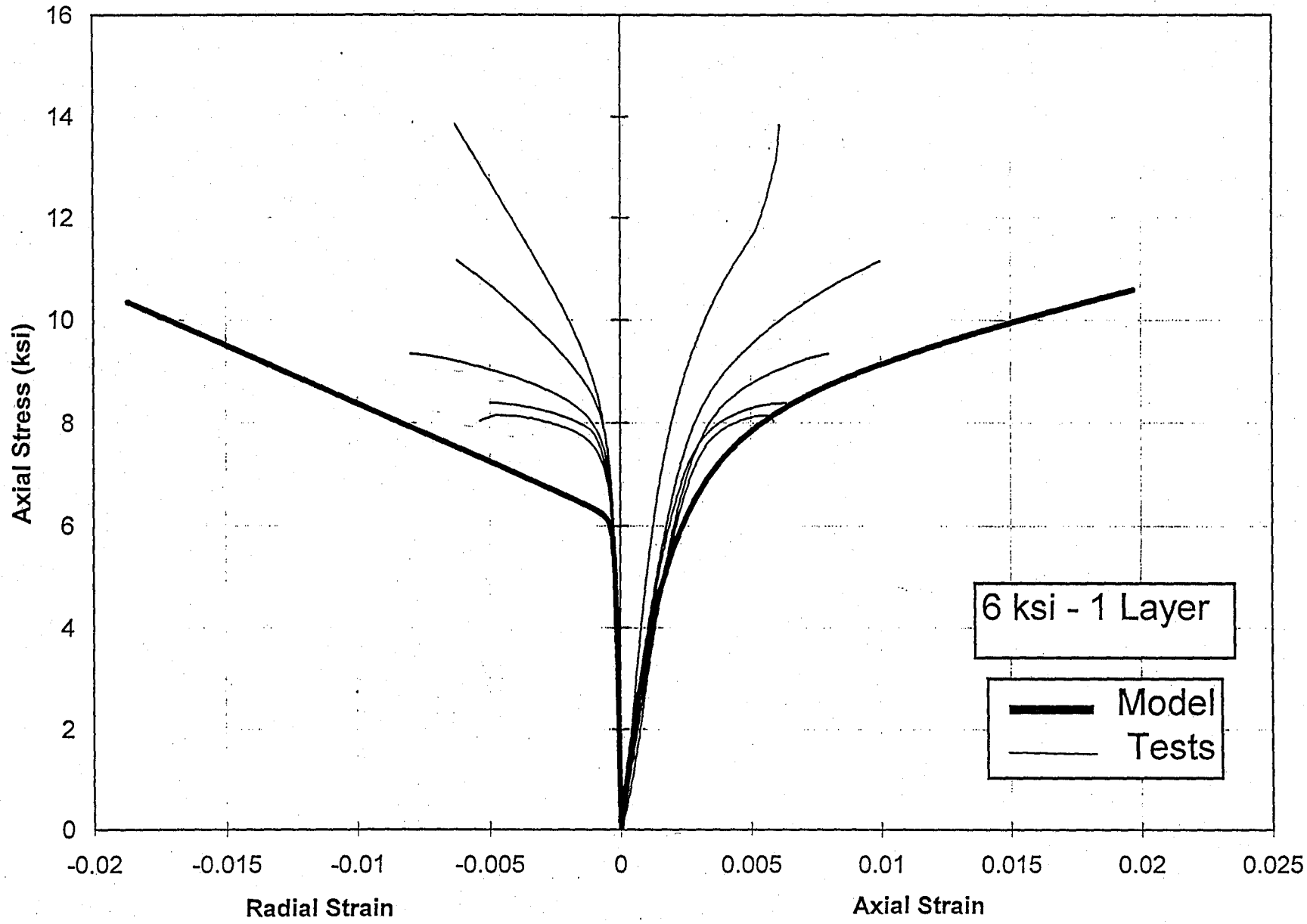

Figure 4.9 Comparison of confinement model with the 6 ksi, 1-layer specimens

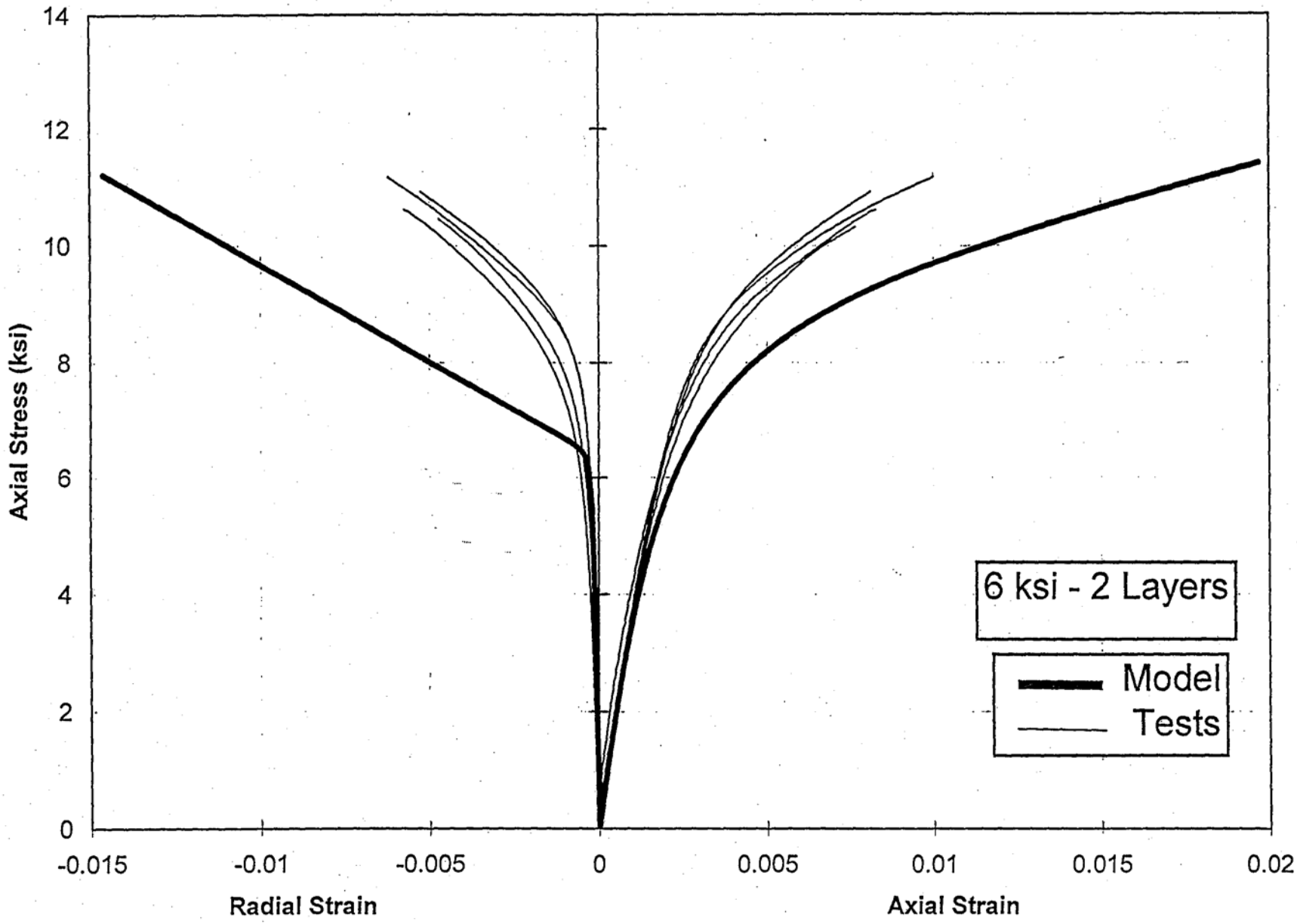

Figure 4.10 Comparison of confinement model with the 6 ksi, 2-layer specimens

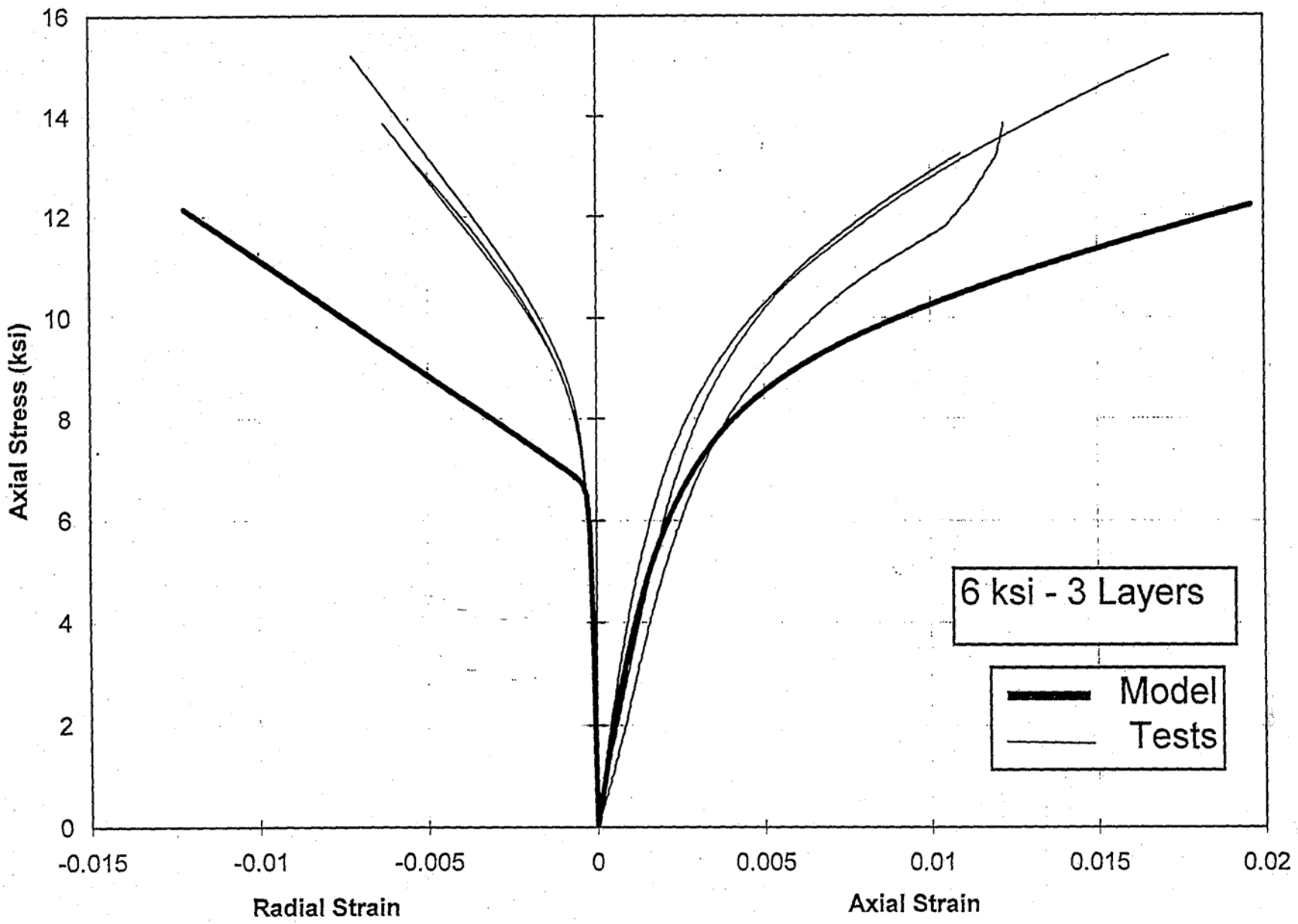

Figure 4.11 Comparison of confinement model with the 6 ksi, 3-layer specimens

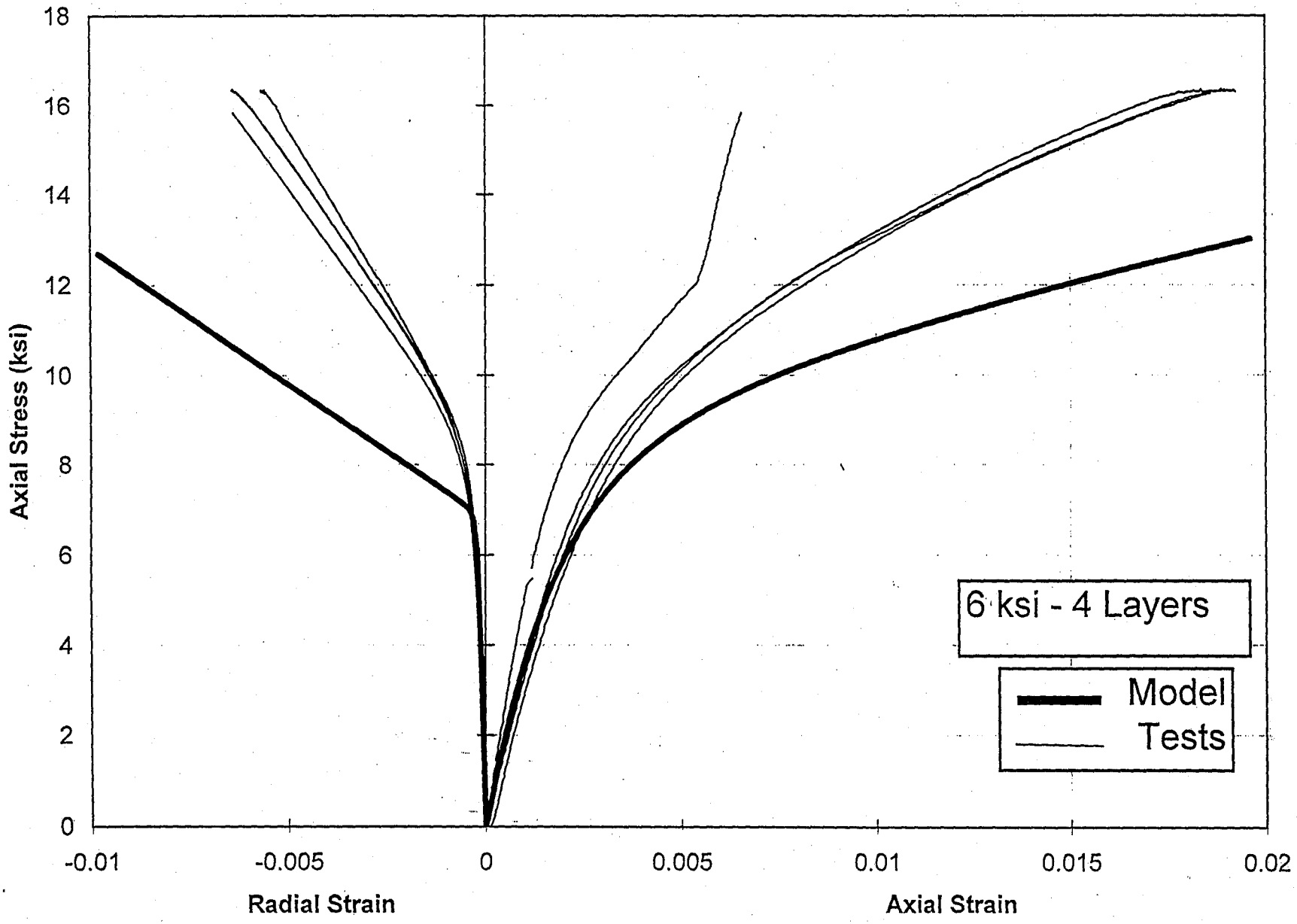

Figure 4.12 Comparison of confinement model with the 6 ksi, 4-layer specimens

CHAPTER 5

FINITE ELEMENT MODELING

5.1. Introduction

Applicability of finite element (FE) modeling to FRP-confined concrete was originally studied as part of the project on fiberglass tubes (Mirmiran 1997a) with ANSYSE^{ED} software. The FE mesh consisted of 48 concrete elements and 24 jacket elements for the top quarter of the column. Six slices through the length of the column, and three sectors within the section were established. For concrete, the 3-D reinforced concrete (SOLID65) element was chosen without the use of smeared reinforcement. For the jacket, the membrane shell (SHELL41) element was selected with linear-elastic materials. In order to limit the effect of jacket to confinement only, its elastic modulus in the axial direction was set close to zero. The stress-strain curve for unconfined concrete was input as a multi-linear kinematic hardening using the model of Ahmad & Shah (1982). Von Mises yield criterion was selected for the analysis. The model 'was first validated for the case of active confinement (hydrostatic pressure), and the results seem to match the experiments. Good agreement was also noted for concrete-filled steel tubes. However, results for FRP-confined concrete were not acceptable, as the model deviated from the experimental results. The main conclusion from the study was that Von Mises yield criterion is not an acceptable criterion for modeling concrete by itself since it does not consider the effect of hydrostatic stress. The better approach would be to use DruckerPrager plasticity. Similar studies have been conducted at the University of Sherbrooke (Rochette and Labossiere 1996) who reported reasonably good agreement with the experimental results. In this chapter, the plasticity approach is described, and the modeling procedure is outlined. Then, the results of FE analysis are compared with the experimental data.

5.2 Plasticity Approach

Rate-independent plasticity constitutes an irreversible straining that occurs in a material once the yield surface is reached. ANSYS® program provides several options to characterize different types of material behavior; classical bilinear kinematic hardening, multi-linear kinematic hardening, bilinear isotropic hardening, multi-linear isotropic hardening, anisotropic, and Drucker-Prager (DP). Plasticity theory provides a mathematical relationship that characterizes the elasto-plastic response of materials. There are three ingredients in the rate-independent plasticity theory in the ANSYS® program; the yield criterion, flow rule, and the hardening rule. The yield criterion determines the stress level at which yielding is initiated. For triaxial state of stress, an equivalent stress (σ_e) is defined as

$$\sigma_e = f(\{\sigma\}) \tag{5.1}$$

where {a} is the stress tensor. Once a_e equals the material yield parameter a_y, the material develops plastic strains. In the stress space, this is termed as having reached the yield surface. The flow rule determines the direction of plastic straining and is given by:

$$\{d\epsilon^{pl}\}=\lambda \left\{\frac{\partial Q}{\partial \sigma}\right\} \tag{5.2}$$

where X is the plastic multiplier. which determines the amount of plastic straining, and Q is a function of stress termed the plastic potential which determines the direction of plastic straining. If Q is set equal to the yield function, the *flow* rule will be termed associative and the plastic strains occur in a direction normal to the yield surface. The hardening rule describes the changing of the yield surface with progressive yielding so that the stress states for subsequent yielding can be established. Hardening can either be isotropic (or work), or kinematic. In isotropic hardening, the yield surface remains centered about its initial centerline and expands in size as the plastic strains develop. In kinematic hardening, the yield surface remains constant in size and the surface translates in the stress space with progressive yielding.

The DP model assumes an elastic-perfectly plastic material response with an associative or non-associative flow rule, a Von Mises yield criterion with dependence on hydrostatic stress. The equivalent stress for DP model is

$$\sigma_e = 3\beta\sigma_m + \left[\frac{1}{2}\{s\}^T[M]\{s\}\right]^{\frac{1}{2}} \tag{5.3}$$

where σ_m is the mean (hydrostatic) stress, {s} is the deviatoric stress, [M] is a special diagonal matrix, and β is a material constant given by

$$\beta = \frac{2\sin\phi}{\sqrt{3}(3-\sin\phi)} \tag{5.4}$$

where (is the angle of internal friction, and the yield parameter of the material is defined as

$$\sigma_y = \frac{6c\cos\phi}{\sqrt{3}(3-\sin\phi)} \tag{5.5}$$

where c is the cohesion value of the material. The yield surface for the DP model is a circular cone with the material parameters (3 and a_y chosen such that it corresponds to the outer aspices of the hexagonal Mohr-Coulomb yield surface. An angle of dilatancy (ϕ_f) is defined for establishing the flow rule. If $\phi_f = \phi$, then the flow rule is associative, meaning that the plastic straining occurs normal to the yield surface and that there will be a volumetric expansion of the material with plastic strains. However, if ($\phi < \phi$, the flow rule is non-associative and there will be less volumetric expansion. Clearly, if ϕ_f is zero, there will be no volumetric expansion. The cohesion value (c) and the angle of internal friction (ϕ) are related as follows:

and

$$k_1 = \frac{1+\sin\phi}{1+\sin\phi} \tag{5.7}$$

where f'_{co} is unconfined strength of concrete, and k_1 is the confinement effectiveness factor. Confinement effectiveness was first suggested by Richart et al. (1928) in a linear relation as below:

$$f'_{cu} = f'_{co} + k_l \, f_r \tag{5.8}$$

where f'_{C},, is the confined strength of concrete, and f, is the confinement pressure given by:

$$f_r = \frac{2 f_j t_j}{D} \tag{5.9}$$

where f is the jacket strength, t_j is the jacket thickness, and D is the core diameter. A value of $k_1 = 4.1$ was suggested by Richart et al. (1928). *For* this value of k_1, and a concrete strength of 4000 psi, values of c and ~ are calculated from (5.6) and (5.7) as 988 psi and 37.43°. Confinement models of Mander et al. (1988) and Samaan et al. (1998) have proposed other (non-linear) forms of confinement effectiveness. A study by Rochette and Labossiere (1996) suggests the following relationships for c and ϕ(after simplifications):

$$\phi = \sin^{-1} \frac{3}{1+1.592332 f'_{co}\,(ksi)} \tag{5.10}$$

$$c(psi) = \left(f'_{co}\,(psi) - 1256\right)\frac{3-\sin\phi}{6\cos\phi} \tag{5.11}$$

In the present study, the values suggested by Rochette and Labossiere (1996) are used. Moreover, a sensitivity analysis was conducted on the dilatancy angle (4)), and it was found out that the dilatancy angle should beset equal to zero, which makes the flow'rule non-associative and the volumetric expansion negligible.

5.3 Modeling

ANSYS® program (Version 5.3) was used in this study. Only the top quarter of the cylinder was modeled in uniaxial'compression under displacement control. A parametric input was developed that is explained below:

Element Types

Concrete was modeled by the six- or eight-noded SOLIID65 element. The 6-noded elements were used as wedges in the first annular division around the center of the cylinder. The jacket was

modeled by the four-noded SHELL41 for FRP, and SBELL43 for steel jackets, since the latter has an elasto-plastic stress-strain capability.

Material Properties

Modulus of elasticity of concrete is calculated automatically from its unconfined strength using Equation (4.3) unless the user prefers the ACI approach (57,0001f ~$_o$) or direct input. The c and values are calculated using Equations (5.10) and (5.11), unless the user prefers one of the models by Richart et al. (1928), Mander et al. (1988), Samaan et al. (1998), or a direct input. The user inputs the dilation as a percentage between 0 and 100. The default dilatancy angle is zero, unless the user prefers partial or full associative flow rule and volumetric expansion. The shell material is assumed linear elastic for FRP, and bilinear kinematic for steel. In order to limit the effect of jacket to confinement only, its elastic modulus in the axial direction -was set close to zero.

Model Geometry and Boundary Conditions

The user inputs the core diameter and the number of divisions in the radial and angular directions as well as the number of depth-wise slices. The program-automatically establishes the entire mesh in the cylindrical coordinate system. As for the boundary conditions, three planes of symmetry exist; XY, XZ, and YZ. All nodes on each plane of symmetry are fixed only in the direction normal to that plane, and are free to move within that plane.

Loading Control

Loading is applied in a displacement control mode to simulate the loading mechanism in an NITS machine. All nodes on the top surface (i.e., at the loading plate) are tied together. so as to enforce a uniform compression. The time steps are created automatically based on the user's expectation and input of the ultimate axial strain of confined concrete.

Post Processing

There are two types ofpost-processing in ANSYS® program; general and time-history. The latter provides a step-by-step variation of any desired variable such as stress or strain at various nodes or within any element in the model. The former provides plotting and listing capabilities for the ultimate results (th' last time step), such as deformations, contour plots of stresses and strains (plastic and elastic), etc. The parametric program developed under this study allows an automatic output of the time-history for the following variables; axial stress in concrete, axial and radial strain in concrete, and hoop stress in the jacket.

5.4 Results and Discussion

The general discretized model ofthe top quarter ofthe confined cylinders is shown in Figure 5.1. The dashed lines represent the undeformed edges (original shape), while the solid lines represent the deformed shape of the specimen. In this particular model a total of 6^3=216 elements were used. . But a sensitivity analysis showed that a total of 90 elements (3x5x6) will suffice in producing accurate results. Figure 5.2 shows the contours of the equivalent Von Mises total strains. The data used in the analysis are the same as those for the confinement model (see Table 4.1). The data from time-history FE analysis was transported into Excel to develop the stress-strain response. The

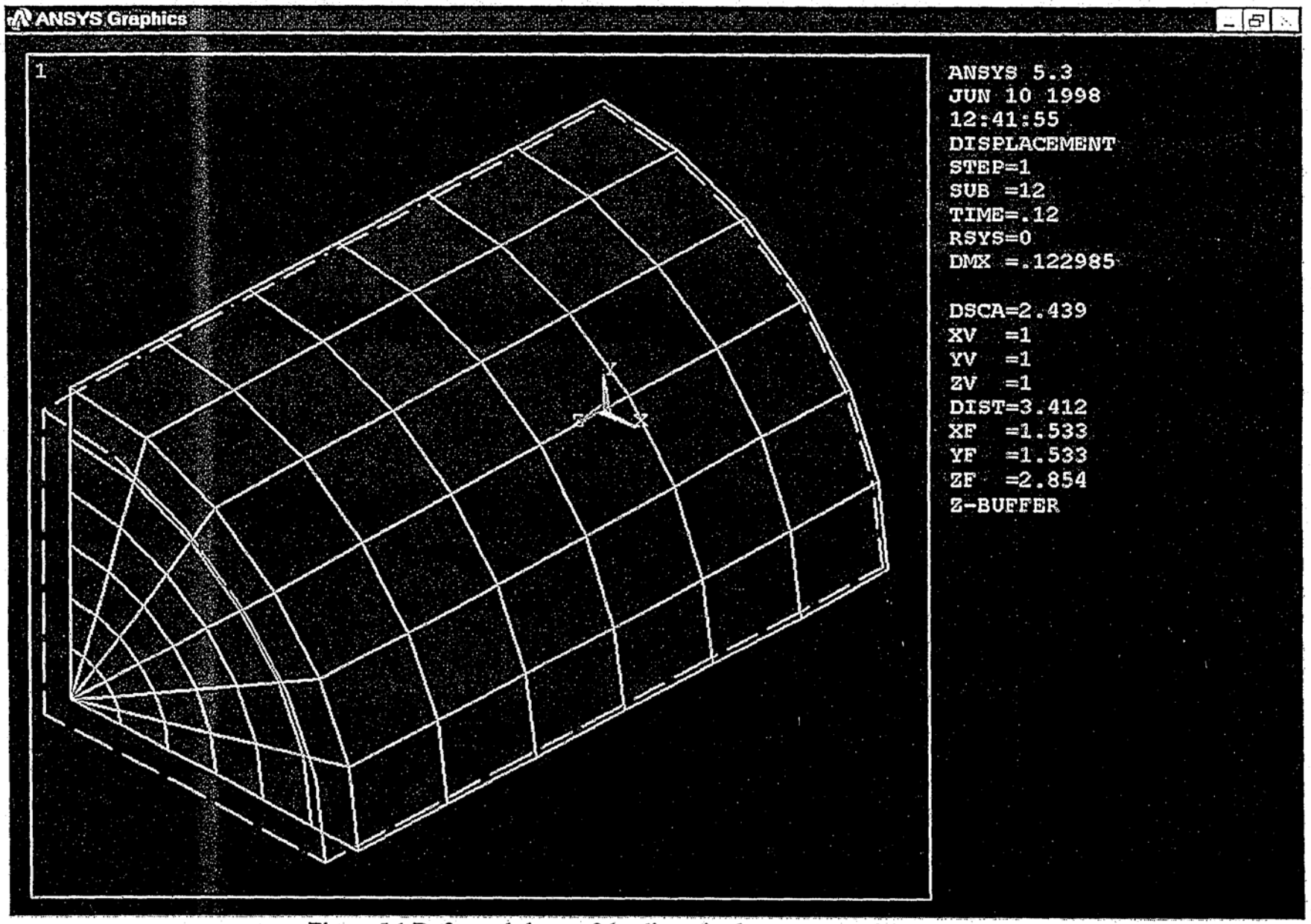

Figure 5.1 Deformed shape of the discretized top quarter of the specimen

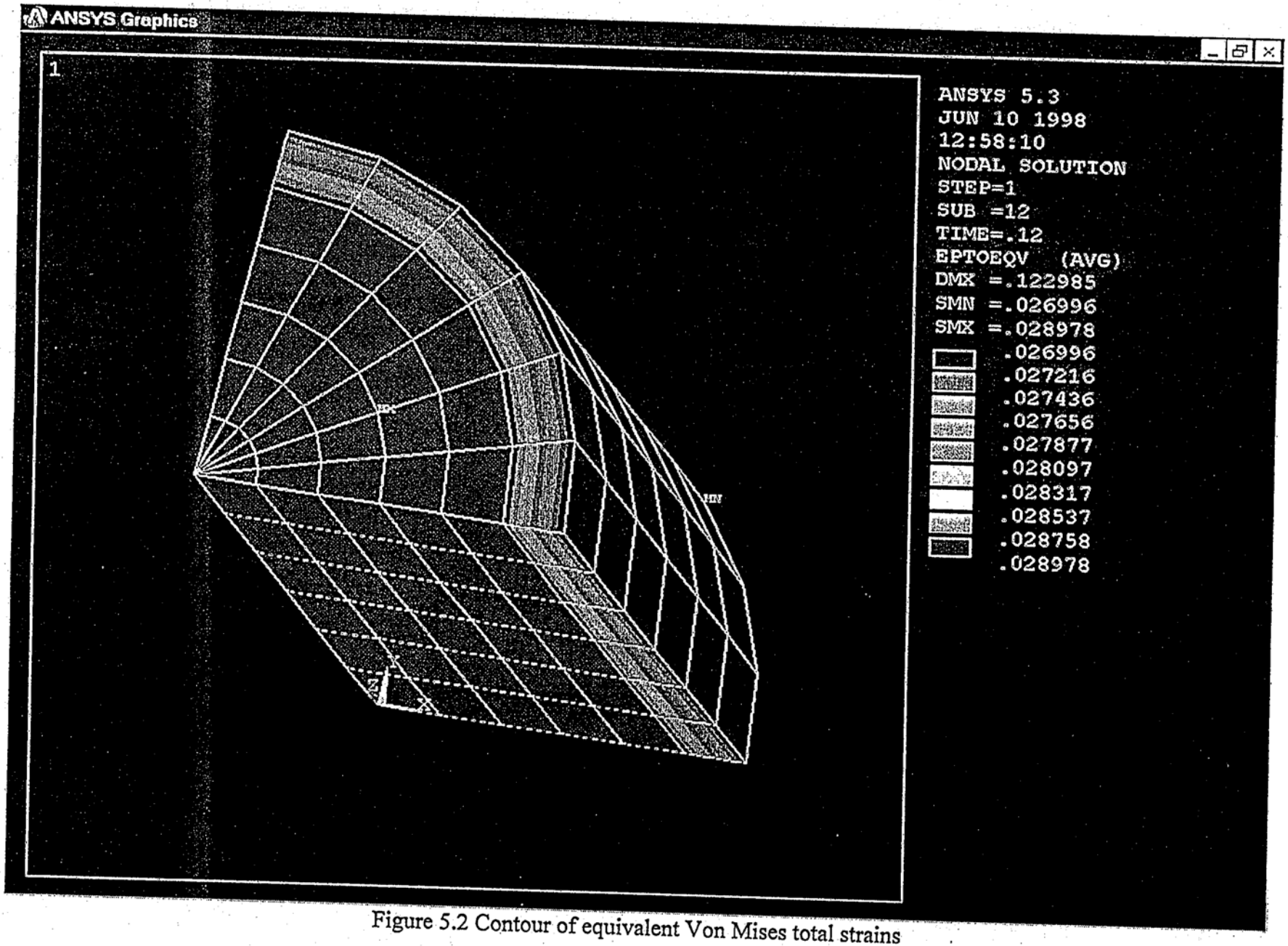

Figure 5.2 Contour of equivalent Von Mises total strains

predicted stress-strain curves of the FE model are plotted in Figures 5.3-5.7 for- the 3 ksi specimens with 1-5 layers, and in Figures 5.8-5.11 for the 6 ksi specimens with 1-4 layers. Generally a better prediction is- obtained for the 3 ksi specimens as compared to the 6 ksi specimens. This may be due to the fact that the bend point of their stress-strain curves is much higher than the assumed values.

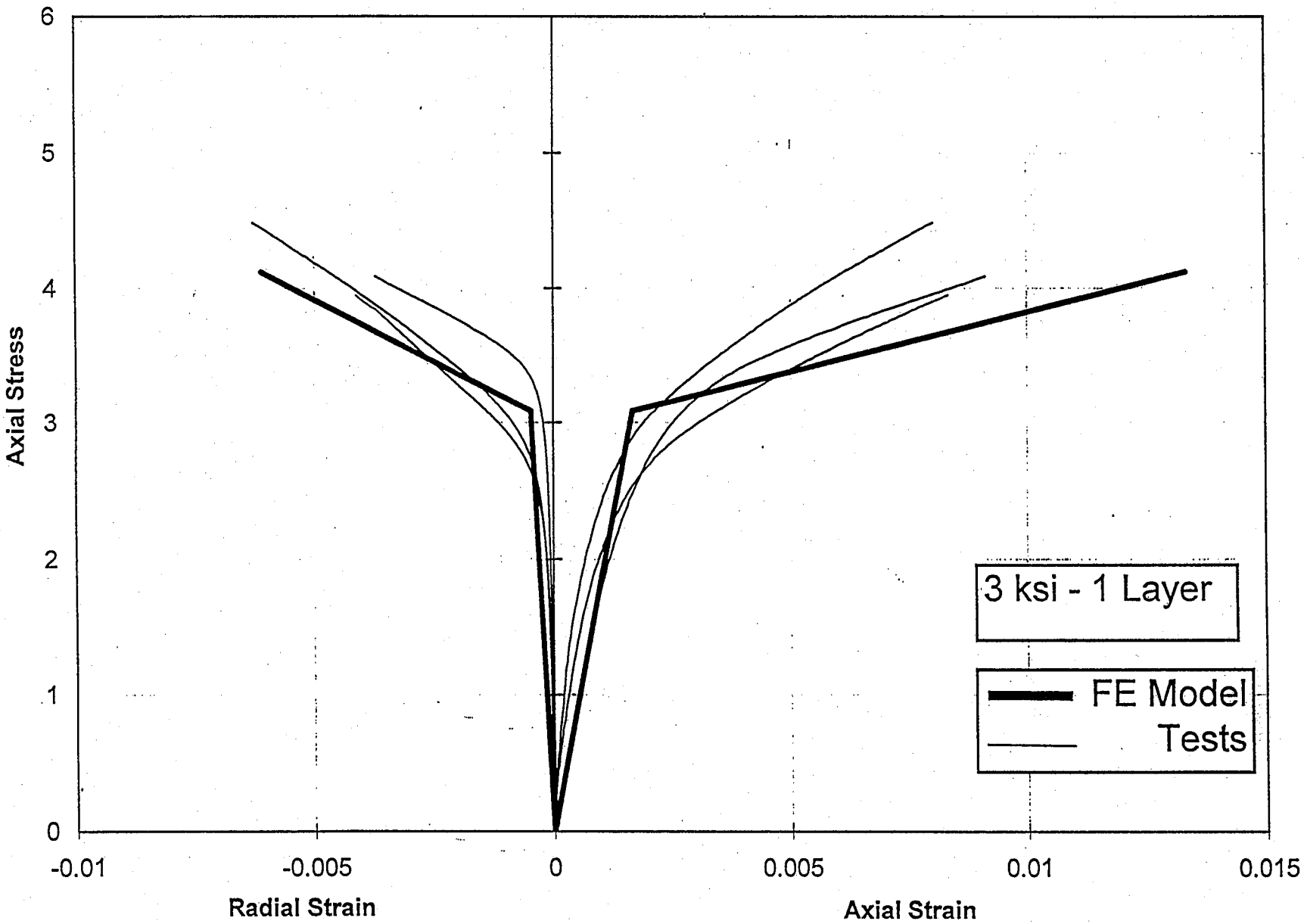

Figure 5.3 Comparison of FE model with the 3 ksi, 1-layer specimens

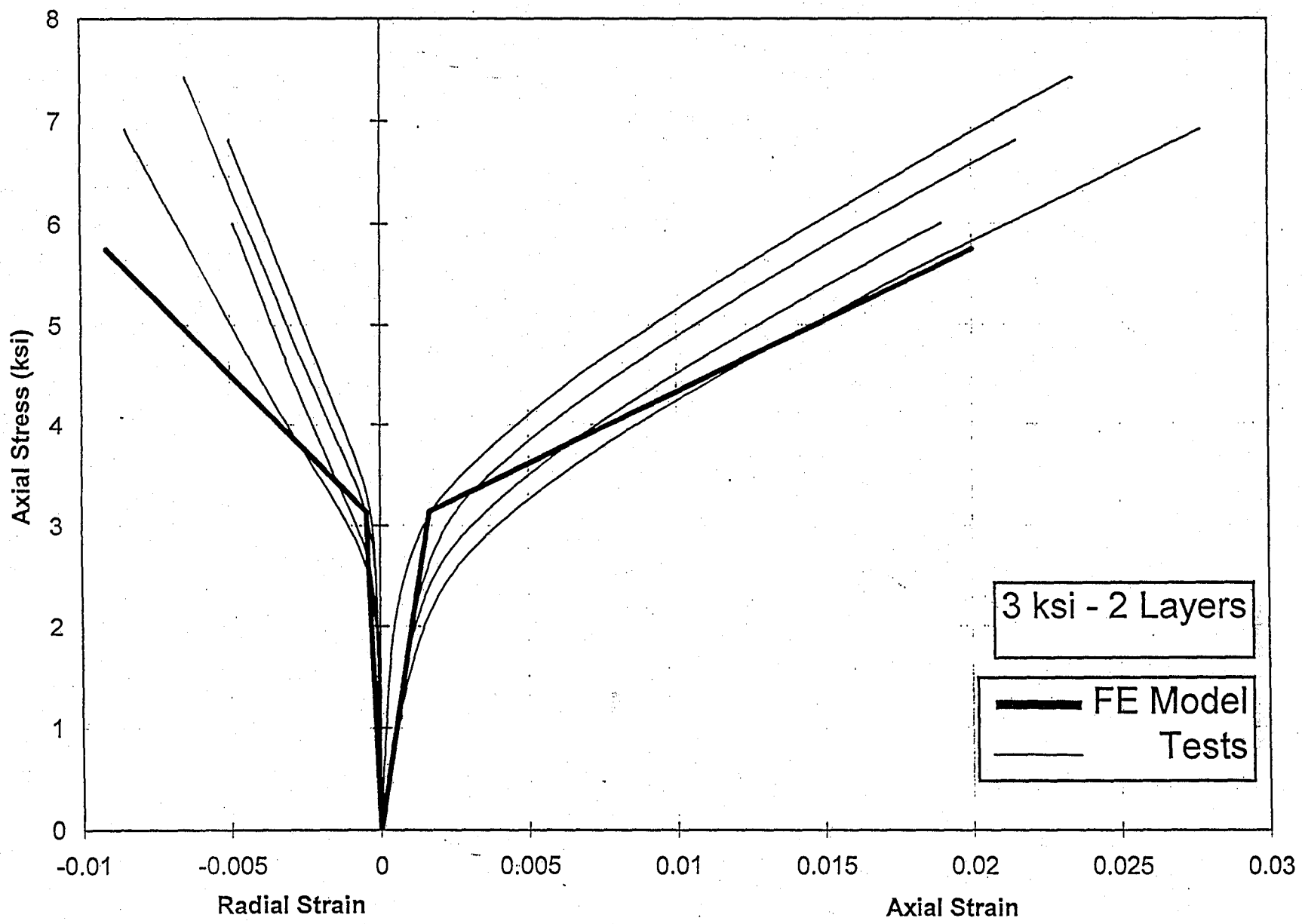

Figure 5.4 Comparison of FE model with the 3 ksi, 2-layer specimens

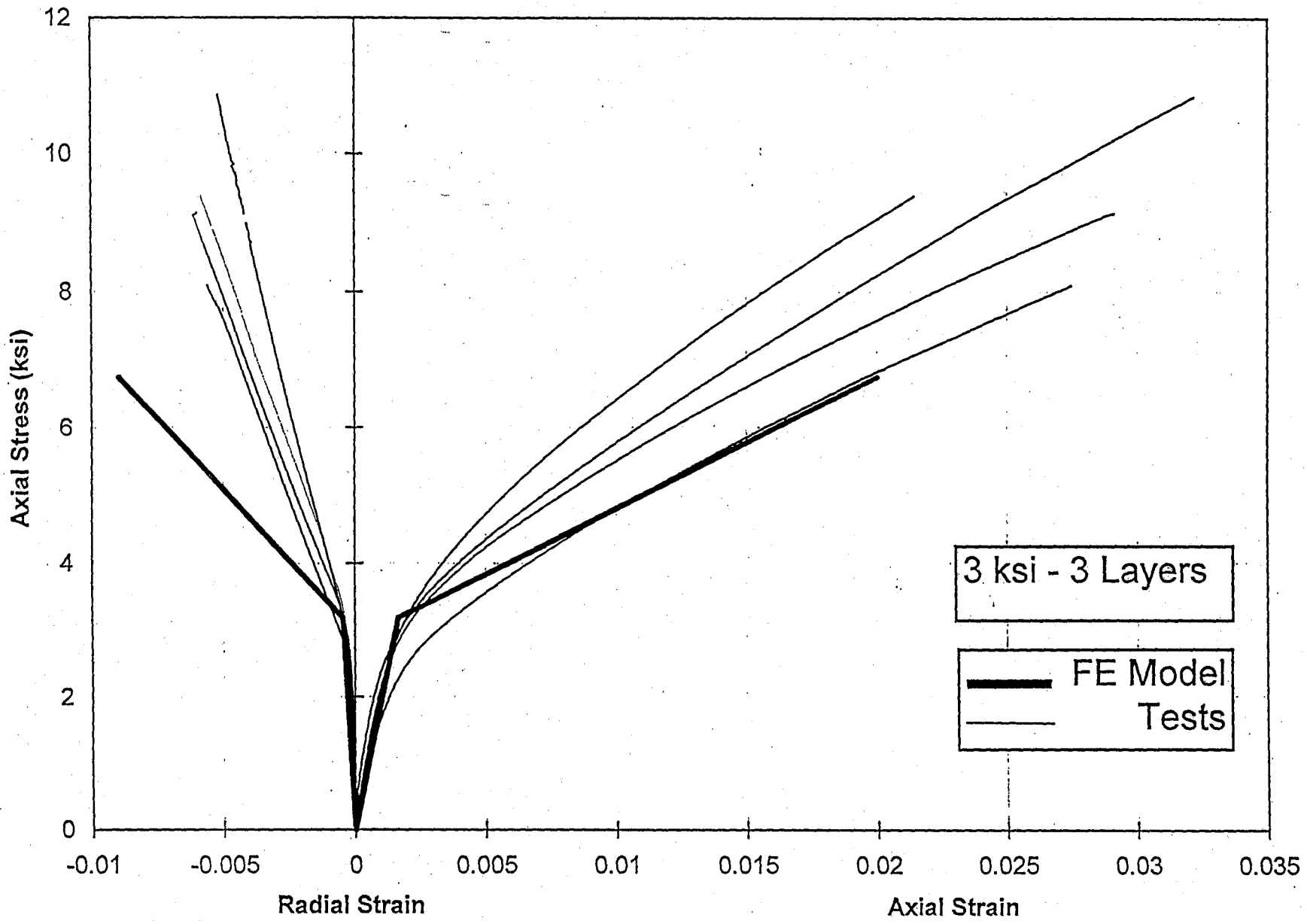

Figure 5.5 Comparison of FE model with the 3 ksi, 3-layer specimens

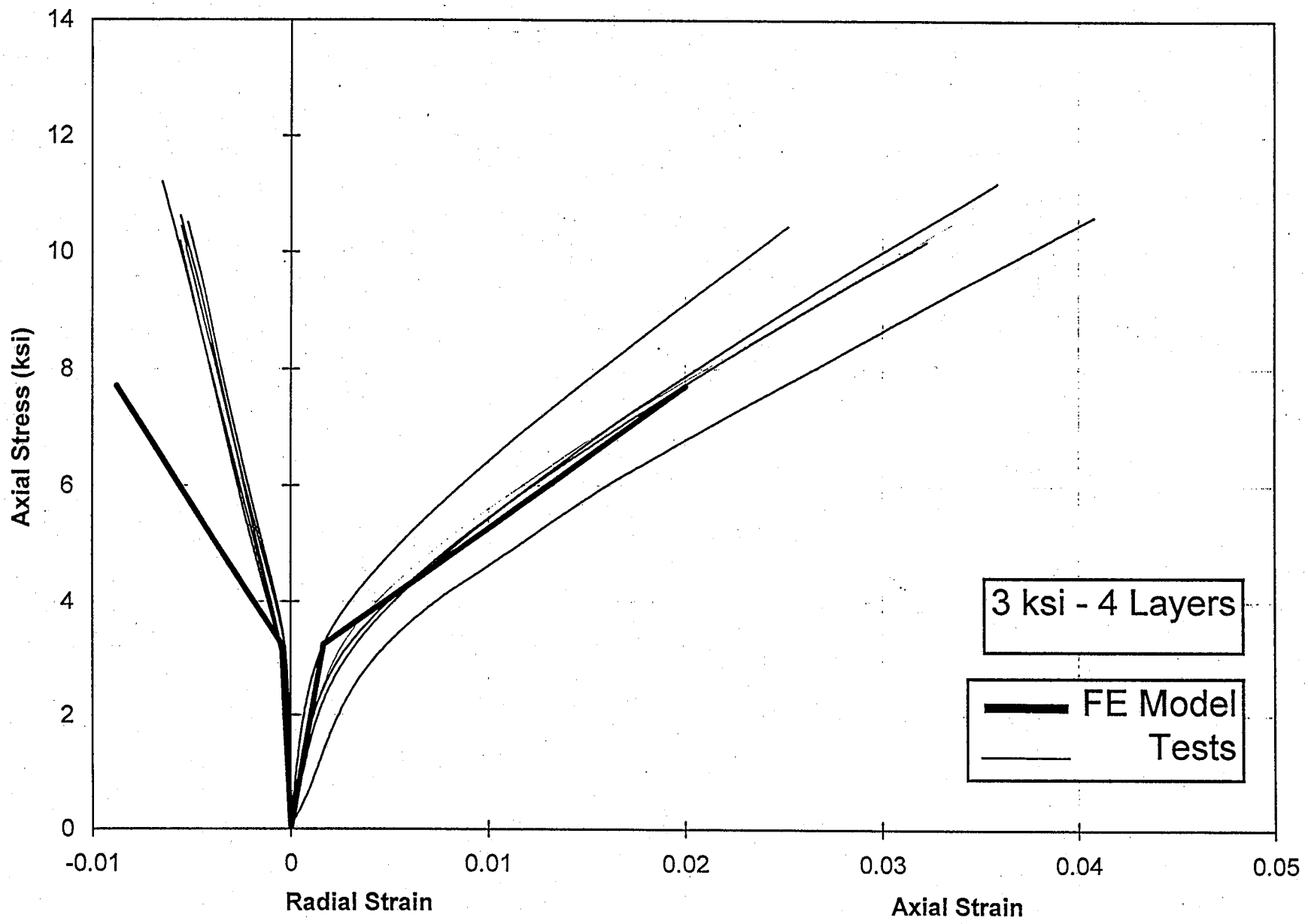

Figure 5.6 Comparison of FE model with the 3 ksi, 4-layer specimens

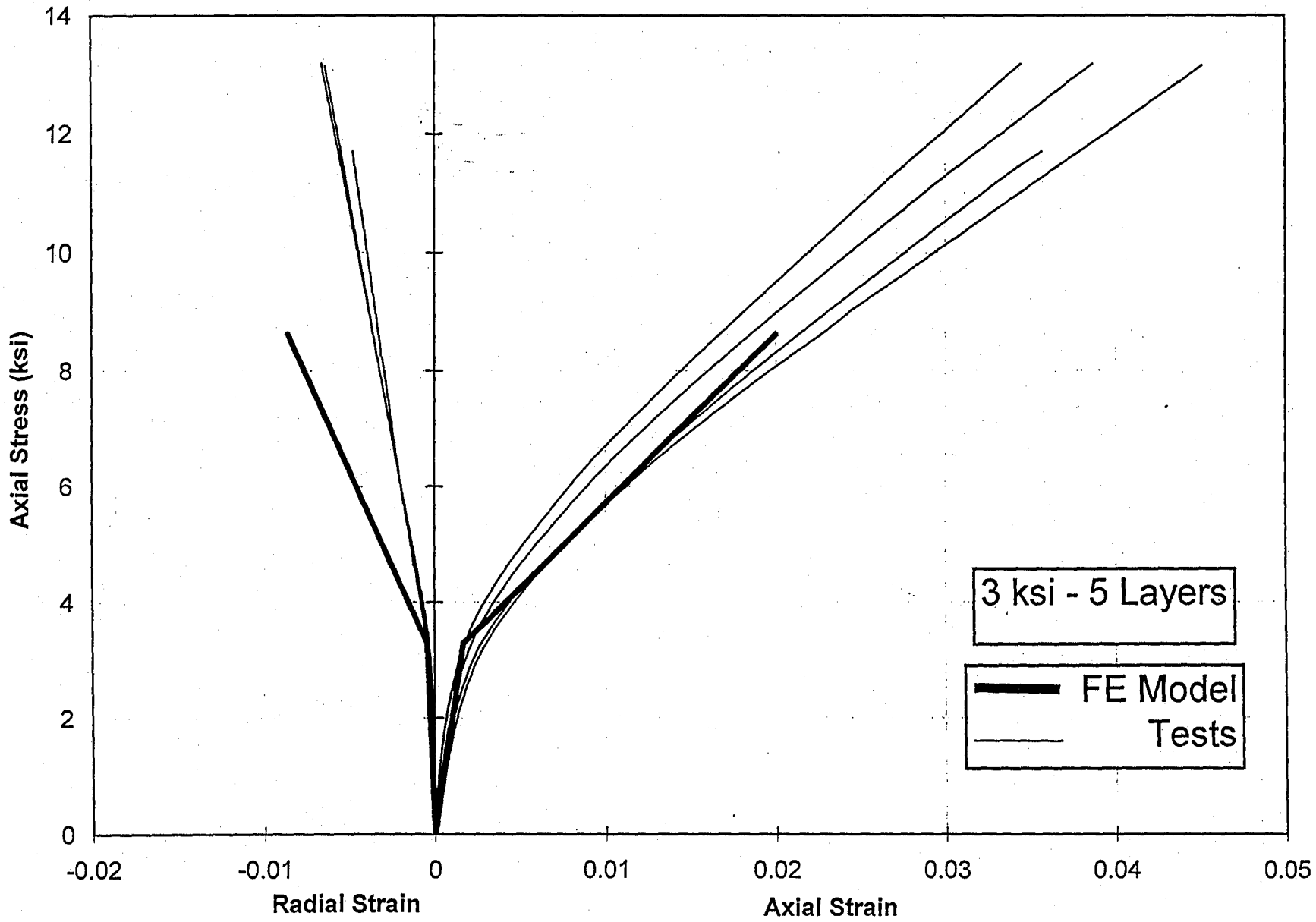

Figure 5.7 Comparison of FE model with the 3 ksi, 5-layer specimens

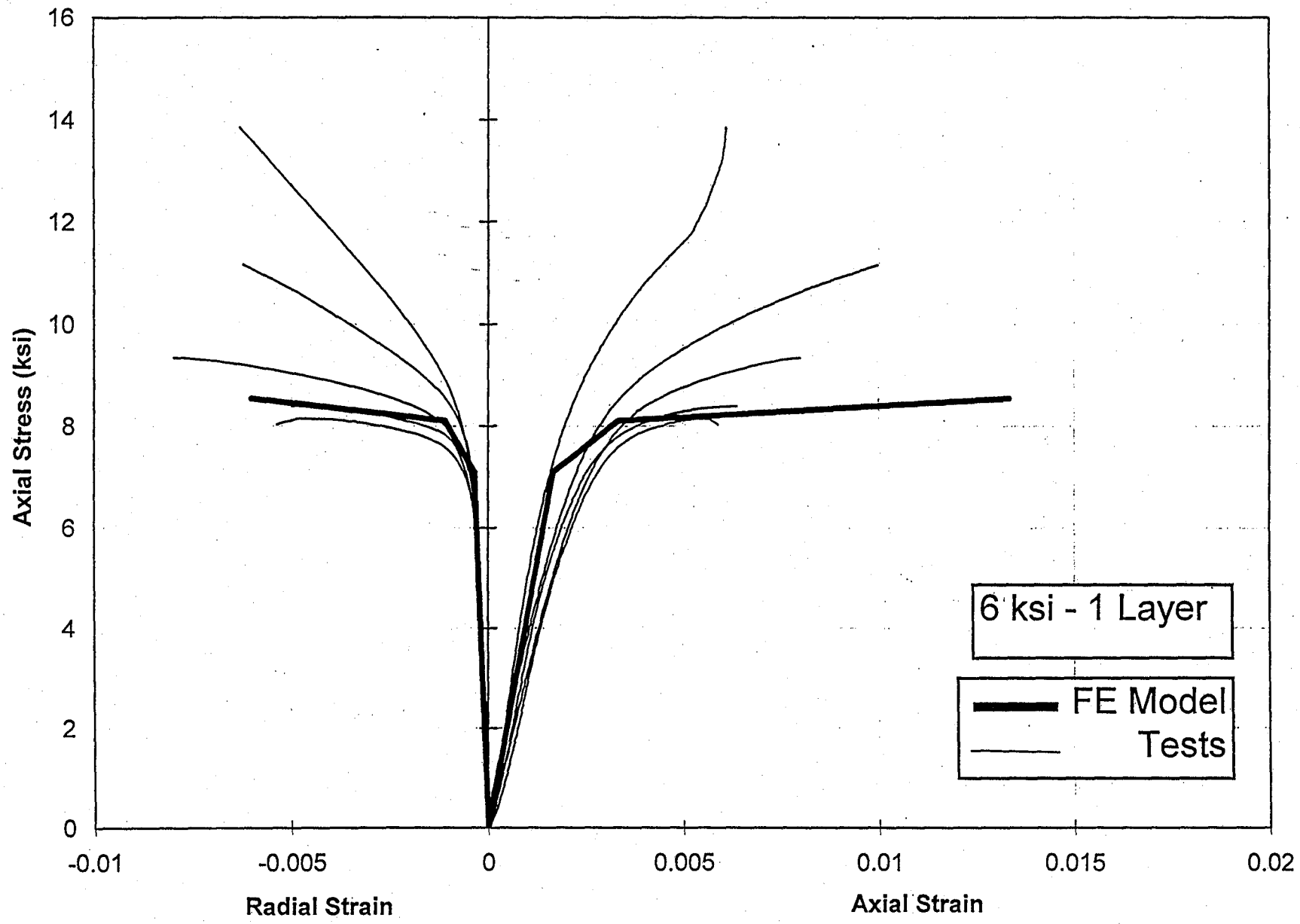

Figure 5.8 Comparison of FE model with the 6 ksi, 1-layer specimens

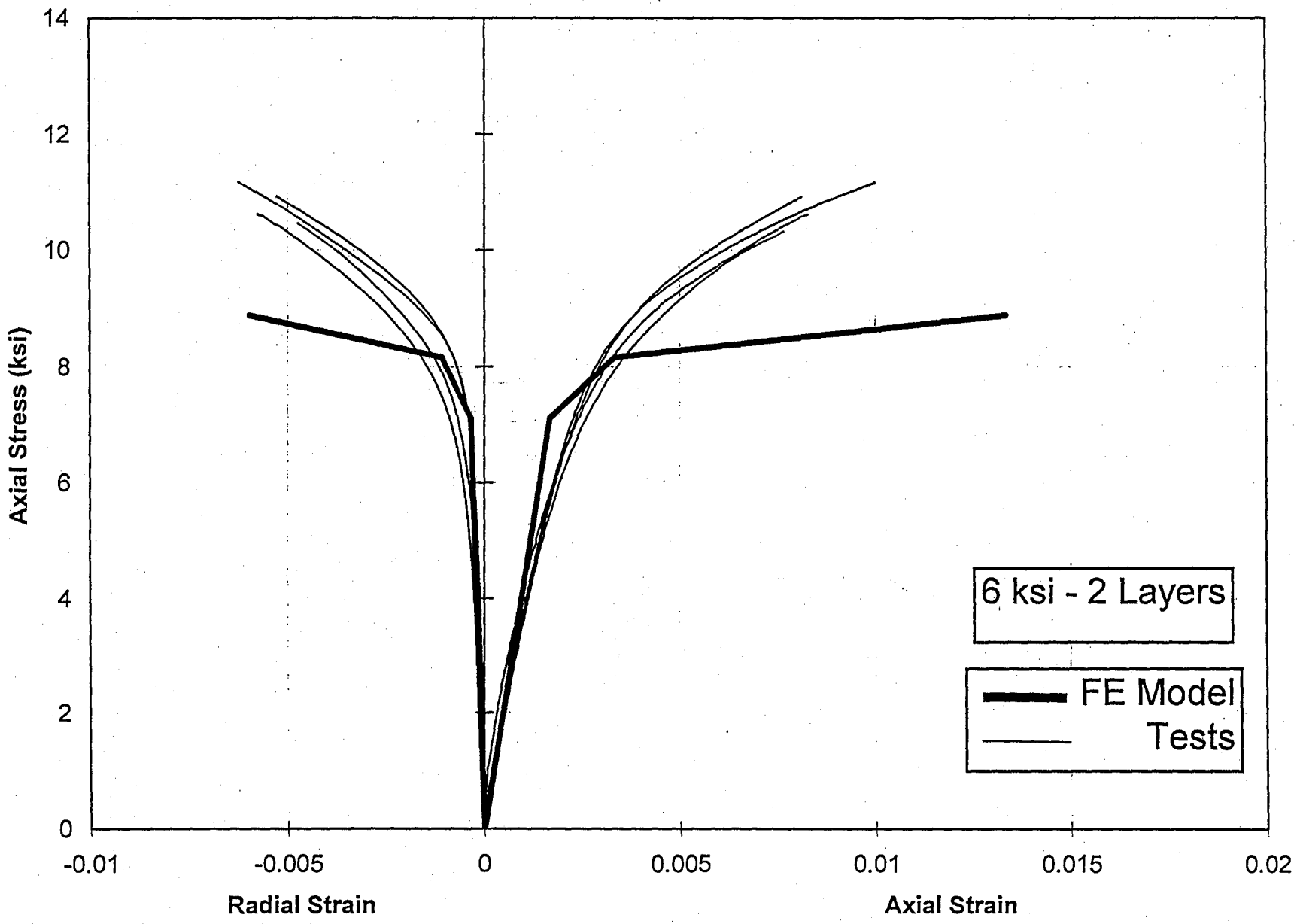

Figure 5.9 Comparison of FE model with the 6 ksi, 2-layer specimens

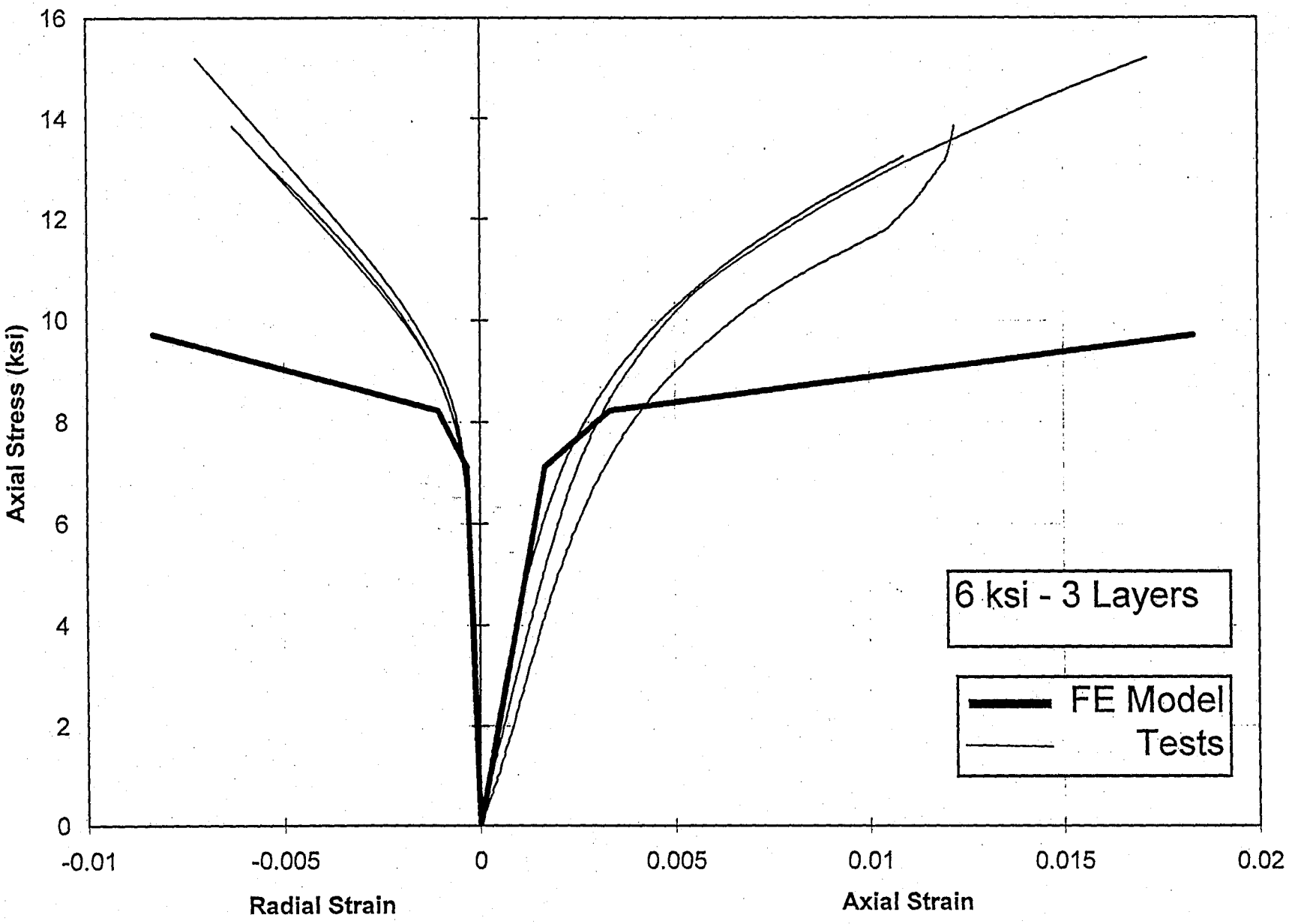

Figure 5.10 Comparison of FE model with the 6 ksi, 3-layer specimens

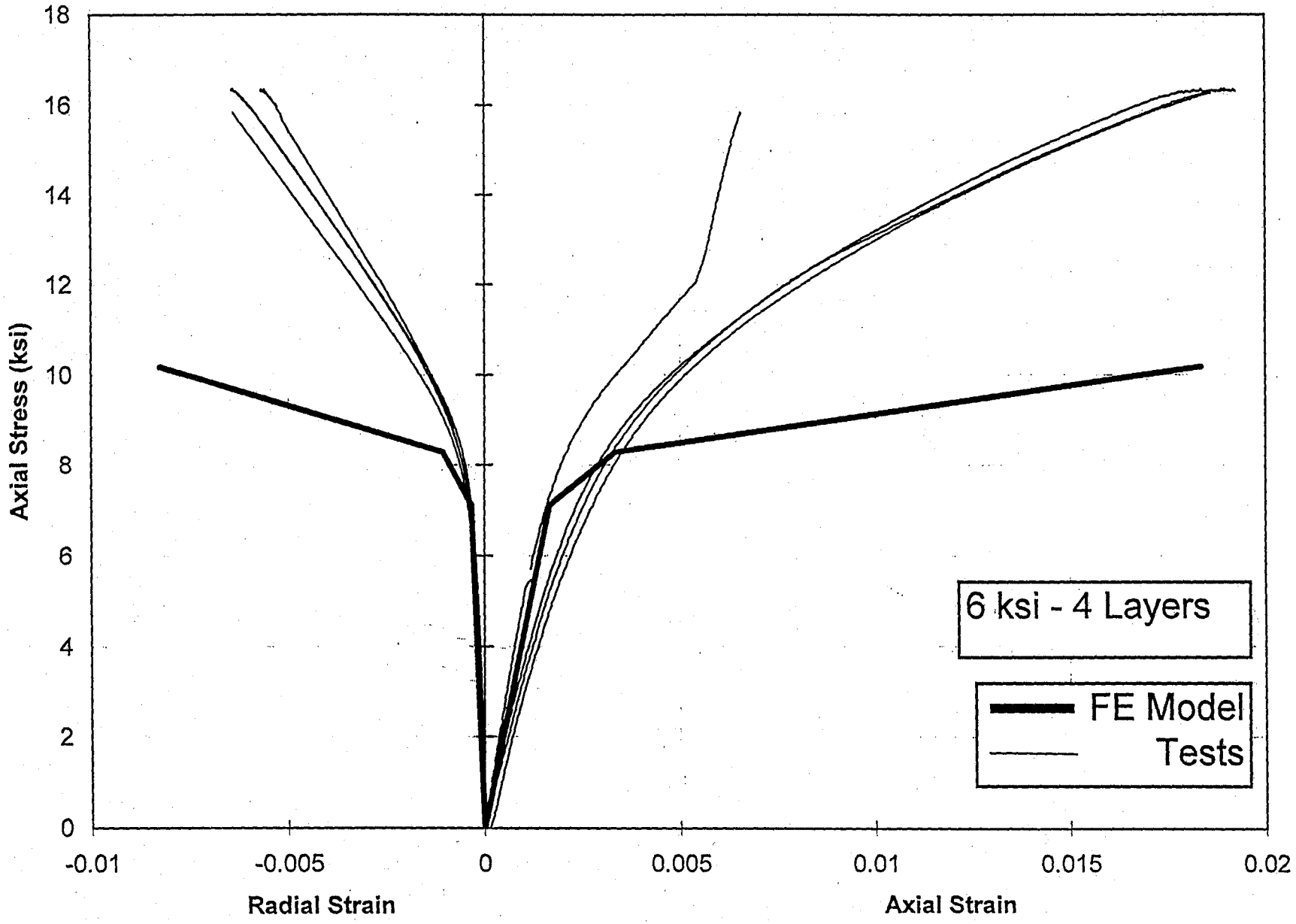

Figure 5.11 Comparison of FE model with the 6 ksi, 4-layer specimens

CHAPTER 6

CONCLUSIONS

Fiber-wrapping offers a high strength, low weight, and corrosion-resistant jacket which can be easily and quickly installed with negligible increase in the column's cross-section. Since the first application of fiber-wrapping technique to concrete chimneys in Japan (Katsumata and Yagi 1990), there has been an abundance of studies on the use of this technique. It has been put into practice in several states including California, Nevada, New York, and Vermont. Both carbon and glass fibers have been utilized, although carbon fibers are more expensive.

Since use of fiber composites *for* confinement of concrete is relatively new, theoretical work in this area is limited to the models that were originally developed for transverse steel reinforcement. However, it has been shown that concrete behaves very differently when confined by elasto plastic materials such as steel as compared to linearly elastic materials such as fiber composites (Mirmiran and Shahawy 1997a). Applying the same models to fiber-wrapped concrete may result in overestimating the strength and unsafe design. In the absence of reliable models, construction industry *may* be forced to either avoid the use of advanced composites, or to incorporate high "factors of safety," making composite construction less economical. The PI has previously developed such a model for glass-wrapped concrete columns (Mirmiran 1997a&b). There is a need to extend the work to carbon-wrapped concrete columns.

The experimental component of this study was conducted by the Florida Department of Transportation, Structural Research Laboratory, Tallahassee, FL. A total of 55:6" x 12" concrete .cylinders including 45 carbon-wrapped and 10 control (unconfined) specimens were tested in uniaxial compression. Two parameters were considered in the experimental program; concrete strength (3 and 6 ksi), and number of layers of carbon fabric (1-Slayers). Typical failure of carbonwrapped specimens was marked by fiber fracture at or near the mid-height of the specimens. Since the fabric was uni-directional (at 0°), a band or ring was typically formed as a result of the shearing off and separation of the fabric in the hoop direction. The response of carbon-wrapped specimens is generally bilinear, although more curvilinear than the response of glass-wrapped concrete. The first slope follows the modulus of elasticity of unconfined concrete, while the second slope depends on the number of layers and the stiffness of the jacket. As for volumetric response, the 6 ksi specimens behave very similar to the glass-wrapped concrete, in that the direction of dilation *is* reversed as the jacket takes over beyond the. critical stage of concrete. However, the 3 ksi specimens do not even show any expansion, as the carbon wrap appears to be stiff enough to restrain any dilation tendency of concrete. For both concrete batches, thicker jackets show faster recovery of

dilation as well as higher compaction rates. The dilation response of carbon-wrapped concrete appears to be generally the same as that of glass-wrapped concrete.

The confinement model that was developed for the glass-wrapped concrete predicted the response of carbon-wrapped specimens rather well. However, due to lack of accurate data on the properties of the jacket, it was not feasible to get better predictions, or to better evaluate the model. The finite element analysis with the non-associative Drucker-Prager type plasticity proved very effective for modeling of carbon-wrapped specimens. The differences were again attributed to the lack of accurate data on the properties of the jacket.

Carbon-wrapping of concrete column adds to its strength and ductility. The behavior of carbon-wrapped concrete is in general very similar to that of glass-wrapped concrete. The bilinear confinement that was developed for glass-wrapped concrete can be applied to carbon-wrapped concrete. However, a better fit can be obtained by re-calibrating the model for an entire database that consists of both carbon-wrapped and glass-wrapped concrete. Such database needs to be accompanied by a set of accurate coupon tests on the properties of the jacket. The finite element modeling is also useful in predicting the response of carbon-wrapped concrete. A more accurate estimate of jacket properties make the analysis fit the test results better.

REFERENCES

Ahmad, S.H., Khaloo, A.R., and Irshaid, A. (1991). "Behavior of concrete spirally confined by fiberglass filaments." *Mag. Concr. Res.*, 43(156), 143-148.

Ahmad, S.H., and Shah, S.P. (1982). "Stress-strain curves of concrete confined by spiral reinforcement." *ACI J.*, 79(6), 484-490.

ANSYS®. (1996). *Online Manual*, Version 5.3.

Ballinger, C., Maeda, T., and Hoshijima, T. (1993). "Strengthening of reinforced concrete chimneys, columns and beams with carbon fiber reinforced plastics." *Proc. Int. Symp. Fiber-Reinforced-Plastic reinforcement for Concrete Structures*, Nanni, A., and Dolan, C.W., ed., ACI, SP 138, 233-247.

Bavarian, B., Shively, J., Ehrgott, R., and Di Julio, R. (1996). "External support of concrete structures using composite materials." *Proc. 1st Int. Conf. Composites in Infrastructure*, Saadatmanesh, H., Ehsani, M.R., ed., Tuscon, AZ., 917-928.

Elwi, A.A., and Murray, D.W. (1979). "A 3D hypoelastic concrete constitutive relationship." *J. Engrg. Mech. Div.*, ASCE, 105(4), 623-641.

Fardis, M.N., and Khalili, H. (1981). "Concrete encased in fiberglass-reinforced plastic." *ACI J.*, 78(6), 440-446.

Fardis, M.N., and Khalili, H.H. (1982). "FRP-encased concrete as a structural material." *Magazine of Concrete Research*, 34(121), 191-201.

"Florida, Oregon protect bridge substructures." (1991). *Civil Engrg.*, 61(10), 18-19.

Fyfe, E.R. (1995). "Testing and field performance of the high strength fiber wrapping system." *Proc. Structures Congress XIII*, ASCE, Boston, MA., 603-606.

Garmestani, H. (1997). "Mechanical and microscopy analysis of carbon fiber reinforced polymeric matrix composite materials." *Final Report*, Florida Department of Transportation, Contract No. B-9949, Tallahassee, FL.

Jin, L., Saadatmanesh, H., and Ehsani, M.R. (1994). "Seismic retrofit of existing reinforced concrete columns by glass-fiber composites." *Proc. Materials Engrg. Conf.*, ASCE, 758-763, New York,

N.Y.

Karabinis, A.I., and Kiousis, P.D. (1994). "Effects of confinement on concrete columns: plasticity approach." *J. Struct. Engrg.*, ASCE, 120(9), 2747-2767.

Katsumata, H., and Yagi, K. (1990). "Applications of retrofit method with carbon fiber for existing reinforced concrete structures." *Proc. 22nd Joint UJNR Panel Meeting on Repair and Retrofit of Existing Structures*, National Institute for Standards and Testing (NIST), Gaithersburg, MD.

Kurt, C.E. (1978). "Concrete-filled structural plastic columns." *J. Struct. Div.*, ASCE, 104(1), 55-63.

Lahlou, K., Aïtcin, P.C., and Chaallal, O. (1992). "Behavior of high-strength concrete under confined stresses." *Cement & Concrete Composites*, 14, 185-193.

Madas, P., and Elnashai, A.S. (1992). "A new passive confinement model for the analysis of concrete structures subjected to cyclic and transient dynamic loading." *J. Earthquake and Struct. Dynamics*, 21, 409-431.

Mander, J.B., Priestley, M.J.N., and Park, R.J.T. (1988). "Theoretical stress-strain model for confined concrete." *J. Struct. Engrg.*, ASCE, 114(8), 1804-1826.

Mastrapa, J.C. (1997). "Effect of construction bond on confinement with fiber composites." *M.S. thesis*, University of Central Florida, Orlando, FL.

Mirmiran, A. (1997a). "Analytical and experimental investigation of reinforced concrete columns encased in fiberglass tubular jackets and use of fiber jacket for pile splicing." *Final Report*, Florida Department of Transportation, Contract No. B-9135, Tallahassee, FL.

Mirmiran, A. (1997b). "FRP-concrete composite column and pile jacket splicing - phase 2." *Final Report*, Contract No. B-9895, Florida Department of Transportation, Tallahassee, FL.

Mirmiran, A., and Shahawy, M. (1995). "A novel FRP-concrete composite construction for the infrastructure." *Proc. Structures Congress XIII*, ASCE, Boston, MA, 1663-1666.

Mirmiran, A., and Shahawy, M. (1997a). "Dilation characteristics of confined concrete." *Mechanics of Cohesive-Frictional Materials*, 2(3), 237-249.

Mirmiran, A., and Shahawy, M. (1997b). "Behavior of concrete columns confined by fiber composites." *J. Struct. Engrg.*, ASCE, 123(5), 583-590.

Monti, G., and Spoelstra, M.R. (1997). "Fiber-section analysis of RC bridge piers retrofitted with FRP jackets." *Proc. Structures Congress XV Building to Last*, ASCE, Portland, Ore., 884-888.

Nanni, A., and Bradford, N.M. (1995). "FRP-jacketed concrete under uniaxial compression." *Constr. and Bldg. Materials*, 9(2), 115-124.

Pantazopoulou, S.J. (1995). "Role of expansion on mechanical behavior of concrete." *J. Struct. Engrg.*, ASCE, 121(12), 1795-1805.

Picher, F. (1995). "Confinement of concrete cylinders with unidirectional carbon epoxy components". *M.S. Thesis*, University of Sherbrooke, Quebec, Canada.

Picher, F., Rochette, P., and Labossiere, P. (1996). "Confinement of concrete cylinders with CFRP." *Proc. 1st Int'l. Conf. Composites in Infrastructure*, Saadatmanesh, H., Ehsani, M.R., ed., Tuscon, AZ., 829-841.

Priestley, M.J.N., and Seible, F. (1996). *Seismic design and retrofit of bridges.* John Wiley and Sons, New York, N.Y.

Richard, R.M., and Abbott, B.J. (1975). "Versatile elastic-plastic stress-strain formula." *J. Engrg. Mech.*, ASCE, 101(4), 511-515.

Richart, F. E., Brandtzaeg, A., and Brown, R. L. (1928). "A study of the failure of concrete under combined compressive stresses." *Engrg. Experiment Station Bulletin No. 185*, University of Illinois, Urbana, IL.

Rochette, P., and Labossiere, P. (1996). "A plasticity approach for concrete columns confined with composite materials." *Adv. Composite Mater. in Bridges and Struct.*, M.M. El-Badry, (Ed.), Canadian Society for Civil Engineering, 359-366.

Saadatmanesh, H., Ehsani, M.R., and Li, M.W. (1994). "Strength and ductility of concrete columns externally reinforced with fiber composite straps." *ACI Struct. J.*, 91(4), 434-447.

Samaan, M., Mirmiran, A., and Shahawy, M. (1998). "Modeling of concrete confined by fiber composites." *J. Struct. Engrg.*, ASCE, In Press.

Xiao, Y., Martin, G.R., Yin, Z., and Ma, R. (1996). "Seismic retrofit of reinforced concrete bridge columns using a prefabricated composite wrapping system." *Proc. 1st Int. Conf. Composites in Infrastructure*, Saadatmanesh, H., and Ehsani, M.R., ed., Tucson, AZ., 903-916.

Zagers, K. (1998). "Nonlinear modeling of concrete-filled FRP tubes using the finite element method." *M.S. thesis*, University of Central Florida, Orlando, FL.